

Two-Loop Vertices in Quantum Field Theory: Infrared and Collinear Divergent Configurations*

GIAMPIERO PASSARINO[†] and SANDRO UCCIRATI[‡]

*Dipartimento di Fisica Teorica, Università di Torino, Italy
INFN, Sezione di Torino, Italy*

A comprehensive study is performed of two-loop Feynman diagrams with three external legs which, due to the exchange of massless gauge-bosons, give rise to infrared and collinear divergencies. Their relevance in assembling realistic computations of next-to-next-to-leading corrections to physical observables is emphasised. A classification of infrared singular configurations, based on solutions of Landau equations, is introduced. Algorithms for the numerical evaluation of the residues of the infrared poles and of the infrared finite parts of diagrams are introduced and discussed within the scheme of dimensional regularization. Integral representations of Feynman diagrams which form a generalization of Nielsen - Goncharov polylogarithms are introduced and their numerical evaluation discussed. Numerical results are shown for all different families of multi-scale, two-loop, three-point infrared divergent diagrams and successful comparisons with analytical results, whenever available, are performed. Part of these results has already been included in a recent evaluation of electroweak pseudo-observables at the two-loop level.

Key words: Feynman diagrams, Multi-loop calculations, Vertex diagrams, Infrared divergencies

PACS Classification: 11.15.-q, 11.15.Bt, 12.38.Bx, 02.90.+p, 02.60.-x, 02.70.Wz

*Work supported by MIUR under contract 2001023713_006.

[†]giampiero@to.infn.it

[‡]uccirati@to.infn.it

Contents

1	Introduction	2
2	Notations and Conventions	3
2.1	Integrals and integration measures	3
2.2	Alphameric classification of Feynman diagrams	4
2.3	Basic quadratic forms	4
3	Tools for virtual infrared divergencies	5
3.1	Infrared singularities and Landau equations	5
3.2	Sector decomposition	7
3.3	Integrable singularities and sector decomposition	8
3.4	Infrared power-counting	8
3.5	Infrared singularities and hypergeometric functions	8
3.6	Threshold behavior and Mellin-Barnes transforms	9
3.7	Old and new Bernstein - Sato - Tkachov functional relations	10
4	Derivatives of two-loop self-energies and infrared poles.	13
5	Infrared divergent two-loop vertices	13
5.1	The V^E diagram	14
5.2	The V^I diagram	15
5.2.1	Extraction of UV and IR poles	15
5.3	The V^M diagram	17
5.3.1	Evaluation of V^M , cases a) and b)	18
5.3.2	Evaluation of V_c^M	22
5.4	The V^G diagram	24
5.5	The V^K diagram	25
5.6	Evaluation of the V^K cases	26
5.6.1	Evaluation of V_a^K	28
5.6.2	Evaluation of V_b^K	29
5.6.3	Evaluation of V_c^K	32
5.6.4	Evaluation of V_d^K	35
5.7	The V^H diagram	37
5.8	Collinear limits of V^H	42
5.9	A detailed study of the V^H configurations	45
6	Behaviour of two - loop vertices in the collinear limit	46
7	Numerical Results	47
8	Conclusions	49
A	Taylor and Laurent expansion of Euler's functions	50
B	Nielsen polylogarithms	50
C	Properties of the hypergeometric function	50
D	Computation of the integral $J_{nm}^{kh}(i)$	51
E	Useful expansions	52
F	Tables of numerical results	53

1 Introduction

This paper belongs to a series devoted to numerical evaluation of the multi-loop, multi-leg Feynman diagrams that appear in any renormalizable quantum field theory. In [1] (hereafter I) the general strategy has been designed and in [2] (hereafter II) a complete list of results has been derived for two-loop functions with two external legs, including their infrared divergent on-shell derivatives. Results for one-loop multi-leg diagrams have been shown in [3] and additional material can be found in [4]. Two-loop three-point functions for infrared convergent configurations have been considered in [5] (hereafter III), two-loop tensor integrals in [6].

Many mass scales appear in the computation of physical observables within the Standard Model, generating serious difficulties for the familiar analytical approach. Our purpose is to overcome these problems through a numerical approach. The application of our techniques has recently contributed to the evaluation of the two-loop fermionic correction to the effective electroweak mixing angle and of the full Higgs-mass dependence of the bosonic ones [7].

The approach described in [1] is primarily intended for evaluation of multi-loop diagrams with internal massive lines. However, QED and QCD are integral part of any realistic calculation and they lead to infrared singularities. Therefore, any method aimed to a numerical evaluation of diagrams must be able to handle the infrared problem and infrared/collinear configurations should be treatable within the same class of algorithms used for the non-infrared cases or within some simple extension of the latter.

For one-loop diagrams we have seen that our methods allow us to extract the infrared pole in dimensional regularization with a residue and a finite part that can be treated numerically [3]. The procedure has been extended in II to cover the on-shell derivative of two-point functions which are needed in the treatment of external legs.

It is the purpose of this paper to extend the study of infrared divergencies to two-loop three-point functions. All diagrams are computed within the scheme of dimensional regularization [8] with space-time dimensionality $n = 4 - \epsilon$. Each loop in a diagram contributes at most one soft (zero gauge-boson mass) and one collinear (for zero fermion mass) $1/\epsilon$ term but the global order of the pole at $\epsilon = 0$ can be greater than two due to simultaneous occurrence of ultraviolet poles which are removed by the introduction of counter-terms.

To accomplish our goals we need an automatized procedure for handling infrared (and collinear) configurations: Landau equations [9] represent the proper tool since a necessary condition for the presence of infrared divergencies is that the Landau equations are fulfilled. Therefore, for each topology we build individual diagrams by filling all the lines with the line content of the theory, disregarding those configurations with vertex content not allowed by the theory itself. The generated result is examined and Landau equations studied for those diagrams that contain massless gauge-boson: if they are fulfilled then we have an infrared divergent configuration. The residue of the infrared pole(s) and the corresponding infrared finite part are then computed numerically.

This part of the procedure is relatively easy while the difficult task is connected to the numerical evaluation of residues and of finite parts. They will be given in terms of multi-dimensional integrals over Feynman parameters with integrands that are not positive defined and, according to our strategy, their evaluation requires introduction of smoothness algorithms.

Smoothness requires that, after suitable manipulations, the kernel in the integral representation and its first N derivatives be continuous functions and, ideally, N should be as large as possible. However, in most of the cases we will be satisfied with absolute convergence, e.g. logarithmic singularities of the kernel. This is particularly true when the large number of terms required by obtaining continuous derivatives of higher order leads to large numerical cancellations.

There is a general approach for extracting infrared poles which goes under the name of sector decomposition [10]. We have examined this technique which, despite its great intrinsic possibilities, has its own problems: to name one it has been applied (so far) mainly to unphysical kinematics where infrared residues and finite parts are given in terms of positive definite integrands, i.e. it will not work properly around thresholds where the Feynman integrands are known to change their sign and imaginary parts show up. For recent developments see, however, ref. [11].

In our experience the form of the integrand, after many iterations of the sector decomposition technique,

is such that one can hardly imagine to design adequate smoothness algorithms. For this reason we have, quite often, privileged algorithms that keep under control the smoothness of the Feynman integrand at each step of the extraction of the infrared singularities. Usage of the whole machinery of hypergeometric functions has shown particularly useful in this respect.

One may wonder why to devote additional efforts to the problem of computing infrared divergent diagrams, given the spectacular success of analytical evaluation in QED/QCD: here we refer, in particular to the results by [12], by [13] and by [14] but also to [16].

The actual reason for pursuing this line of research is that QED and QCD are embedded in a more general theory, e.g. the standard model of fundamental interactions; from this point of view their handling is much more complicated. For instance there will be more than one mass scale for infrared divergent configurations, like in the decay of charged gauge-bosons and, with few exceptions, the analytical approach works only for very few scales or in the approximation where the scales themselves are arranged according to some fixed hierarchy, $m \ll M$ etc.

We are not claiming that a purely numerical approach is the final solution, rather one should carefully mix (semi) analytical extraction of dominant corrections (e.g. leading and sub-leading collinear logarithms) with numerical evaluation of sub-dominant, process-dependent, terms; the latter should be transformed in a way that allows for a safe, stable, integration where apparent singularities of the integrand are absent or limited to a minimum amount. Whenever a cancellation of dominant terms is foreseen we have to organize the calculation in such a way that these terms drop out before any numerical integration is attempted. From this point of view the technique of reduction of an arbitrary diagram to generalized scalar integrals is not always the best choice; master integrals quite often are individually more divergent (e.g. in the collinear limit) than the complete answer. Our technique does not grant any privilege to master integrals – from a computational point of view – and, therefore, seems more appropriate in handling the problem.

The outline of the paper will be as follows: in Section 2 we define our conventions. In Section 3 we review some of the tools that have been introduced to study infrared divergencies in quantum field theory. The connection between infrared divergent configurations and Landau equations is described in Section 3.1, in Section 3.2 and 3.3 we present the procedure of sector decomposition while an alternative technique for extracting ultraviolet (if any) and infrared poles, based on properties of the hypergeometric function is given in Section 3.5. In Section 3.6 we present a discussion of threshold singularities. Starting with Section 5 we present our results for all configurations, from Section 5.1 to Section 5.7. In Section 5.9 we present an explicit example of our procedure for classifying infrared divergent diagrams. Numerical results are summarized in Section 7. In Appendix we give a collection of technical details.

2 Notations and Conventions

Our conventions for dealing with arbitrary two-loop diagrams have been introduced in Sect. 2 of II. Conventions that are specific for three-point functions have been introduced in Sect. 2 of III; also the various families of two-loop vertex diagrams have been classified in III but, for the reader's convenience, they are repeated in Figs. 3–11.

2.1 Integrals and integration measures

In particular, to keep our results as compact as possible, we introduce the following notations where $x_0 = y_0 = 1$:

$$\begin{aligned} \int dS_n(\{x\}) f(x_1, \dots, x_n) &\equiv \prod_{i=1}^n \int_0^{x_{i-1}} dx_i f(x_1, \dots, x_n), \\ \int dC_n(\{x\}) f(x_1, \dots, x_n) &\equiv \int_0^1 \prod_{i=1}^n dx_i f(x_1, \dots, x_n), \end{aligned} \tag{1}$$

Also, the so-called '+'-distribution will be extensively used, e.g.

$$\begin{aligned}
\int dC_n(\{z\}) \int_0^1 dx \frac{f(x, \{z\})}{x} \Big|_+ &= \int dC_n(\{z\}) \int_0^1 dx \frac{f(x, \{z\}) - f(0, \{z\})}{x}, \\
\int dC_n(\{z\}) \int_0^1 dx \frac{f(x, \{z\})}{x-1} \Big|_+ &= \int dC_n(\{z\}) \int_0^1 dx \frac{f(x, \{z\}) - f(1, \{z\})}{x-1}, \\
\int dC_n(\{z\}) \int_0^1 dx \frac{f(x, \{z\}) \ln^n x}{x} \Big|_+ &= \int dC_n(\{z\}) \int_0^1 dx \frac{[f(x, \{z\}) - f(0, \{z\})] \ln^n x}{x}.
\end{aligned} \tag{2}$$

The last relation in Eq.(2) is used for evaluating integrals of the following type:

$$\int_0^1 dx \frac{f(x)}{x^{1-\epsilon}} = \frac{f(0)}{\epsilon} + \int_0^1 dx \frac{f(x)}{x} \Big|_+ + \epsilon \int_0^1 dx \frac{f(x) \ln x}{x} \Big|_+ + \mathcal{O}(\epsilon^2). \tag{3}$$

Since we will have to split integrals during the evaluation of diagrams we have introduced a special notation:

$$\int_{a,c}^{c,b} dx F_{1\oplus 2; A}(x) = \int_a^c dx F_{1; A}(x) + \int_c^b dx F_{2; A}(x). \tag{4}$$

In other cases we have to integrate over a triangle, for which we introduce the special notation ($\bar{X} = 1 - X$)

$$\int_{(0, \bar{X}, x_1)} dx_2 dx_3 = \int_0^{\bar{X} x_1} dx_2 \int_0^{x_2/\bar{X}} dx_3 + \int_{\bar{X} x_1}^{x_1} dx_2 \int_0^{(x_1-x_2)/X} dx_3, \tag{5}$$

2.2 Alphameric classification of Feynman diagrams

In our conventions any scalar two-loop diagram is identified by a capital letter (S, V etc, for self-energies, vertices etc) indicating the number of external legs and by a triplet of numbers (α, β and γ) giving the number of internal lines (in the q_1, q_2 and $q_1 - q_2$ loops respectively). There is a compact way of representing this triplet: assume that $\gamma \neq 0$, i.e. that we are dealing with non-factorizable diagrams, then we introduce $\kappa = \gamma_{\max} [\alpha_{\max} (\beta - 1) + \alpha - 1] + \gamma$ for each diagram. Furthermore, we can associate a letter of the alphabet to each κ : for $G = V$ we have $\alpha_{\max} = 2$ and $\gamma_{\max} = 2$, therefore, the following correspondence holds:

$$121 \rightarrow E, \quad 131 \rightarrow I, \quad 141 \rightarrow M, \quad 221 \rightarrow G, \quad 231 \rightarrow K, \quad 222 \rightarrow H. \tag{6}$$

For $G = S$ we have $\alpha_{\max} = 2$ and $\gamma_{\max} = 1$, therefore

$$111 \rightarrow A, \quad 121 \rightarrow C, \quad 131 \rightarrow E, \quad 221 \rightarrow D. \tag{7}$$

This classification is extensively used throughout the paper where we omit the suffix 0 for scalar diagrams.

2.3 Basic quadratic forms

An x -dependent mass is always defined as

$$m_x^2 = \frac{m_1^2}{x} + \frac{m_2^2}{1-x}. \tag{8}$$

In the following we introduce some quadratic forms that are widely used throughout the paper.

$$\chi(x; P^2; m, M) \equiv -P^2 x^2 + (P^2 - m^2 + M^2)x + m^2 = -P^2 (x - X_\chi)^2 + B_\chi, \tag{9}$$

where we define

$$B_\chi = \frac{1}{4P^2} \lambda(-P^2, m^2, M^2), \quad X_\chi = \frac{P^2 - m^2 + M^2}{2P^2}, \quad \bar{X}_\chi = 1 - X_\chi. \tag{10}$$

Here $\lambda(x, y, z) = x^2 + y^2 + z^2 - 2(xy + xz + yz)$ is the usual Källén lambda - function. If no ambiguity will arise we will simply write $\chi(x)$. Furthermore, we introduce

$$\overline{\chi}(x; P^2; m, M) \equiv \chi(1-x; P^2; m, M) = -P^2 x^2 + (P^2 - M^2 + m^2)x + M^2 = -P^2(x - \overline{X}_\chi)^2 + B_\chi, \quad (11)$$

$$\beta(x, y; P^2; m, M) \equiv -P^2 x^2 + (P^2 - m^2 + M^2)xy + m^2 y^2 = -P^2(x - X_\chi y)^2 + B_\chi y^2, \quad (12)$$

$$\overline{\beta}(x, y; P^2; m, M) \equiv -P^2 x^2 + (P^2 - M^2 + m^2)xy + M^2 y^2 = -P^2(x - \overline{X}_\chi y)^2 + B_\chi y^2. \quad (13)$$

Once again, we will drop irrelevant arguments if no ambiguity may arise. These quadratic forms will play a major role in the evaluation of the diagrams considered in this paper.

3 Tools for virtual infrared divergencies

Before starting a comprehensive study of two-loop, infrared divergent, vertices we collect in this Section a set of tools which are relevant for the general analysis of infrared divergencies in a spontaneously broken quantum field theory.

First, we recall the classification of infrared configurations based on the study of Landau equations; we then move to a short review of the techniques which go under the general name of sector decomposition; the use of these techniques for handling integrable singularities in the evaluation of Feynman diagrams is also discussed. Alternative techniques based on a representation of infrared divergent diagrams through hypergeometric functions will be illustrated by means of simple examples. Mellin - Barnes techniques will be introduced to study infrared configurations around their normal thresholds and to extract collinear limits. Finally, we will present some of our new techniques which represent an extension of the Bernstein - Sato functional relations [17].

3.1 Infrared singularities and Landau equations

As explained in the Introduction, the classification of infrared divergent Feynman diagrams is most conveniently based on the use of Landau equations [9]. The whole procedure is better illustrated in terms of a simple scalar one-loop triangle. Consider the following Feynman parametric representation of the diagram:

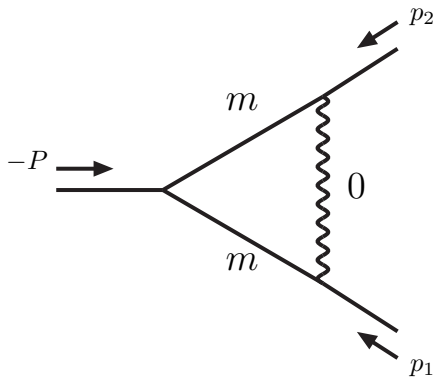


Figure 1: The scalar one-loop, three-point Green function with one massless internal line. All momenta are flowing inwards.

$$C_0(p_1^2, p_2^2, P^2; m, 0, m) = \frac{\mu^\epsilon}{i\pi^2} \int_0^1 dx \int_0^x dy V_C^{-1-\epsilon/2}(x, y),$$

$$V_C(x, y) = -p_2^2 x^2 - p_1^2 y^2 - 2p_1 \cdot p_2 xy + (p_2^2 - m^2)x - (p_2^2 - P^2 - m^2)y + m^2. \quad (14)$$

To regularize infrared divergencies we use the scheme of dimensional regularization, with the space-time dimensionality $n = 4 - \epsilon$ and where μ is the 't Hooft unit of mass. In principle one should carefully

distinguish between ultraviolet and infrared regulators ($\epsilon > 0$ or $\epsilon < 0$) but for a comprehensive discussion we refer to [18].

It is important to recall that a necessary condition for the presence of infrared divergencies is that the Landau equations are fulfilled. A proper solution of the set of Landau equations for the one-loop vertex of Fig. 1 requires that

$$P^2 = -\frac{1}{2m_2^2} \left\{ 2m_2^2(m_1^2 + m_3^2) - (m_1^2 + m_2^2 + p_1^2)(m_3^2 + m_2^2 + p_2^2) \pm \left[\lambda(-p_1^2, m_1^2, m_2^2)\lambda(-p_2^2, m_3^2, m_2^2) \right]^{1/2} \right\}, \quad (15)$$

which, for $m_2 = 0$ and $m_1 = m_3 = m$ is satisfied if $p_1^2 = p_2^2 = -m^2$ and P^2 is unconstrained¹. The corresponding V_C reads

$$V_C(x, y) = m^2(1-x)^2 + m^2y^2 + (P^2 + 2m^2)(1-x)y, \quad (16)$$

showing that $V_C = 0$ for $x = 1$ and $y = 0$. The parametrization in Eq.(14) is certainly not the most convenient one to evaluate the residue of infrared pole but this choice has been made deliberately, having in mind the more complex two-loop cases.

In any software package designed to compute (automatically) physical observables the classification of the infrared cases must be a built-in procedure. The study of the Landau equations for a given family of diagrams is the most elegant way to classify its infrared divergent configurations. Again we refer to the one-loop vertex for illustration. The Landau equations are

$$\alpha_1(q^2 + m_1^2) = 0, \quad \alpha_2((q + p_1)^2 + m_2^2) = 0, \quad \alpha_3((q + p_1 + p_2)^2 + m_3^2) = 0, \quad (17)$$

$$\alpha_1 q_\mu + \alpha_2 (q + p_1)_\mu + \alpha_3 (q + p_1 + p_2)_\mu = 0. \quad (18)$$

A solution of the system with $\alpha_i \neq 0, \forall i$ gives the leading singularity.

Let us multiply Eq.(18) by q , by p_1 and by p_2 to obtain an homogeneous system of three equations where we use $q^2 = -m_1^2$ etc, from Eq.(17). A necessary and sufficient condition to have a proper solution, i.e. not all the $\alpha_i = 0$, requires the determinant of coefficients to be zero, thus fixing a relation between internal and external masses. Any configuration that satisfy this constraint is a Landau singularity for the diagram which, however, does not necessarily imply that the diagram itself diverges at that configuration. For the C_0 function this corresponds to the well-known anomalous threshold.

Consider the following case: $p_{1,2}^2 = -m^2, m_{1,3} = m$ and $m_2 = 0$. It is easily found that the anomalous threshold condition is satisfied, therefore the configuration is a Landau singularity; however, the question is of which kind. Let us insert the above values into the homogeneous system, what we obtain is

$$m^2 \alpha_1 + \left(\frac{1}{2}P^2 + m^2\right) \alpha_2 = 0, \quad \left(\frac{1}{2}P^2 + m^2\right) \alpha_1 + m^2 \alpha_3 = 0. \quad (19)$$

First of all we observe that it is not either $\alpha_1 = 0$ or $q^2 = -m_1^2$, etc; it can be both. Secondly, our configuration, where $P^2 = (p_1 + p_2)^2$ is unconstrained, is a singularity. Finally these is a special case of the general configuration discussed (P^2 free) which is even more singular giving, in the infrared case, the true leading Landau singularity. To have $\alpha_{1,3} \neq 0$ we must require $P^2 = -4m^2$ which gives, in the annihilation channel, the well-known threshold singularity on top of the infrared one. This condition emerges also from the following argument: inserting $p_{1,2}^2 = -m^2$ in the anomalous threshold condition one obtains $m_2^2 P^2 = 0$, and $m_2^2(m_2^2 - P^2 - 4m^2) = 0$, corresponding to the two signs of Eq.(15). In a certain sense the constraint $P^2 = -4m^2$ is buried inside the anomalous threshold condition. To summarize: that all the propagators in a diagram are on-shell and that the consistency relation is satisfied does not necessarily imply that all α_i are different from zero: the infrared case is a clear example. Note the presence of a potential singularity also at $P^2 = 0$ which, however, is not physical, i.e. is not lying on the physical Riemann sheet. The latter fact can be seen by inspecting the explicit analytical result,

$$C_0^{\text{IR}} = \frac{2}{\beta P^2} \ln \frac{\beta + 1}{\beta - 1} \frac{1}{\epsilon} + \text{IR finite}, \quad \beta^2 = 1 + 4 \frac{m^2}{P^2}. \quad (20)$$

¹In our metric spacelike p implies positive p^2 . Further $p_4 = i p_0$ with p_0 real for a physical four-momentum.

Our strategy for the general classification of infrared divergent configurations will be on a diagram-by-diagram basis; we assume a certain number of zero internal masses with at least one unconstrained external momentum. Then we fix the remaining parameters to satisfy the consistency relation for the Landau equations. Finally, we return to the original set of Landau equations and look for additional constraints that are necessary in order to generate the true leading singularity. The presence of a threshold-like singularity on top of the infrared poles is the sign that, after extracting these poles, we still have complications for the residual integrations that cannot be solved with a naive use of the method to be described in the next subsection.

3.2 Sector decomposition

Once a diagram has been identified as infrared divergent we must proceed with the extraction of the infrared pole(s) and with the evaluation of the infrared residue(s) and of the finite part.

To continue our discussion we reconsider Eq.(14) and change variables, $x = 1 - x'$ and $y = (1 - x')y'$. Next we split the integration by using $1 = \theta(x - y) + \theta(y - x)$, remap the two integrals into $[0, 1]^2$ and obtain

$$C_0^{IR} = \frac{\mu^\epsilon}{i\pi^2} \int_0^1 dx \int_0^1 dy \left[(x^{-1-\epsilon} - x^{-\epsilon}) \chi_x^{-1-\epsilon/2} + (y^{-1-\epsilon} - x y^{-\epsilon}) \chi_y^{-1-\epsilon/2} \right],$$

$$\chi_x = m^2 \left[(1+y)^2 + x y (x y - 2 - 2 y) \right] + P^2 y (1-x),$$

$$\chi_y = m^2 \left[(1+x)^2 + x y (x y - 2 - 2 x) \right] + P^2 x (1-x y). \quad (21)$$

The infrared pole can now be extracted, giving $C_0^{IR} = P_{IR} + F_{fin}$,

$$P_{IR} = 2 \frac{\mu^\epsilon}{i\pi^2} \int_0^1 dx dy x^{-1-\epsilon} \left[m^2 (1+y)^2 + P^2 y \right]^{-1-\epsilon/2} = -\frac{2}{\epsilon} \frac{\mu^\epsilon}{i\pi^2} \int_0^1 dy \left[m^2 (1+y)^2 + P^2 y \right]^{-1-\epsilon/2}. \quad (22)$$

This procedure of extracting infrared poles, known as sector decomposition [10], cannot be applied in its naive version to three-point functions. The reason is that the residue of the infrared pole(s) is now given by an integral where the integrand is not positive defined over the parametric hyper-cube and, therefore, we cannot perform a straightforward numerical integration, at least if we want to avoid brute force and time consuming methods. Note that in our procedure we will use the van der Bij - Veltman parametrization [19] of two-loop integrals and not the more familiar Cvitanovic - Kinoshita one [20].

To summarize the complete algorithm of sector decomposition, we perform the following steps (for each family of diagrams): At first, infrared and eventually collinear divergent configurations are selected by using the corresponding set of Landau equations which have been derived, diagram-by-diagram in III. Examples for two-loop vertices are given in Figs. 5–12. For a similar classification in QED with a massive regulator we refer to [24]. sector decomposition is applied to a graph G leading to an expression

$$G = \sum_{l=0}^L \frac{g_l(\epsilon)}{\epsilon^l} = \sum_{l=0}^L \frac{G_l}{\epsilon^l}, \quad G_l = \frac{1}{B_l^\zeta} \int_S dx \mathcal{G}_l(x), \quad (23)$$

since each loop contributes at most one soft and collinear $1/\epsilon^2$ term (ϵ being the dimensional regulator) the highest value for L in a two-loop diagram is four; higher values in the Laurent expansion are only possible if ultraviolet divergencies are also present. In those cases the proper procedure is: ultraviolet poles are removed by local counter-terms, analytical continuation in ϵ is performed and infrared poles are extracted. Smoothness algorithms are derived for each component G_l , as indicated in Eq.(23), where x is a vector of Feynman parameters, S is some simplex, \mathcal{G}_l is an integrable function (in the limit $\delta \rightarrow 0$) and B_l^ζ is a function of masses and external momenta whose zeros correspond to true singularities of G , if any. Smoothness requires that the kernel in Eq.(23) and its first N derivatives be continuous functions and, ideally, N should be as large as possible. However, in most of the cases we will be satisfied with absolute convergence, e.g. logarithmic singularities of the kernel. This is particularly true around the zeros of B_l^ζ where the large number of terms required by obtaining continuous derivatives of higher order leads to large numerical cancellations.

3.3 Integrable singularities and sector decomposition

As it will become evident in the following sections, where we explicitly evaluate the diagrams, most of our integral representations will have the form

$$G = \int_S dx \frac{1}{A(x)} \ln \left[1 + \frac{A(x)}{B(x)} \right], \quad \text{or} \quad G(x) = \int_S dx \frac{1}{A(x)} \text{Li}_n \left(\frac{A(x)}{B(x)} \right), \quad (24)$$

where x is a vector of Feynman parameters, S is some simplex and A, B are multivariate quadratic forms. Eq.(24) generalizes the Nielsen-Goncharov family of polylogarithms [26] based on monomials in one variable, see Appendix B. Our integral representations are well-behaved around $A(x) \approx 0$ but numerical instabilities could arise when simultaneously $A(x) \approx B(x) \approx 0$ as it will always be the case for collinear singularities. A nice solution to this problem [21] is to adopt a sector decomposition to factorize their common zero. Eventually, for some special configuration of internal masses and external invariants, this procedure will describe the correct behavior around a genuine singularity of G , e.g. A and B having a common zero of the same order. An example is provided by the following integral,

$$J(a) = \int_0^1 dx dy \frac{1}{x} \ln \left[1 + \frac{x}{x+ay} \right] = \int_0^1 dx dy \left[\ln \left(1 + \frac{1}{1+ay} \right) + \frac{1}{x} \ln \left(1 + \frac{x}{x+a} \right) \right]. \quad (25)$$

After performing a sector decomposition in Eq.(25) we obtain that $a = 0$ is indeed an end-point singularity of J . All our numerical results are based on additional sector decompositions of integrands of the form shown in Eq.(24), although this is not explicitly indicated in the text.

3.4 Infrared power-counting

Before continuing the discussion on the evaluation of infrared divergent configurations it is convenient to introduce the concept of infrared power-counting. Given any parametric representation of a Feynman diagram we perform transformation of variables such that $0 \leq x_i \leq 1$ with

$$G = \int dC_N \chi_N^{-\mu}, \quad \chi_N = \sum_{l_1 \dots l_n} a_{l_1 \dots l_n} \prod_{i=1}^n x_i^{l_i} \theta \left(\sum_{i=1}^n l_i - L \right) \quad (26)$$

and $\chi_N = 0$, for $x_i = 0$, $\forall i$, with $L \geq 1$. After introducing polar coordinates the integral can be written as

$$G = \int d\Omega_{n-1} \int_0^{R(\Omega)} dr r^{n-\mu L-1} \chi_{N,\text{red}}^{-\mu}(r, \Omega), \quad (27)$$

with $\chi_{N,\text{red}}(0, \Omega) \neq 0$. Define A, B such that $n - \mu L - 1 = A - B \epsilon$. If $A \geq 0$ the integration does not lead to an ϵ -pole and the corresponding diagram is infrared safe. A typical example is represented by V^E of Fig. 3 where, although $\chi_E = 0$ at the hedge of the integration region, power-counting shows that no infrared pole arises.

3.5 Infrared singularities and hypergeometric functions

We have seen in the previous sections that a general method for extracting the infrared poles (within dimensional regularization) of Feynman diagrams is based on sector decomposition. However, in most of the two-loop cases sector decomposition has drawbacks: first of all the number of generated sectors tends to increase considerably and then the procedure creates new integrands with polynomials of very high degree, the higher the number of iterations the higher the degree. The consequence is that one cannot find an adequate smoothness algorithm to handle the final integration. We give a second, alternative, procedure once again illustrated in terms of a C_0 function.

The polynomial V_C of Eq.(14) can be rewritten ($P^2 = -s$, $p_i^2 = -m^2$) as

$$V_C(x, y) = m^2 x^2 + m^2 y^2 + (s - 2m^2)xy - 2m^2 x - (s - 2m^2)y + m^2, \quad (28)$$

and we perform the transformation $y = y' + \alpha x$ with $m^2 \alpha^2 + (s - 2m^2)\alpha + m^2 = 0$. This transformation is designed to make V linear in x and, whenever possible we always seek for a transformation that makes the Feynman integrand linear in one of the variables. After some straightforward manipulation we obtain $i\pi^2 C_0 = \mu^\epsilon (C_0^1 + C_0^2)$ weher

$$C_0^1 = (1 - \alpha) \int_0^1 dy \int_0^y dx V_1^{-1-\epsilon/2}(x, y), \quad C_0^2 = \alpha \int_0^1 dy \int_0^y dx V_2^{-1-\epsilon/2}(x, y), \quad (29)$$

with V -polynomials given by

$$\begin{aligned} V_1 &= \left[s(1 + \alpha)y - s + 2(1 - \alpha)m^2 \right] x - \alpha s y^2 - 2(1 - \alpha)m^2 y + m^2, \\ V_2 &= \left[\alpha s + 2(1 - \alpha)m^2 \right] x y - \left[\alpha s - (2\alpha - 1)m^2 \right] y^2. \end{aligned} \quad (30)$$

In Eq.(29) the x -integration has the general form

$$I_i(y) = \int_0^y dx \left[B_i(y) - A_i(y)x \right]^{-1-\epsilon/2} = y B_i^{-1-\epsilon/2} {}_2F_1(1 + \epsilon/2, 1; 2; \frac{A_i}{B_i} y). \quad i = 1, 2. \quad (31)$$

Using well-known properties of the hypergeometric function we obtain, for $|\arg(-z)| < \pi$,

$${}_2F_1(1 + \frac{\epsilon}{2}, 1; 2; z) = \frac{2}{\epsilon} \left[-{}_2F_1(1, 1 + \frac{\epsilon}{2}; 1 + \frac{\epsilon}{2}; 1 - z) + (1 - z)^{-\epsilon/2} {}_2F_1(1, 1 - \frac{\epsilon}{2}; 1 - \frac{\epsilon}{2}; 1 - z) \right] \quad (32)$$

from which we derive

$$I_i(y) = -\frac{2}{A_i \epsilon} B_i^{-\epsilon/2} \left[1 - \left(1 - \frac{A_i}{B_i} y \right)^{-\epsilon/2} \right]. \quad (33)$$

Given the form of A_1 in Eq.(30) we can simply expand around $\epsilon = 0$ obtaining

$$C_0^1 = (\alpha - 1) \int_0^1 dy \frac{1}{A_1(y)} \ln \left[1 - \frac{A_1(y)}{B_1(y)} y \right], \quad (34)$$

which is well-behaved for $A_1(y) = 0$. However, for $i = 2$, we find

$$A_2(y) = a(s, m^2) y, \quad B_2(y) = b(s, m^2) y^2, \quad (35)$$

$$a(s, m^2) = -\alpha s + 2(\alpha - 1)m^2 = \frac{1}{4} \beta(\beta + 1)^2 m^2, \quad b(s, m^2) = -\alpha s + (2\alpha - 1)m^2 = \frac{1}{16} (\beta + 1)^4 m^2. \quad (36)$$

Therefore, C_0^2 is infrared divergent and we get

$$\begin{aligned} C_0^2 &= \frac{\alpha}{a(s, m^2)} b^{-\epsilon/2}(s, m^2) \int_0^1 dy y^{-1-\epsilon} \ln \left[1 - \frac{a(s, m^2)}{b(s, m^2)} y \right] \left\{ 1 - \frac{\epsilon}{4} \ln \left[1 - \frac{a(s, m^2)}{b(s, m^2)} y \right] \right\} \\ &= 2 \frac{\alpha}{a(s, m^2)} \ln \frac{\beta - 1}{\beta + 1} \left[\frac{1}{\epsilon} - \frac{1}{2} \ln \frac{\beta - 1}{\beta + 1} - \frac{1}{2} \ln b(s, m^2) \right], \end{aligned} \quad (37)$$

with $\beta^2 = 1 - 4m^2/s$. The infrared pole has been isolated and infrared residue and finite part are already in a form that allows for direct numerical integration. For a general diagram they are rational functions of the residual Feynman parameters and we have been able to derive adequate smoothness algorithms for their integration.

3.6 Threshold behavior and Mellin-Barnes transforms

In computing infrared residues and finite parts of diagrams we face one additional complication: in general we end up with integrands which are not positive definite. Therefore, around those configurations of the external parameters where threshold singularities occur the algorithm has to be modified. The general

idea is to isolate the singular behavior and to write, for the regular part, an expansion in some Källén function of the external parameters. We borrow the relevant technique from another problem, the large energy expansion of Feynman diagrams which is best performed by using Mellin-Barnes transforms [22].

The whole idea is better illustrated with a simple example. Consider the infrared residue of C_0 :

$$P_{IR} = -\frac{2}{\epsilon} \frac{\mu^\epsilon}{i\pi^2} B_{1+\epsilon/2}(-m^2; m^2, P^2 + 4m^2),$$

$$B_\alpha(p^2; m_1^2, m_2^2) = \int_0^1 dx [\chi(x) - i\delta]^{-\alpha}, \quad \chi(x) = -p^2 x^2 + (p^2 + m_2^2 - m_1^2)x + m_1^2, \quad (38)$$

and $\delta \rightarrow 0_+$. Let x_\pm be the roots of $\chi - i\delta = 0$. If they are complex or real but external ($\notin [0, 1]$) then the numerical evaluation is straightforward; when they are real and internal ($\in [0, 1]$) the integration contour can be distorted and the integral can be computed unless a pinch will occur in $[0, 1]$ [23] (or an end-point singularity); this happens for $\lambda(-P^2, m^2, m^2) = 0$.

The integral in Eq.(38) is simple enough to be computed analytically but in our approach we will pretend to treat it numerically; distortion is performed, unless a pinch occurs. Then the question will arise of what to do around those parametric regions where $\lambda = 0$. Here we describe our solution for extracting the leading and sub-leading behavior of P_{IR} around $\lambda = 0$. First we rewrite χ as

$$\chi(x) = m^2(x - x_0)^2 - \frac{\lambda}{4m^2} - i\delta, \quad x_0 = \frac{s}{2m^2} - 1, \quad (39)$$

and consider the case $P^2 = -s$ with $s \geq 0$. Further, we assume that $0 \leq x_0 \leq 1$ and obtain

$$B_\alpha = \frac{m^{-2\alpha}}{2\pi i} \int_0^1 dx \int_{-i\infty}^{+i\infty} ds B(s, \alpha - s) \rho^{\alpha-s} Q^{-s}, \quad \rho^{-1} = -\frac{\lambda}{4m^4} - i\delta, \quad Q = (x - x_0)^2 - i\delta. \quad (40)$$

where B denotes the Euler beta-function. Eq.(40) is valid in the vertical strip $0 < \text{Re } s < \alpha$. We choose $\alpha < 1/2$, require $0 < \text{Re } s < 1/2$ and perform analytical continuation to obtain

$$\int_0^1 dx Q^{-s} = \sum_{X=x_0}^{1-x_0} \frac{X^{1-2s}}{1-2s}. \quad (41)$$

Since we are interested in the limit $|\rho| \rightarrow \infty$, the s -integral will be closed over the right-hand complex half-plane at infinity, with simple poles at $s = 1/2$ and $s = \alpha + k$ $k \geq 0$. In this way we obtain

$$B_\alpha = B\left(\frac{1}{2}, \alpha - \frac{1}{2}\right) m^{-2\alpha} \left(-\frac{\lambda}{4m^4} - i\delta\right)^{1/2-\alpha} + \text{sub-leading}, \quad s \rightarrow 4m^2. \quad (42)$$

The result can be easily generalized to the case of unequal masses. In this case we have also have a pseudo-threshold, $s = (m_1 - m_2)^2$, which is not a singularity on the first Riemann sheet since $x_0 \notin [0, 1]$.

3.7 Old and new Bernstein - Sato - Tkachov functional relations

For all one-loop multi-leg diagrams we have developed computational techniques based on the proposal introduced in I. Most of two-loop infrared convergent diagrams can be computed by following the same strategy. However, some extension has to be introduced to deal with the general case. To derive new algorithms, we recall the definition of Bernstein - Sato polynomials [17]: if $V(x)$ is a polynomial in several variables then there is a non-zero polynomial $b(\mu)$ and a differential operator $\mathcal{P}(\mu)$ with polynomial coefficients such that

$$\mathcal{P}(\mu) V^{\mu+1}(x) = b(\mu) V^\mu(x). \quad (43)$$

The Bernstein-Sato polynomial is the monic polynomial of smallest degree amongst such $b(\mu)$. If $V(x)$ is a non-negative polynomial then $V^\mu(x)$, initially defined for μ with non-negative real part, can be analytically continued to a meromorphic distribution-valued function of μ by repeatedly using the functional equation

$$V^\mu(x) = \frac{1}{b(\mu)} \mathcal{P}(\mu) V^{\mu+1}(x). \quad (44)$$

The Bernstein - Sato - Tkachov theorem [25] tells us that for any finite set of polynomials $V_i(x)$, where $x = (x_1, \dots, x_n)$ is a vector of Feynman parameters, there exists an identity of the following form (hereafter a BST identity):

$$\mathcal{P}(x, \partial) \prod_i V_i^{\mu_i+1}(x) = B_V \prod_i V_i^{\mu_i}(x). \quad (45)$$

where \mathcal{P} is a polynomial of x and $\partial_i = \partial/\partial x_i$; B_V and all coefficients of \mathcal{P} are polynomials of μ_i and of the coefficients of $V_i(x)$. Furthermore, if the polynomial V is of second degree we have a master formula, due to F. V. Tkachov [25]. We write the polynomial as $V(x) = x^t H x + 2 K^t x + L$, where $x^t = (x_1, \dots, x_n)$, H is an $n \times n$ matrix, K is an n vector. The solution to the problem of determining the polynomial \mathcal{P} is as follows:

$$\mathcal{P} = 1 - \frac{(x - X_V)^t \partial_x}{2(\mu + 1)}, \quad B_V = L - K^t H^{-1} K, \quad X_V = -H^{-1} K. \quad (46)$$

Therefore we have:

$$V^\mu(x) = \frac{1}{B_V} \left[1 - \frac{(x - X_V)^t \partial_x}{2(\mu + 1)} \right] V^{\mu+1}(x), \quad V^{-1}(x) = \frac{1}{B_V} \left[1 - \frac{1}{2} (x - X_V)^t \partial_x \ln V(x) \right]. \quad (47)$$

The list of BST relations must be extended to cover infrared singular cases. It often happens that $V(x)$ is not complete and so other BST relations, originally defined in Eq.(45), are needed. A typical example is when V is linear in one variable $V(x, y) = h(x - x_0)^2 + cy + b$. For this polynomial the H matrix is singular and it can be easily shown that the following relations hold:

$$V^\mu = \frac{1}{b} \left[1 - \frac{(x - x_0) \partial_x + 2y \partial_y}{2(\mu + 1)} \right] V^{\mu+1}, \quad V^\mu = \frac{1}{c} \frac{1}{\mu + 1} \partial_y V^{\mu+1}. \quad (48)$$

A better way to proceed without loss of generality is to introduce a \mathcal{P}_0 and a \mathcal{P}_1 with the property that

$$\mathcal{D}_\pm = \mathcal{P}_0 \pm \mathcal{P}_1^t \partial_x, \quad \mathcal{D}_+ V(x) = B_V. \quad (49)$$

BST relations can be written as

$$V^\mu(x) = \frac{1}{B_V} \left[\mathcal{P}_0 + \frac{1}{\mu + 1} \mathcal{P}_1^t \partial_x \right] V^{\mu+1}(x), \quad \text{for } \mu \neq -1; \quad V^{-1}(x) = \frac{1}{B_V} \left[\mathcal{P}_0 + \mathcal{P}_1^t \partial_x \ln V(x) \right]. \quad (50)$$

A first extension of Eq.(47) is given by the following example:

$$V^{-1}(x) \ln^n V(x) = \frac{1}{B_V} \left[\mathcal{P}_0 + \frac{1}{n+1} \mathcal{P}_1^t \partial_x \ln V(x) \right] \ln^n V(x). \quad (51)$$

Eq.(51) can be easily generalised to arbitrary powers of V :

$$V^\mu(x) \ln^n V(x) = \frac{1}{B_V} \left\{ \mathcal{P}_0 \ln^n V(x) + \sum_{k=0}^n \frac{n!}{(n-k)!} \frac{(-1)^k}{(\mu+1)^{k+1}} \mathcal{P}_1^t \partial_x \ln^{n-k} V(x) \right\} V^{\mu+1}(x). \quad (52)$$

As a next step we seek for similar relations, holding for Nielsen polylogarithms [26] and for the hypergeometric function [27]. These new relations can be obtained with the help of the following formulae:

$$\frac{d}{dx} \text{Li}_{n+1}(x) = \frac{1}{x} \text{Li}_n(x), \quad \frac{d}{dx} {}_2F_1(a-1, b; c; x) = \frac{a-1}{x} \left[{}_2F_1(a, b; c; x) - {}_2F_1(a-1, b; c; x) \right]. \quad (53)$$

Given a generic polynomial $A(x)$, it is easily verified that

$$\frac{1}{V} \text{Li}_n \left(\frac{A}{V} \right) = \frac{1}{B_V} \left[\frac{1}{A} \text{Li}_n \left(\frac{A}{V} \right) \mathcal{D}_+ A - \mathcal{P}_1^t \partial_x \text{Li}_{n+1} \left(\frac{A}{V} \right) \right], \quad (54)$$

$$\begin{aligned}
V^{-a} {}_2F_1(a, b; c; \frac{A}{V}) &= \frac{1}{B_V} \left\{ \frac{V^{1-a}}{A} \left[{}_2F_1(a, b; c; \frac{A}{V}) \mathcal{D}_+ A - {}_2F_1(a-1, b; c; \frac{A}{V}) \mathcal{P}_1^t \partial_x A \right] \right. \\
&\quad \left. + \frac{\mathcal{P}_1^t}{1-a} \partial_x \left[V^{1-a} {}_2F_1(a-1, b; c; \frac{A}{V}) \right] \right\}. \tag{55}
\end{aligned}$$

In particular for $n = 0, 1$, we have $\text{Li}_0(x) = x/(1-x)$ and $\text{Li}_1(x) = -\ln(1-x)$, for which the corresponding relations are

$$\frac{1}{V} \frac{A}{V-A} = \frac{1}{B_V} \left[\frac{1}{V-A} \mathcal{D}_+ A + \mathcal{P}_1^t \partial_x \ln \left(1 - \frac{A}{V} \right) \right], \tag{56}$$

$$\frac{1}{V} \ln \left(1 - \frac{A}{V} \right) = \frac{1}{B_V} \left[\frac{1}{A} \ln \left(1 - \frac{A}{V} \right) \mathcal{D}_+ A + \mathcal{P}_1^t \partial_x \text{Li}_2 \left(\frac{A}{V} \right) \right]. \tag{57}$$

When the BST factor, B_V , vanishes we have:

$$\frac{1}{V-A} \mathcal{D}_+ A = -\mathcal{P}_1^t \partial_x \ln \left(1 - \frac{A}{V} \right), \quad \text{for } B_V = 0. \tag{58}$$

Another set of (new) relations is obtained starting from known properties of polylogarithms,

$$\frac{d}{dx} \frac{\text{Li}_{n+1}(x)}{x} = \frac{1}{x^2} \left[\text{Li}_n(x) - \text{Li}_{n+1}(x) \right]. \tag{59}$$

For $x = A/V$, when $n = 1$, we easily obtain:

$$\frac{A}{V^2} \ln \left(1 - \frac{V}{A} \right) = \frac{1}{B_V} \left[A \mathcal{D}_- \frac{1}{V} \ln \left(1 - \frac{V}{A} \right) + \mathcal{P}_1^t \partial_x \ln \left(1 - \frac{A}{V} \right) \right]. \tag{60}$$

Using Eq.(60) for $n = 2$, we obtain:

$$\frac{A}{V^2} \text{Li}_2 \left(\frac{V}{A} \right) = \frac{1}{B_V} \left\{ A \mathcal{D}_- \frac{1}{V} \text{Li}_2 \left(\frac{V}{A} \right) + \mathcal{P}_1^t \partial_x \left[\frac{A}{V} \ln \left(1 - \frac{V}{A} \right) - \ln \left(1 - \frac{A}{V} \right) \right] \right\} \tag{61}$$

The same procedure can be iterated to get a similar relation for $A/V^2 \text{Li}_n(V/A)$.

One can derive other relations of this type but here we have restricted our attention to those which are actually used in this paper. Their application in computing Feynman integrals is based on the integration by parts of the terms containing $\mathcal{P}_1^t \partial_x$ (when it is not applied just on A).

After applying BST relations we end up with integrands which show a *less* divergent behaviour with respect to the original one; in most cases the integrand is smooth enough to allow for a stable numerical integration. When this is not the case we reiterate the use of BST functional relations; they are followed by a second integration by parts, etc, etc.

A typical example of smoothness algorithm corresponds to apply a BST functional relation to Eq.(22). In this case we obtain

$$i \pi^2 m^2 P_{IR} = -\frac{2}{\epsilon} \left(\frac{\mu}{m} \right)^\epsilon \int_0^1 dy v^{-1-\epsilon/2}(y), \quad v(y) = y^2 + (z+2)y + 1, \quad z = \frac{P^2}{m^2}; \tag{62}$$

$$\int_0^1 dy v^{-1-\epsilon/2}(y) = -\frac{4}{z(z+4)} \left[1 - \frac{1}{4}(z+4) \ln(z+4) + \frac{1}{2} \int_0^1 dy \ln v(y) + \mathcal{O}(\epsilon) \right], \tag{63}$$

showing the additional threshold singularity at $P^2 = -4m^2$. Note the absence of a singularity at $P^2 = 0$ on the first Riemann sheet.

4 Derivatives of two-loop self-energies and infrared poles.

In II we have defined the on-shell derivative of a two-point function, where possibly some of the internal masses are zero, as the $\partial/\partial p^2$ derivative evaluated at the mass shell of one of the non-zero internal masses. These derivatives are used to construct wave function renormalization factors and a complete list of results has been shown in II.

Here, we briefly review the subject; consider the on-shell derivative of S^C (for the simplest topology S^A the on-shell derivative is infrared finite). Once again, a necessary condition for the presence of infrared divergencies is that the Landau equations are fulfilled: for S^C , we see that $s = (m_1 + m_2 \pm m_4)^2$ and $m_3^2 = (m_1 + m_2)^2$ are satisfied by $m_2 = m_4 = 0$, $m_1 = m_3 = m$ and $s = m^2$. It is easily seen that S^C is not infrared divergent but its derivative with respect to p^2 shows an infrared pole when computed on-shell. To continue our discussion we consider the case $m_2 = m_4 = 0$ and $m_1 = m_3 = m$, a typical example of which is shown in Fig. 2. After a straightforward calculation we obtain

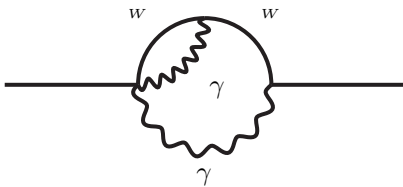


Figure 2: A two-loop diagram contribution to the W -boson self-energy.

$$S_p^C = \frac{1}{m^2} \left(\frac{\mu^2}{\pi m^2} \right)^\epsilon \left[-\frac{2}{\epsilon^2} - 2(2 - \gamma) \frac{1}{\epsilon} - 7 + \gamma(4 - \gamma) - \frac{1}{2} \zeta(2) + \mathcal{O}(\epsilon) \right]. \quad (64)$$

Results for $S_p^E \equiv S_p^{131}$ have been derived in Sect 7.4 of II; results for $S_p^D \equiv S_p^{221}$ have been derived in Sect 7.9 of II; γ is the Euler constant and ζ the Riemann zeta function.

5 Infrared divergent two-loop vertices

Starting with this section we present a detailed discussion, diagram - by - diagram, of two-loop infrared divergent vertices. Once again, evaluating a specific diagram means to derive a set of algebraic manipulations that return a multi-dimensional integral representation of the diagram for which numerical methods can be safely applied. For infrared configurations this means evaluating both the residues of the infrared poles and the finite parts. Special limits always require additional refinements of the procedure. The key ingredients in our derivation are: BST functional relations, the whole machinery of hypergeometric functions and Mellin-Barnes transforms.

Several diagrams belong to the general G^{1N1} family which is specified in terms of a set of momenta k_i which are linear combinations of the external momenta p_j ; $k_i = p_1 + \dots + p_i$. Our parametrization is as follows:

$$G^{1N1} = - \left(\frac{\mu^2}{\pi} \right)^\epsilon \Gamma(N - 2 + \epsilon) \int_0^1 dx \int dS_N(y, u_1, \dots, u_{N-1}) \left[x(1-x) \right]^{-\epsilon/2} (1-y)^{\epsilon/2-1} \chi_{1N1}^{2-N-\epsilon}, \quad (65)$$

$$\chi_{1N1} = u^t \mathcal{H}u + 2\mathcal{K}^t u + (m_x^2 - m_3^2)(1-y) + m_3^2,$$

where we have introduced the following quantities:

$$\mathcal{H}_{ij} = -p_i \cdot p_j, \quad \mathcal{K}_i = \frac{1}{2} (k_i^2 - k_{i-1}^2 + m_{i+3}^2 - m_{i+2}^2), \quad i, j = 1, \dots, N-1 \quad (66)$$

and where the x -dependent mass is defined in Eq.(8). Three out of six of the non-trivial two-loop vertex families can be described in terms of the representation of Eq.(65).

5.1 The V^E diagram

The V^E diagram of Fig. 3 is representable as

$$\pi^4 V^E = \mu^{2\epsilon} \int d^n q_1 d^n q_2 \frac{1}{[1]_E [2]_E [3]_E [4]_E}, \quad (67)$$

$$[1]_E = q_1^2 + m_1^2, \quad [2]_E = (q_1 - q_2)^2 + m_2^2, \quad [3]_E = (q_2 - p_2)^2 + m_3^2, \quad [4]_E = (q_2 - P)^2 + m_4^2. \quad (68)$$

Although V^E does not exhibit infrared poles it is simple enough to illustrate our procedure. A necessary

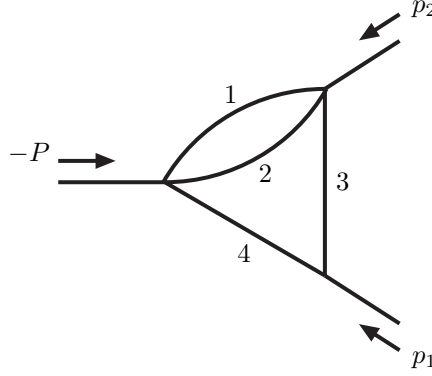


Figure 3: The irreducible two-loop vertex diagrams V^E . External momenta are flowing inwards.

condition for the presence of infrared singularities is that the corresponding Landau equations are fulfilled. For V^E this requires the condition $A P^4 + 2 B P^2 + C = 0$, with coefficients

$$A = m_3^2, \quad B = -\left[p_2^2 + (m_1 + m_2)^2 - m_3^2\right] (p_1^2 - m_3^2 + m_4^2) - 2 m_3^2 (p_1^2 + p_2^2),$$

$$C = \frac{1}{4 m_3^2} \left[B^2 - \lambda(-p_1^2, m_3^2, m_4^2) \lambda(-p_2^2, (m_1 + m_2)^2, m_3^2) \right]. \quad (69)$$

Let us concentrate on infrared divergencies due to photons. Then any tri-linear vertex has at most one photon line and any quadri-linear one has at most two photon lines. We are looking for solutions of the Landau equations where two external momenta are on some mass-shell and the third one is unconstrained. The procedure will be as follows:

Let $m_1 = 0$ and P^2 be a free parameter. We immediately find that Landau equations admit a solution with $\alpha_i \neq 0, \forall i$ if $m_3 = 0, p_1^2 = -m_4^2, p_2^2 = -m_2^2$.

Let $m_1 = 0$ and p_1^2 be free, we find $m_2 = 0, P^2 = -m_4^2, p_2^2 = -m_3^2$.

Let $m_1 = 0$ and p_2^2 be free, we find $m_4 = 0, P^2 = -m_2^2, p_1^2 = -m_3^2$.

Another possibility is to start with $m_3 = 0$. We proceed as follows:

Let $m_3 = 0$ and P^2 be free. We obtain $p_1^2 = -m_4^2, p_2^2 = -(m_1 + m_2)^2$, which is of no interest since we do not expect a theory with such a peculiar relation among masses.

Let $m_3 = 0$ and p_1^2 be free. We obtain $m_1 + m_2 = 0$, which is of no interest because it requires three photon lines in the same vertex.

Let $m_3 = 0$ and p_2^2 be free. We obtain $m_4 = 0, p_1^2 = 0, P^2 = -(m_1 + m_2)^2$, again of no interest.

Because of the symmetry of the diagram the $m_2 = 0$ and $m_4 = 0$ cases are already covered. Consider $m_1 = m_3 = 0$ and $p_1^2 = -m_4^2, p_2^2 = -m_2^2$. Using Eq.(65) we obtain

$$\chi_E(x, y, z) = -m_2^2 \frac{1-y}{1-x} - m_2^2 (1-y)^2 - m_4^2 z^2 - (P^2 + m_2^2 + m_4^2) (1-y) z + m_2^2 (1-y), \quad (70)$$

showing that $\chi_E = 0$ for the specified configuration at $y = 1$ and $z = 0$. However, χ_E appears with exponent $-\epsilon$ in the parametric representation for V^E so that no infrared pole will show up. To continue our analysis we consider the following cases:

$m_1 = m_3 = 0$ and P^2 free. We obtain $p_1^2 = -m_4^2$, $p_2^2 = -m_2^2$.

$m_1 = m_3 = 0$ and p_1^2 or p_2^2 free. We obtain that $m_2 = 0$ and the case is of no interest because it requires three photon lines in a vertex.

The last case is $m_1 = m_3 = m_4 = 0$ which requires either $p_1^2 = 0$ or $m_2 = 0$, i.e. more than two photon lines in a vertex.

5.2 The V^I diagram

The V^I family of diagrams, shown in Fig. 4, is representable as

$$\pi^4 V^I = \mu^{2\epsilon} \int d^n q_1 d^n q_2 \frac{1}{[1]_I [2]_I [3]_I [4]_I [5]_I}, \quad (71)$$

with propagators

$$\begin{aligned} [1]_I &= q_1^2 + m_1^2, & [2]_I &= (q_1 - q_2)^2 + m_2^2, & [3]_I &= q_2^2 + m_3^2, \\ [4]_I &= (q_2 + p_1)^2 + m_4^2, & [5]_I &= (q_2 + P)^2 + m_5^2. \end{aligned} \quad (72)$$

Referring to Section 3.1 we see that the leading Landau singularity for V^I is equivalent to the sub-leading

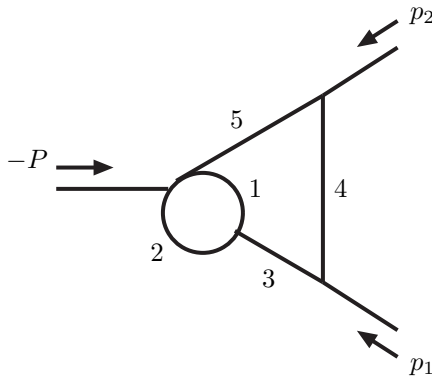


Figure 4: The irreducible two-loop vertex diagrams V^I . External momenta are flowing inwards.

one, with $\alpha_1 = \alpha_2 = 0$, when the peculiar condition $m_3 = m_1 + m_2$ is added. Therefore we discuss first those infrared configurations that correspond to sub-leading Landau singularities, and postpone the special case $m_3 = m_1 + m_2$.

If $\alpha_3 = 0$ the reduced diagram, i.e. the one where the third propagator is shrunk to a point, corresponds to a V^E topology which is free from infrared poles, as explicitly shown in Section 5.1.

If $\alpha_1 = \alpha_2 = 0$ the reduced diagram is a one loop three-point function and the classification of the infrared singularities is simpler. We obtain: 1) $m_3 = 0$, $P^2 = -m_5^2$, $p_1^2 = -m_4^2$, or 2) $m_4 = 0$, $p_1^2 = -m_3^2$, $p_2^2 = -m_5^2$, or 3) $m_5 = 0$, $P^2 = -m_3^2$, $p_2^2 = -m_4^2$. They correspond to the configurations shown in Fig. 5 (the first and the third are actually the same).

5.2.1 Extraction of UV and IR poles

For both configurations 1) \equiv 3) and 2) we perform the transformation $y = 1 - y'$; the diagram reads as follows:

$$V_i^I = - \left(\frac{\mu^2}{\pi} \right)^\epsilon \Gamma(1 + \epsilon) \int_0^1 dx \int dS_2(\{z\}) \int_0^{1-z_1} dy [x(1-x)]^{-\epsilon/2} y^{\epsilon/2-1} (a_{i;I} y + Z_{i;I})^{-1-\epsilon} \quad (73)$$

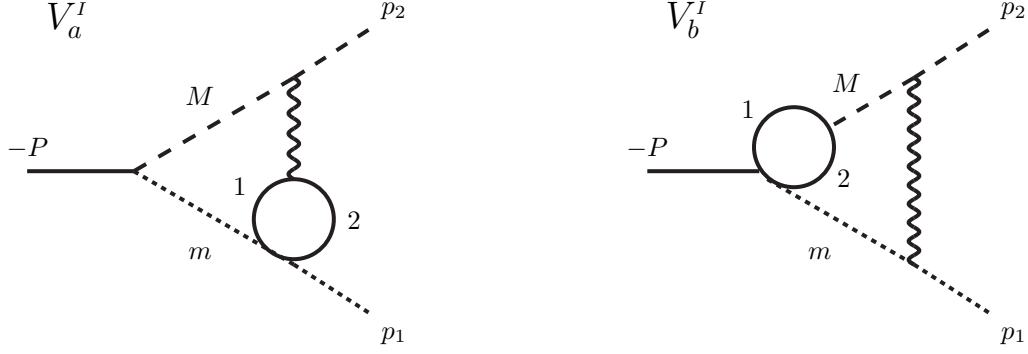


Figure 5: The V^I infrared configurations. The photon line represents a general massless particle while the dashed and the continuous lines represent different massive particles. The mass of the two particles in the bubble are m_1 and m_2 .

where $i = a, b$, and $a_{a;I} = m_x^2$, $a_{b;I} = m_x^2 - M^2$, with m_x^2 defined in Eq.(8), and

$$Z_{a;I} = \beta(z_2, z_1; P^2; m^2, M^2) \quad Z_{b;I} = \beta(1 - z_1, 1 - z_2; P^2; m^2, M^2) \quad (74)$$

and β defined in Eq.(12). V^I is also ultraviolet divergent and we look first for a procedure that extracts the ultraviolet pole. Consider the innermost integral appearing in Eq.(73)

$$\mathcal{Y}_{i;I} = Z_{i;I}^{-1-\epsilon} \int_0^{1-z_1} dy y^{\epsilon/2-1} \left(1 + \frac{a_{i;I}}{Z_{i;I}} y\right)^{-1-\epsilon}. \quad (75)$$

It is convenient to evaluate this integral in terms of an hypergeometric function [27]:

$$\mathcal{Y}_{i;I} = \frac{2}{\epsilon} Z_{i;I}^{-1-\epsilon} z_1^{\epsilon/2} {}_2F_1\left(1 + \epsilon, \frac{\epsilon}{2}; 1 + \frac{\epsilon}{2}; -\frac{1}{\zeta_{i;I}}\right), \quad \zeta_{i;I} = \frac{Z_{i;I}}{a_{i;I}(1 - z_1)}. \quad (76)$$

Using a well-known property of hypergeometric functions (see appendix C) we obtain

$$\mathcal{Y}_{i;I} = \frac{2}{\epsilon} \frac{\Gamma^2(1 + \epsilon/2)}{\Gamma(1 + \epsilon)} a_{i;I}^{-\epsilon/2} Z_{i;I}^{-1-\epsilon/2} - \frac{2}{2 + \epsilon} a_{i;I}^{-1-\epsilon} (1 - z_1)^{-1-\epsilon/2} {}_2F_1\left(1 + \epsilon, 1 + \frac{\epsilon}{2}; 2 + \frac{\epsilon}{2}; -\zeta_{i;I}\right), \quad (77)$$

with the result that the ultraviolet pole has been extracted. The second term in Eq.(77) is finite, so we can set $\epsilon = 0$, obtaining for V_i^I :

$$V_i^I = -\left(\frac{\mu^2}{\pi}\right)^\epsilon \frac{2}{\epsilon} \Gamma^2\left(1 + \frac{\epsilon}{2}\right) \mathcal{X}_{i;I} \mathcal{Z}_I + \int_0^1 dx \int dS_2(\{z\}) \frac{\ln(1 + \zeta_{i;I})}{Z_{i;I}} + \mathcal{O}(\epsilon), \quad (78)$$

$$\mathcal{X}_{i;I} = \int_0^1 dx [x(1-x)]^{-\epsilon/2} a_{i;I}^{-\epsilon/2}, \quad \mathcal{Z}_I = \int dS_2(\{z\}) Z_{i;I}^{-1-\epsilon/2}. \quad (79)$$

In the last expression we have dropped out the index i for \mathcal{Z}_I , since both cases produce the same result (it is easily seen by transforming $z_1 \rightarrow 1 - z_1$, $z_2 \rightarrow 1 - z_2$ and $z_1 \leftrightarrow z_2$, for the case b).

The second term in Eq.(78) is well-behaved when integrated over x , z_1 and z_2 and additional manipulations are not needed. As far as the first term is concerned we can write, after some straightforward manipulation,

$$\mathcal{X}_{i;I} = 1 - \frac{\epsilon}{2} \int_0^1 dx \ln V_{i;I} + \frac{\epsilon^2}{8} \int_0^1 dx \ln^2 V_{i;I} \quad (80)$$

where the two new quadratic forms are

$$V_{a;I} = m_1^2(1-x) + m_2^2 x, \quad V_{b;I} = \chi(x; -M^2; m_1^2, m_2^2). \quad (81)$$

For \mathcal{Z}_I we map the integration region into the square $[0, 1]^2$ obtaining:

$$\mathcal{Z}_I = \int dS_2(\{z\}) \beta^{-1-\epsilon/2}(z_2, z_1; P^2; m^2, M^2) = \int dC_2(\{z\}) z_1^{-1-\epsilon} \chi^{-1-\epsilon/2}(z_2) = -\frac{1}{\epsilon} \int_0^1 dz \chi^{-1-\epsilon/2}(z). \quad (82)$$

where β has been defined in Eq.(12). For the z_2 -integral we use one BST iteration, integrate by parts and expand in ϵ obtaining:

$$\mathcal{Z}_I = \mathcal{R}_1^I \epsilon^{-1} + \mathcal{R}_2^I + \mathcal{R}_3^I \epsilon, \quad (83)$$

where the coefficients in the ϵ expansion are

$$\mathcal{R}_i^I = \frac{(-1)^n}{2^n n! B_\chi} \left\{ \int_0^1 dz \ln^{n-1} \chi(z) \left[\ln \chi(z) + 2n \right] - L_\chi^n \right\} \quad L_\chi^n = \overline{X}_\chi \ln^n \chi(1) + X_\chi \ln^n \chi(0). \quad (84)$$

The BST factor B_χ and co-factor X_χ are collected in Eq.(10). Of course, the BST method fails when masses and external momenta are such that B_χ is very small. The general solution to this problem is based on the method of Mellin-Barnes transforms. For this particular diagram, however, the situation is very easy. Referring to Eq.(82) we have integrals of the form

$$\mathcal{Z}_I = -\frac{1}{\epsilon} H_I, \quad H_I = \int_0^1 dz \chi_I^{-1-\epsilon/2}(z), \quad \chi_I(z) \equiv \chi(z; p^2; m_a^2, m_b^2) \quad (85)$$

which we want to evaluate in the limit $B_\chi \rightarrow 0$ (χ is defined in Eq.(9)). The integral in Eq.(85) is a B_α function of Eq.(38) and can be evaluated for an arbitrary values of the exponent α . Setting $\alpha = 1 + \epsilon/2$ in Eq.(38) we obtain

$$\begin{aligned} B_{1+\epsilon/2}(p^2; m_a^2, m_b^2) &= \left[B\left(\frac{1}{2}, \frac{1+\epsilon}{2}\right) \rho^{(1+\epsilon)/2} - \sum_{X=a}^{1-a} \frac{X^{-1-\epsilon}}{1+\epsilon} + \mathcal{O}(\rho^{-1}) \right] s^{-1-\epsilon/2}. \\ &= \left\{ \pi \rho^{1/2} - \sum_{X=a}^{1-a} \frac{1}{X} - \frac{\epsilon}{2} \left[\pi \rho^{1/2} \ln \frac{4s}{\rho} - \sum_{X=a}^{1-a} \frac{\ln X^2 s + 2}{X} + \mathcal{O}(\rho^{-1}) \right] \right\} s^{-1}, \quad (86) \end{aligned}$$

where B is the Euler beta function and where we have introduced

$$p^2 = -s, \quad \rho = -\frac{4s^2}{\lambda - i\delta}, \quad a = \frac{s + m_a^2 - m_b^2}{2s}, \quad \lambda = \lambda(s, m_a^2, m_b^2), \quad (87)$$

where $\lambda(x, y, z)$ is the Källén function and where we assume $s > 0$. Collecting all pieces together, we get:

$$\overline{V_i^I} = - \left(\frac{\mu^2}{\pi} \right)^\epsilon \Gamma(1+\epsilon) \left(\frac{1}{\epsilon^2} V_{-2}^{i;I} + \frac{1}{\epsilon} V_{-1}^{i;I} + V_0^{i;I} \right) \quad (88)$$

$$\begin{aligned} V_{-2}^{i;I} &= 2 \mathcal{R}_1^I, & V_{-1}^{i;I} &= 2 \mathcal{R}_2^I - \mathcal{R}_1^I \int_0^1 dx \ln V_{i;I}, \\ V_0^{i;I} &= 2 \mathcal{R}_3^I - \frac{\zeta(2)}{2} \mathcal{R}_1^I - \int_0^1 dx \left[\mathcal{R}_2^I \ln V_{i;I} - \frac{\mathcal{R}_1^I}{4} \ln^2 V_{i;I} - \int dS_2(\{z\}) \frac{\ln(1+\zeta_{i;I})}{Z_{i;I}} \right]. \end{aligned} \quad (89)$$

5.3 The V^M diagram

The V^M family of diagrams, given in Fig. 6, is representable as

$$\pi^4 V^M = \mu^{2\epsilon} \int d^n q_1 d^n q_2 \frac{1}{[1]_M [2]_M [3]_M [4]_M [5]_M [6]_M}, \quad (90)$$

$$[1]_M = q_1^2 + m_1^2, \quad [2]_M = (q_1 - q_2)^2 + m_2^2, \quad [3]_M = q_2^2 + m_3^2,$$

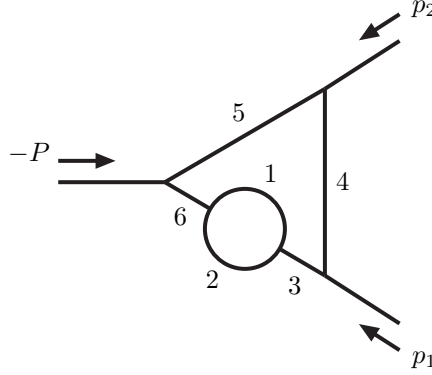


Figure 6: The irreducible two-loop vertex diagrams V^M . External momenta are flowing inwards.

$$[4]_M = (q_2 + p_1)^2 + m_4^2, \quad [5]_M = (q_2 + P)^2 + m_5^2, \quad [6]_M = q_2^2 + m_6^2. \quad (91)$$

If $m_3 \neq m_6$ then V^M is the difference of two V^I diagrams,

$$V^M = \frac{1}{m_6^2 - m_3^2} \left[V^I(P^2; m_1, m_2, m_3, m_4, m_5) - V^I(P^2; m_1, m_2, m_6, m_4, m_5) \right]. \quad (92)$$

In general Landau equations are the same for V^M and for V^I so that the classification of potentially infrared singular V^M vertices follows closely the discussion presented in the previous section (see Fig. 7), the main difference being in the exponent of the integrand. Configuration c) is a special case of configuration b) and will be treated in a second step.

5.3.1 Evaluation of V^M , cases a) and b)

For the first two configurations of Fig. 7 we have

$$V_i^M = - \left(\frac{\mu^2}{\pi} \right)^\epsilon \Gamma(2 + \epsilon) \int_0^1 dx \int dS_2(\{z\}) \int_0^{1-z_1} dy [x(1-x)]^{-\epsilon/2} y^{\epsilon/2-1} (1-z_1-y) (a_{i;M} y + Z_{i;M})^{-2-\epsilon} \quad (93)$$

where $i = a, b$, $a_{a;M} = m_x^2$, $a_{b;M} = m_x^2 - M^2$, with m_x^2 defined in Eq.(8) and with

$$Z_{a;M} = \beta(z_2, z_1; P^2; m^2, M^2) \quad Z_{b;M} = \beta(1-z_1, 1-z_2; P^2; m^2, M^2) \quad (94)$$

and β defined in Eq.(12). V^M is also ultraviolet divergent and we need, once more, a procedure for extracting the ultraviolet pole. Consider the innermost integral in Eq.(93)

$$\begin{aligned} V_i^M &= - \left(\frac{\mu^2}{\pi} \right)^\epsilon \Gamma(2 + \epsilon) \int_0^1 dx \int dS_2(\{z\}) [x(1-x)]^{-\epsilon/2} \mathcal{Y}_{i;M}, \\ \mathcal{Y}_{i;M} &= Z_{i;M}^{-2-\epsilon} \int_0^{1-z_1} dy y^{\epsilon/2-1} (1-z_1-y) \left(1 + \frac{a_{i;M}}{Z_{i;M}} y \right)^{-2-\epsilon}. \end{aligned} \quad (95)$$

The integral of Eq.(95) is expressible in terms of hypergeometric functions,

$$\int_0^b dy y^{s-1} (1 + \alpha y)^{-\nu} = \frac{1}{s} b^s {}_2F_1(\nu, s; s+1; -b\alpha), \quad \text{Re } s > 0, \quad |\arg(1 + \alpha b)| < \pi. \quad (96)$$

The result is further transformed according to well-known properties (see appendix C) and we obtain that:

$$\mathcal{Y}_{i;M} = \frac{1}{\Gamma(2 + \epsilon)} Z_{i;M}^{-1-\epsilon/2} a_{i;M}^{-\epsilon/2} \left[\Gamma\left(2 + \frac{\epsilon}{2}\right) \Gamma\left(\frac{\epsilon}{2}\right) (1-z_1) Z_{i;M}^{-1} - \Gamma^2\left(1 + \frac{\epsilon}{2}\right) a_{i;M}^{-1} \right] + \Phi_{i;M}, \quad (97)$$

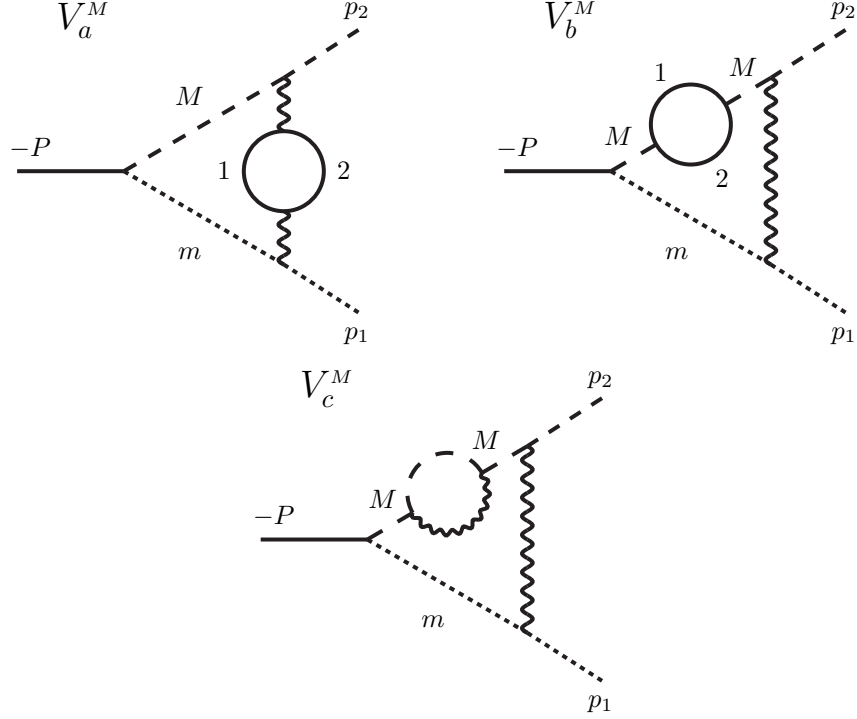


Figure 7: The V^M infrared configurations. The photon line represents a massless particle while the dashed and the solid lines represent different massive particles. Furthermore, the masses of the two particles in the bubble are m_1 and m_2 .

where the function $\Phi_{i;M}$ is defined by the following relation:

$$\begin{aligned} \Phi_{i;M} &= a_{i;M}^{-2-\epsilon} (1-z_1)^{-1-\epsilon/2} \left[-\frac{2}{4+\epsilon} {}_2F_1\left(2+\epsilon, 2+\frac{\epsilon}{2}; 3+\frac{\epsilon}{2}; -\zeta_{i;M}\right) \right. \\ &\quad \left. + \frac{2}{2+\epsilon} {}_2F_1\left(2+\epsilon, 1+\frac{\epsilon}{2}; 2+\frac{\epsilon}{2}; -\zeta_{i;M}\right) \right] = \frac{1}{a_{i;M} Z_{i;M}} \left[1 - \frac{\ln(1+\zeta_{i;M})}{\zeta_{i;M}} \right], \end{aligned} \quad (98)$$

where we used $\zeta_{i;M} = Z_{i;M}/a_{i;M}(1-z_1)$. In Eq.(98) we have put $\epsilon = 0$ and the last result follows after using the well-known relations for the hypergeometric function collected in appendix C.

After inserting these relations in Eq.(95) we obtain

$$V_i^M = - \left(\frac{\mu^2}{\pi} \right)^\epsilon \Gamma^2 \left(1 + \frac{\epsilon}{2} \right) \left[\left(\frac{2}{\epsilon} + 1 \right) \mathcal{X}_{i;M}^1 Z_{i;M}^1 - \mathcal{X}_{i;M}^2 Z_M^2 \right] - J_{i;M}. \quad (99)$$

where we have introduced

$$\begin{aligned} \mathcal{X}_{i;M}^n &= \int_0^1 dx [x(1-x)]^{-\epsilon/2} a_{i;M}^{1-n-\epsilon/2}, \quad \mathcal{Z}_{i;M}^1 = \int dS_2(\{z\}) (1-z_1) Z_{i;M}^{-2-\epsilon/2}, \\ \mathcal{Z}_M^2 &= \int dS_2(\{z\}) Z_M^{-1-\epsilon/2}, \quad J_{i;M} = \int dS_2(\{z\}) \int_0^1 dx \Phi_{i;M}, \end{aligned} \quad (100)$$

Note that $\mathcal{X}_{i;M}^1$ has been already computed while analyzing the V^I diagram, Eq.(80) and Eq.(81); therefore

$$\mathcal{X}_{i;M}^1 = \mathcal{X}_{i;I}, \quad V_{a,b;M} = V_{a,b;I}, \quad (101)$$

For $\mathcal{X}_{i;M}^2$ we distinguish between the two cases a) and b). The computation of $\mathcal{X}_{a;M}^2$ is straightforward, since $a_{a;M}$ is positive definite in $x \in [0, 1]$, and gives

$$\mathcal{X}_{i;M}^2 = \mathcal{X}_{i;M}^{2,0} + \mathcal{X}_{i;M}^{2,1} \epsilon, \quad i = a, b; \quad \mathcal{X}_{a;M}^{2,n} = \frac{(-1)^n}{2^n n!} \int_0^1 dx x (1-x) V_{a;M}^{-1} \ln^n V_{a;M} \quad (102)$$

For $\mathcal{X}_{b;M}^2$ instead we use the BST-method to increase the power of $V_{b;M}$ and obtain:

$$\mathcal{X}_{b;M}^{2,0} = -\frac{1}{2B_M} \int_0^1 dx \left(\alpha_M \ln V_{b;M} - \frac{1}{3} \right), \quad \mathcal{X}_{b;M}^{2,1} = -\frac{1}{2B_M} \int_0^1 dx \left\{ \ln V_{b;M} \left[x(1-x) - \frac{\alpha_M}{4} \ln V_{b;M} \right] \right\}, \quad (103)$$

where we use

$$a_M = 3x^2 - 2(1 + X_M)x + X_M, \quad X_M = \frac{M^2 + m_1^2 - m_2^2}{2M^2} \quad B_M = -\frac{\lambda(M^2, m_1^2, m_2^2)}{4M^2} \quad (104)$$

The case $B_M = 0$ requires $M = m_1 \pm m_2$ which in all realistic situations means $m_1(m_2) = 0$ and $m_2(m_1) = M$. This is equivalent to configuration c) which will be treated in the next subsection.

When examining $\mathcal{Z}_{i;M}^1$ we transform $z_2 \rightarrow z_1 z_2$ for $i = a$ and $z_1 \rightarrow 1 - z_1$, $z_2 \rightarrow 1 - z_2$, $z_1 \leftrightarrow z_2$, $z_2 \rightarrow z_1 z_2$ for $i = b$. In both cases the z_1 integration can be performed, giving

$$\begin{aligned} \mathcal{Z}_{a;M}^1 &= \int dC_2 (1 - z_1) z_1^{-3-\epsilon} \chi(z_2)^{-2-\epsilon/2} = \frac{1}{(1+\epsilon)(2+\epsilon)} \int_0^1 dz_2 \chi(z_2)^{-2-\epsilon/2}. \\ \mathcal{Z}_{b;M}^1 &= \int dC_2 z_1^{-2-\epsilon} z_2 \chi(z_2)^{-2-\epsilon/2} = -\frac{1}{1+\epsilon} \int_0^1 dz_2 z_2 \chi(z_2)^{-2-\epsilon/2}. \end{aligned} \quad (105)$$

For the z_2 -integration we use twice the BST-method followed by integration by parts and expand around $\epsilon = 0$ obtaining:

$$\mathcal{Z}_{i;M}^1 = \frac{1}{4B_\chi} (\mathcal{R}_0^{i;M} + \mathcal{R}_1^{i;M} \epsilon) \quad i = a, b \quad (106)$$

$$\begin{aligned} \mathcal{R}_0^{a;M} &= \frac{1}{2B_\chi} \left[S_\chi^{01} - \bar{X}_\chi \ln M^2 - X_\chi \ln m^2 + 2 \right] + \frac{\bar{X}_\chi}{M^2} + \frac{X_\chi}{m^2} \\ \mathcal{R}_1^{a;M} &= -\frac{1}{8B_\chi} (S_\chi^{02} + 8S_\chi^{01} + 8) + \frac{1}{8} \bar{X}_\chi \left(\frac{\ln M^2}{B_\chi} - \frac{4}{M^2} \right) (\ln M^2 + 4) + \frac{1}{8} \bar{X}_\chi \left(\frac{\ln m^2}{B_\chi} - \frac{4}{m^2} \right) (\ln m^2 + 4) \\ \mathcal{R}_0^{b;M} &= -\frac{X_\chi}{B_\chi} (S_\chi^{01} - \bar{X}_\chi \ln M^2 - X_\chi \ln m^2 + 2) - 2 \frac{\bar{X}_\chi}{M^2} \\ \mathcal{R}_1^{b;M} &= \frac{1}{4B_\chi} \left[X_\chi S_\chi^{02} - 8S_\chi^{11} + 14X_\chi S_\chi^{01} - X_\chi^2 \ln m^2 (\ln m^2 + 6) - \bar{X}_\chi \ln M^2 (X_\chi \ln M^2 + 6X_\chi - 4) \right. \\ &\quad \left. - 4 + 12X_\chi \right] + \frac{\bar{X}_\chi}{M^2} (\ln M^2 + 3), \quad S_\chi^{nm} = \int_0^1 dz z^n \ln^m \chi(z). \end{aligned} \quad (107)$$

For \mathcal{Z}_M^2 we can follow the derivation given for V^I :

$$\mathcal{Z}_M^2 = \mathcal{R}_1^M \epsilon^{-1} + \mathcal{R}_2^M, \quad \mathcal{R}_n^M = \mathcal{R}_n^I, \quad (108)$$

with \mathcal{R}_n^I given in Eq.(84). One expression remains to be computed:

$$J_{i;M} = \int dS_2(\{z\}) \int_0^1 dx \frac{1}{a_{i;M} Z_{i;M}} \left[1 - \frac{\ln(1 + \zeta_{i;M})}{\zeta_{i;M}} \right]. \quad (109)$$

Here there is an additional problem, namely the integrand is well-behaved in the limit $Z_{i;M} \rightarrow 0$ but not when $a_{i;M} \rightarrow 0$.

For case a), $a_{a;M}$ never vanishes in the integration interval and we can simply write:

$$J_{a;M} = \int dC_2(\{z\}) \int_0^1 dx \frac{1}{m_x^2 z_1 \chi(z_2)} \left[1 - \frac{\ln(1 + \eta_{a;M})}{\eta_{a;M}} \right], \quad \eta_{a;M} = \frac{z_1^2 \chi(z_2)}{m_x^2 (1 - z_1)}. \quad (110)$$

On the contrary, to compute $J_{b;M}$ is more convenient to reexamine Eq.(98). Setting $\epsilon = 0$ we have:

$$J_{b;M} = - \int dS_2(\{z\}) \int_0^1 dx a_{b;M}^{-2} (1 - z_1)^{-1} \left[\frac{1}{2} {}_2F_1(2, 2; 3; -\zeta_{b;M}) - {}_2F_1(2, 1; 2; -\zeta_{b;M}) \right] \quad (111)$$

As the next step we use the BST relation of Eq.(55) which, in the present case, reads:

$$V_{b;M}^{-2} {}_2F_1(2, b; c; \frac{A_{b;M}}{V_{b;M}}) = \frac{1}{B_M} \left\{ V_{b;M}^{-1} {}_2F_1(2, b; c; \frac{A_{b;M}}{V_{b;M}}) + \frac{x - X_M}{2} \partial_x \left[V_{b;M}^{-1} {}_2F_1(1, b; c; \frac{A_{b;M}}{V_{b;M}}) \right] \right. \\ \left. - \frac{x - X_M}{2} \frac{\partial_x A_{b;M}}{A_{b;M}} V_{b;M}^{-1} \left[{}_2F_1(2, b; c; \frac{A_{b;M}}{V_{b;M}}) - {}_2F_1(1, b; c; \frac{A_{b;M}}{V_{b;M}}) \right] \right\}. \quad (112)$$

where B_M and X_M are defined in Eq.(104) and $A_{b;M} = -x(1-x)Z_{b;M}/(1-z_1)$. After integration by parts we get:

$$J_{b;M} = \frac{1}{2B_M} \int dS_2(\{z\}) \int_0^1 dx \frac{1}{Z_{b;M}} \left\{ 3x(1-x) \left[1 - \frac{\ln(1 + \zeta_{i;M})}{\zeta_{i;M}} \right] + a_M \ln(1 + \zeta_{i;M}) \right\} \quad (113)$$

where $a_M = 3x^2 - 2(1 + X_M)x + X_M$ as defined in Eq.(104). To obtain the last formula we have used the explicit expression for the hypergeometric functions given in appendix C.

The case where masses and momenta are such that B_χ is vanishing small must be treated separately. In the following we will show how Mellin-Barnes techniques can be used in this kinematical situation (for the cases under discussion). For case a) the situation is particularly simple: from Eq.(105) we see that when B_χ is very small we have to evaluate $B_{2+\epsilon/2}(P^2; m^2, M^2)$, which is of the general form of Eq.(38). With $\alpha = 2 + \epsilon/2$ in Eq.(38) and discarding the terms with positive powers of $\lambda(-P^2, m^2, M^2)$ we have,

$$B_{2+\epsilon/2} = \left[B \left(\frac{1}{2}, \frac{3+\epsilon}{2} \right) \rho^{3/2+\epsilon/2} - \frac{1}{3+\epsilon} [a^{-3-\epsilon} + (1-a)^{-3-\epsilon}] + \mathcal{O}(\rho^{-1}) \right] s^{-2-\epsilon/2}, \quad (114)$$

where we have introduced $P^2 = -s$, $\rho = -(4s^2)/\lambda$ and $a = (s + m^2 - M^2)/(2s)$. It suffices to expand the result of Eq.(114) in powers of ϵ and to retain the first two terms in the expansion:

$$B_{2+\epsilon/2} = [I^{(0)} + I^{(1)} \epsilon + \mathcal{O}(\epsilon^2) + \mathcal{O}(\rho^{-1})] s^{-2}, \quad (115)$$

$$I^{(0)} = \frac{\pi}{2} \rho^{3/2} - \frac{1}{3} \sum_{X=a}^{1-a} \frac{1}{X^3}, \quad I^{(1)} = \frac{\pi}{4} \rho^{3/2} \left(1 + \ln \frac{\rho}{4s} \right) + \frac{1}{18} \sum_{X=a}^{1-a} \frac{3 \ln X^2 s + 2}{X^3}. \quad (116)$$

The case b) is quite similar; consider the integral

$$Y_\alpha = \int_0^1 dx x [\chi(x) - i\delta]^{-\alpha} = \int_0^1 dx (x-a) [\chi(x) - i\delta]^{-\alpha} + a B_\alpha, \quad (117)$$

Since $\chi(x) = s[(x-a)^2 + \rho^{-1}]$, the integral in Eq.(117) gives:

$$Y_\alpha = \frac{M^{2(1-\alpha)} + m^{2(1-\alpha)}}{2s(1-\alpha)} + a B_\alpha. \quad (118)$$

Setting $\alpha = 2 + \epsilon/2$ and expanding in ϵ we get:

$$Y_{2+\epsilon/2} = -\frac{1}{2s} \left\{ \frac{1}{M^2} - \frac{1}{m^2} - \frac{\epsilon}{2} \left[\frac{\ln M^2 + 1}{M^2} - \frac{\ln m^2 + 1}{m^2} \right] \right\} + a B_{2+\epsilon/2}, \quad (119)$$

which conclude our discussion. Collecting all pieces together, we get:

$$\boxed{V_i^M} = - \left(\frac{\mu^2}{\pi} \right)^\epsilon \Gamma(1 + \epsilon) \left(\frac{1}{\epsilon} V_{-1}^{i;M} + V_0^{i;M} \right), \quad i = a, b \quad (120)$$

$$V_{-1}^{i;M} = \frac{\mathcal{R}_0^{i;M}}{2B_\chi} - \mathcal{X}_{i;M}^{2,0} \mathcal{R}_1^M, \quad V_0^{i;M} = \frac{\mathcal{R}_1^{i;M}}{2B_\chi} - \frac{\mathcal{R}_0^{i;M}}{4B_\chi} \left(\int_0^1 dx \ln V_{a;M} - 1 \right) - \mathcal{X}_{i;M}^{2,0} \mathcal{R}_2^M - \mathcal{X}_{i;M}^{2,1} \mathcal{R}_1^M + J_{i;M}. \quad (121)$$

5.3.2 Evaluation of V_c^M

Configuration c) of Fig. 7 is a special case of b). For this case the polynomial V_M (see Eq.(101)) takes the form

$$V_{c;M}(x) = x^2 M^2 \quad \text{giving} \quad a_{c;M}(x) = \frac{x}{1-x} M^2. \quad (122)$$

$V_{c;M}(x)$ has a double zero for $x = 0$ and the corresponding BST factor is therefore zero. As a consequence the diagram acquires an extra infrared pole, confirming the presence of a leading Landau singularity. To evaluate this special case, we reconsider Eq.(93), which in the present configuration reads:

$$V_c^M = - \left(\frac{\mu^2}{\pi} \right)^\epsilon \Gamma(2 + \epsilon) \int_0^1 dx \int dS_2(\{z\}) \int_0^{1-z_1} dy [x(1-x)]^{-\epsilon/2} y^{\epsilon/2-1} (1-z_1-y) \left(\frac{xy M^2}{1-x} + Z_{c;M} \right)^{-2-\epsilon}, \quad (123)$$

$$Z_{c;M} = \beta (1-z_1, 1-z_2; P^2; m^2, M^2), \quad (124)$$

with β defined in Eq.(12). We perform the following set of transformations: $y = (1-z_1)y'$, and $z_1 = 1-z'_1$, $z_2 = 1-z'_2$, followed by $z'_1 = z''_1 z'_2$, obtaining:

$$V_c^M = - \left(\frac{\mu^2}{\pi} \right)^\epsilon \Gamma(2 + \epsilon) \int dC_4(x, y, \{z\}) \left(\frac{z_1}{z_2} \frac{y}{x(1-x)} \right)^{\epsilon/2} \frac{1-y}{y} z_1 \left[\frac{xy z_1 M^2}{1-x} + z_2 \chi(z_1) \right]^{-2-\epsilon}, \quad (125)$$

where $\chi(z_1) \equiv \chi(z_1; P^2; m^2, M^2)$ of Eq.(9). Integrating over z_2 gives an hypergeometric function and we use its properties (see appendix C) to get:

$$\begin{aligned} V_c^M &= - \left(\frac{\mu^2}{\pi} \right)^\epsilon \frac{2}{2-\epsilon} \Gamma(2 + \epsilon) \int dC_3(x, y, z) x^{-2-3\epsilon/2} (1-x)^{2+\epsilon/2} z^{-1-\epsilon/2} \\ &\quad \times y^{-3-\epsilon/2} (1-y) (M^2)^{-2-\epsilon} {}_2F_1\left(2 + \epsilon, 1 - \frac{\epsilon}{2}; 2 - \frac{\epsilon}{2}; - \frac{(1-x)\chi(z)}{xyzM^2}\right) \\ &= - \left(\frac{\mu^2}{\pi} \right)^\epsilon \int dC_3(x, y, z) \left[\Gamma\left(1 - \frac{\epsilon}{2}\right) \Gamma\left(1 + \frac{3}{2}\epsilon\right) x^{-1-2\epsilon} (1-x)^{1+\epsilon} z^{-\epsilon} \right. \\ &\quad \times y^{-2-\epsilon} (1-y) (M^2)^{-1-3\epsilon/2} \chi^{-1+\epsilon/2}(z) - \frac{2}{2+3\epsilon} \Gamma(2 + \epsilon) [x(1-x)]^{-\epsilon/2} z^{1+\epsilon/2} \\ &\quad \left. \times y^{-1+\epsilon/2} (1-y) \chi^{-2-\epsilon}(z) {}_2F_1\left(2 + \epsilon, 1 + \frac{3}{2}\epsilon; 2 + \frac{3}{2}\epsilon; - \frac{xyzM^2}{(1-x)\chi(z)}\right) \right]. \quad (126) \end{aligned}$$

In the first term of Eq.(126) the integrations over x and y are trivial and generate the double pole in ϵ . The second term of Eq.(126) shows a single pole, hidden in the y integration, which can be extracted as in Eq.(3). We obtain:

$$V_c^M = - \left(\frac{\mu^2}{\pi} \right)^\epsilon \left(V_{c,0}^M + V_{c,1}^M + V_{c,2}^M \right) \quad (127)$$

$$\begin{aligned} V_{c,0}^M &= \Gamma\left(1 - \frac{\epsilon}{2}\right) \Gamma\left(1 + \frac{3}{2}\epsilon\right) B(-2\epsilon, 2 + \epsilon) B(-1 - \epsilon, 2) (M^2)^{-1-3\epsilon/2} \int_0^1 dz z^{-\epsilon} \chi^{-1+\epsilon/2}(z), \\ V_{c,1}^M &= - \frac{2}{\epsilon} \frac{2}{2+3\epsilon} \Gamma(2 + \epsilon) B\left(1 - \frac{\epsilon}{2}, 1 - \frac{\epsilon}{2}\right) \int_0^1 dz z^{1+\epsilon/2} \chi^{-2-\epsilon}(z), \\ V_{c,2}^M &= \int dC_3(x, y, z) \frac{z}{\chi^2(z)} \frac{(1-x)\chi(z) + xzM^2}{(1-x)\chi(z) + xyzM^2}. \quad (128) \end{aligned}$$

For $V_{c,0}^M$ we perform a Laurent expansion in ϵ which gives:

$$V_{c,0}^M = -\frac{1}{2M^2} \Gamma(1+\epsilon) \left(\mathcal{R}_{-2}^{c;M} \epsilon^{-2} + \mathcal{R}_{-1}^{c;M} \epsilon^{-1} + \mathcal{R}_0^{c;M} \right), \quad (129)$$

$$\begin{aligned} \mathcal{R}_{-2}^{c;M} &= J_0^0, & \mathcal{R}_{-1}^{c;M} &= \left(1 - \frac{3}{2} \ln M^2\right) J_0^0 + \frac{1}{2} J_0^1 - J_1^0, \\ \mathcal{R}_0^{c;M} &= \left(\frac{9}{8} \ln^2 M^2 - \frac{3}{2} \ln M^2 + \frac{11}{4} \zeta(2) + 1\right) J_0^0 + \left(1 - \frac{3}{2} \ln M^2\right) \left(\frac{1}{2} J_0^1 - J_1^0\right) + \frac{1}{8} J_0^2 - \frac{1}{2} J_1^1 + \frac{1}{2} J_2^0, \end{aligned}$$

where J_n^k is defined by:

$$J_n^k = \int_0^1 dz \ln^n z \frac{\ln^k \chi(z)}{\chi(z)} \quad (130)$$

This class of integrals can be treated by using Eq.(51) which, in the present case, reads as follows:

$$\chi^{-1}(z) \ln^k \chi(z) = \frac{1}{B_\chi} \left[\ln^k \chi(z) - \frac{z - X_\chi}{2(k+1)} \partial_z \ln^{k+1} \chi(z) \right]. \quad (131)$$

After integration by parts, we get:

$$\begin{aligned} J_n^0 &= \frac{1}{2B_\chi} \left[\int_0^1 dz \ln^{n-1} z \left(n \frac{z - X_\chi}{z} + \ln z \right) \ln \frac{\chi(z)}{\chi(0)} + 2(-1)^n \Gamma(n+1) \right], & n \geq 1, \\ J_n^1 &= \frac{1}{4B_\chi} \int_0^1 dz \left\{ 4 \ln^n z \ln \chi(z) + \ln^{n-1} z \left(n \frac{z - X_\chi}{z} + \ln z \right) \ln \frac{\chi(z)}{\chi(0)} [\ln \chi(z) + \ln \chi(0)] \right\}, & n \geq 1, \\ J_0^{k-1} &= \frac{1}{2B_\chi} \frac{1}{k} \left\{ \int_0^1 dz \ln^{k-1} \chi(z) [\ln \chi(z) + 2k] - L_\chi^k \right\}, \end{aligned} \quad (132)$$

with L_χ^k given in Eq.(84). The same strategy is adopted for the second integral, thus obtaining:

$$V_{c,1}^M = \Gamma(1+\epsilon) \left(-2 I_0^0 \epsilon^{-1} - I_0^0 - I_1^0 + 2 I_0^1 \right) \quad (133)$$

where I_n^k is now defined by:

$$I_n^k = \int_0^1 dz z \ln^n z \frac{\ln^k \chi(z)}{\chi^2(z)} \quad (134)$$

This class of integrals can be treated by using Eq.(52) which, in the present case, becomes:

$$\chi^{-2}(z) \ln^k \chi(z) = \frac{1}{B_\chi} \left[\chi^{-1}(z) \ln^k \chi(z) + \frac{z - X_\chi}{2} \sum_{l=0}^k \frac{k!}{l!} \partial_z \chi^{-1}(z) \ln^l \chi(z) \right]. \quad (135)$$

After integration by parts, we repeat the whole procedure for I_n^k ; the BST relation to be used in this second step is:

$$\chi^{-1}(z) \ln^k \chi(z) = \frac{1}{B_\chi} \left[\ln^k \chi(z) - \frac{z - X_\chi}{2(k+1)} \partial_z \ln^{k+1} \chi(z) \right]. \quad (136)$$

The second integration by parts gives:

$$\begin{aligned} I_0^k &= \frac{1}{4B_\chi^2} \left\{ \int_0^1 dz \left[\frac{X_\chi}{k+1} \ln^{k+1} \chi(z) - (4z - 5X_\chi) \ln^k \chi(z) - (8z - 5X_\chi) k! \mathcal{L}_{k-1}(z) \right] \right. \\ &\quad \left. - \overline{X}_\chi \left[\frac{X_\chi}{k+1} \ln^{k+1} \chi(1) - (2 - X_\chi) k! \mathcal{L}_k(1) \right] - k! \overline{X}_\chi \left[\overline{X}_\chi \mathcal{L}_{k+1}(0) + 2 \right] \right\} + \frac{k! \overline{X}_\chi}{2 B_\chi} \frac{1 + \mathcal{L}_k(1)}{\chi(1)} \\ I_1^0 &= \frac{1}{4B_\chi^2} \int_0^1 dz \left\{ \left(X_\chi \ln z - 2z + 3X_\chi \right) \ln \chi(z) - \frac{X_\chi^2}{z} \ln \frac{\chi(z)}{\chi(0)} + \overline{X}_\chi^2 \ln \chi(1) - X_\chi^2 \ln \chi(0) - 1 \right\}, \end{aligned} \quad (137)$$

where $\mathcal{L}_k(z) = \sum_{l=1}^k \ln^l \chi(z)/l!$. Finally we evaluate $V_{c,2}^M$. First the integration over y is performed:

$$V_{c,2}^M = \int_0^1 dx \int_0^1 dz \left[\frac{1-x}{x M^2 \chi(z)} + \frac{z}{\chi^2(z)} \right] \ln \left(1 + \frac{x z M^2}{(1-x) \chi(z)} \right). \quad (138)$$

In the second term of Eq.(138) we transform the argument of the logarithm to get

$$V_{c,2}^M = \int_0^1 dx \int_0^1 dz \left[\frac{1-x}{x M^2 \chi(z)} \ln \left(1 + \frac{x z M^2}{(1-x) \chi(z)} \right) + \frac{z}{\chi^2(z)} \ln \left(1 + \frac{(1-x) \chi(z)}{x z M^2} \right) \right] + \ln M^2 I_0^0 + I_1^0 - I_0^1, \quad (139)$$

where I_n^k is given by Eq.(137). The first two terms in Eq.(139) are treated according to Eq.(57) and Eq.(60) which in, the present case, become

$$\begin{aligned} \frac{1}{\chi(z)} \ln \left(1 - \frac{a z}{\chi(z)} \right) &= \frac{1}{B_\chi} \left[\frac{1}{2} \left(1 + \frac{X_\chi}{z} \right) \ln \left(1 - \frac{a z}{\chi(z)} \right) - \frac{z - X_\chi}{2} \partial_z \text{Li}_2 \left(\frac{a z}{\chi(z)} \right) \right], \\ \frac{z}{\chi^2(z)} \ln \left(1 - \frac{\chi(z)}{a z} \right) &= \frac{1}{B_\chi} \left[z \left(1 + \frac{z - X_\chi}{2} \partial_z \right) \frac{1}{\chi(z)} \ln \left(1 - \frac{\chi(z)}{a z} \right) - \frac{z - X_\chi}{2 a} \partial_z \ln \left(1 - \frac{a z}{\chi(z)} \right) \right]. \end{aligned} \quad (140)$$

where $a = -x M^2/(1-x)$. After integration by parts, we finally obtain:

$$\begin{aligned} V_{c,2}^M &= \frac{1}{2 B_\chi} \int_0^1 dx \int_0^1 dz \left\{ \frac{1-x}{x M^2} \left[\frac{X_\chi}{z} \ln \left(1 + \frac{x z M^2}{(1-x) \chi(z)} \right) + \text{Li}_2 \left(-\frac{x z M^2}{(1-x) \chi(z)} \right) \right] \right. \\ &\quad \left. + \frac{X_\chi}{\chi(z)} \ln \left(1 + \frac{(1-x) \chi(z)}{x z M^2} \right) \right\} + \frac{\bar{X}_\chi}{M^2 B_\chi} \zeta(3) + \ln M^2 I_0^0 + I_1^0 - I_0^1 \end{aligned} \quad (141)$$

Collecting all pieces together, we get:

$$\boxed{V_c^M} = - \left(\frac{\mu^2}{\pi} \right)^\epsilon \Gamma(1+\epsilon) \left(\frac{1}{\epsilon^2} V_{-2}^{c;M} + \frac{1}{\epsilon} V_{-1}^{c;M} + V_0^{c;M} \right) \quad (142)$$

$$V_{-2}^{c;M} = -\frac{\mathcal{R}_{-2}^{c;M}}{2 M^2}, \quad V_{-1}^{c;M} = -\frac{\mathcal{R}_{-1}^{c;M}}{2 M^2} - 2 I_0^0, \quad V_0^{c;M} = -\frac{\mathcal{R}_0^{c;M}}{2 M^2} - I_0^0 - I_1^0 + 2 I_0^1 + V_{c,2}^M. \quad (143)$$

5.4 The V^G diagram

This family of diagrams, corresponding to Fig. 8, can be written as

$$\pi^4 V^G = \mu^{2\epsilon} \int d^n q_1 d^n q_2 \frac{1}{[1]_G [2]_G [3]_G [4]_G [5]_G}, \quad (144)$$

where we have introduced the following notation:

$$\begin{aligned} [1]_G &= q_1^2 + m_1^2, & [2]_G &= (q_1 + p_1)^2 + m_2^2, & [3]_G &= (q_1 - q_2)^2 + m_3^2, \\ [4]_G &= (q_2 + p_1)^2 + m_4^2, & [5]_G &= (q_2 + P)^2 + m_5^2. \end{aligned} \quad (145)$$

The leading Landau singularity corresponds to the following four solutions:

$$P^2 = -\frac{1}{4 m_2^2 m_4^2} \left[(m_2^2 - m_3^2 + m_4^2) (p_1^2 + m_1^2 - m_2^2) (-p_2^2 + m_4^2 - m_5^2) - 4 m_2^2 m_4^2 (p_1^2 + p_2^2) \right] \quad (146)$$

$$\begin{aligned} & -\eta (p_2^2 - m_4^2 + m_5^2) (\lambda_{12})^{1/2} + \sigma (p_1^2 + m_1^2 - m_2^2) (\lambda_{13})^{1/2} + \sigma \eta (m_2^2 - m_3^2 + m_4^2) (\lambda_{23})^{1/2} \Big], \\ \lambda_{ij} &= \lambda_i \lambda_j, \quad \lambda_1 = \lambda(m_2^2, m_3^2, m_4^2), \quad \lambda_2 = \lambda(-p_1^2, m_1^2, m_2^2), \quad \lambda_3 = \lambda(-p_2^2, m_4^2, m_5^2). \end{aligned} \quad (147)$$

where $\eta \sigma = \pm 1$. From a study of these conditions it follows that V^E is free from QED - like infrared divergent configurations.

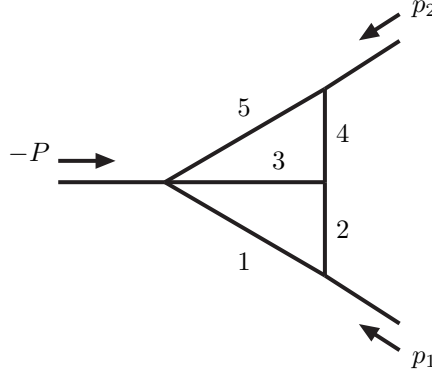


Figure 8: The irreducible two-loop vertex diagrams V^G . External momenta are flowing inwards.

5.5 The V^K diagram

This family of diagrams, depicted in Fig. 9, can be written as

$$\pi^4 V^K = \mu^{2\epsilon} \int d^n q_1 d^n q_2 \frac{1}{[1]_\kappa [2]_\kappa [3]_\kappa [4]_\kappa [5]_\kappa [6]_\kappa}, \quad (148)$$

where we have introduced the following notation for propagators:

$$\begin{aligned} [1]_\kappa &= q_1^2 + m_1^2, & [2]_\kappa &= (q_1 + P)^2 + m_2^2, & [3]_\kappa &= (q_1 - q_2)^2 + m_3^2, \\ [4]_\kappa &= q_2^2 + m_4^2, & [5]_\kappa &= (q_2 + p_1)^2 + m_5^2, & [6]_\kappa &= (q_2 + P)^2 + m_6^2, \end{aligned} \quad (149)$$

The leading Landau singularity for V^K is given in Eq. (321) of III. Our strategy will be to search for

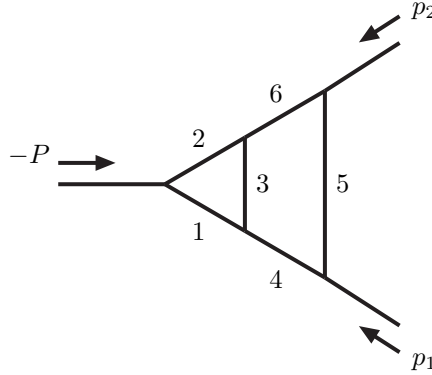


Figure 9: The irreducible two-loop vertex diagrams V^K . External momenta are flowing inwards.

solutions of the Landau equations where two external momenta are on some mass-shell and the third one is unconstrained. Suppose that P^2 is unconstrained, then we must have $m_3 = 0$ and, moreover, the first condition of Eq. (321) of III requires $m_4 = m_1$ and $m_6 = m_2$. The second condition will be written as

$$\begin{aligned} 4 m_3^2 m_4^2 p_2^2 &= (m_1^2 - m_3^2 - m_4^2) (m_2^2 - m_3^2 - m_6^2) (p_1^2 + m_4^2 + m_5^2) - 4 m_3^2 m_4^2 (m_5^2 + m_6^2) \\ &+ \eta_1 (m_1^2 - m_3^2 - m_4^2) \lambda_{23}^{1/2} - \eta_2 (m_2^2 - m_3^2 - m_6^2) \lambda_{13}^{1/2} + \eta_3 (p_1^2 + m_4^2 + m_5^2) \lambda_{12}^{1/2}, \end{aligned} \quad (150)$$

where $\eta_i = \pm 1, i = 1, \dots, 3$. With $m_4 = m_1$ and $m_6 = m_2$ we obtain $\lambda_1 = m_3^2 (m_3^2 - 4m_1^2)$ and $\lambda_2 = m_3^2 (m_3^2 - 4m_2^2)$, so that m_3^2 can be factorized on both sides of Eq.(150). Next, by putting $m_3 = 0$ we obtain

$$m_1^2 (p_2^2 + m_2^2 + m_5^2) + s_4 m_1 m_2 (p_1^2 + m_1^2 + m_5^2) = 0, \quad (151)$$

from which we recognize the familiar infrared configuration with $p_1^2 = -m_1^2$, $p_2^2 = -m_2^2$, and $m_4 = m_1$, $m_6 = m_2, m_3 = m_5 = 0$. which corresponds to configuration b) in Fig. 10. If p_2^2 is unconstrained (the case with p_1^2 leads to the same configuration because of the symmetry of the diagram), we must have $m_4 = 0$. Searching for configurations with two photons, there is only one possibility compatible with the standard model, $m_2 = 0$. Inserting these conditions in the second relation of Eq. (321) of III we obtain $m_1 = m_3 = m_6$ and $p_1^2 = -m_5^2$. Then the first relation of Eq. (321) requires $P^2 = -m_6^2$, leading to configuration d) of Fig. 10. In the following we classify the sub-leading singularities. For the sub-leading singularity corresponding to $\alpha_1 = \alpha_2 = \alpha_3 = 0$ the reduced diagram is a one-loop three-point function where the classification of infrared singular configurations is already known: we obtain three solutions which correspond to the two configurations shown in Fig. 10: The first is $m_4 = 0$, $P^2 = -m_6^2$, $p_1^2 = -m_5^2$, the second is $m_5 = 0$, $p_1^2 = -m_4^2$, $p_2^2 = -m_6^2$, with a third one given by $m_6 = 0$, $P^2 = -m_4^2$, $p_2^2 = -m_5^2$.

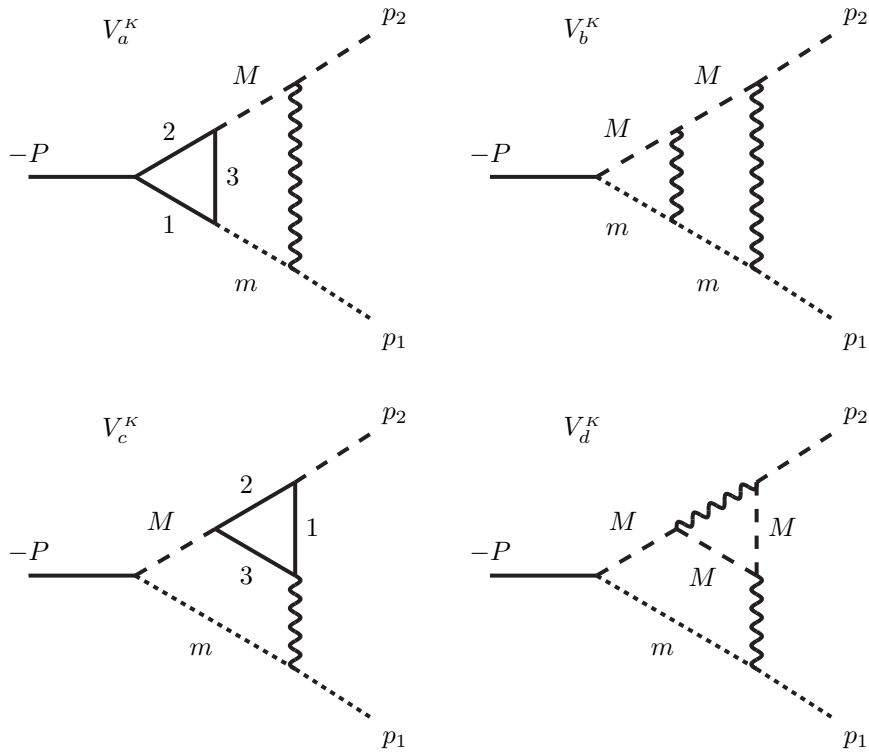


Figure 10: The V^K infrared configurations. The photon line represents a general massless particle while dashed and solid lines refer to different massive particles. The mass of the three particles in the internal triangle are m_1 , m_2 and m_3 .

5.6 Evaluation of the V^K cases

In order to evaluate infrared configurations for this family of diagrams we use the parametrization of Eq.(149). At first we combine propagators $[1]_K - [3]_K$ with Feynman parameters x_1, x_2 ,

$$\pi^4 V^K = \mu^{2\epsilon} \Gamma(3) \int d^n q_1 d^n q_2 \int dS_2(\{x\}) \frac{1}{[4]_K [5]_K [6]_K} \frac{1}{(q_1^2 + 2R_x \cdot q_1 + Q_x^2)^3}, \quad (152)$$

where x -dependent quantities are

$$R_x = (1 - x_1) P - x_2 q_2, \quad Q_x^2 = x_1 (m_1^2 - m_2^2) + x_2 (q_2^2 + m_3^2 - m_1^2) + m_2^2 + (1 - x_1) P^2. \quad (153)$$

Integration over q_1 gives

$$\pi^2 V^\kappa = i \mu^{2\epsilon} \frac{\Gamma(1 + \epsilon/2)}{\pi^{\epsilon/2}} \int dS_2(\{x\}) [x_2(1-x_2)]^{-1-\epsilon/2} \int \frac{d^n q_2}{(q_2^2 + 2P_x \cdot q_2 + M_x^2)^{1+\epsilon/2} [4]_\kappa [5]_\kappa [6]_\kappa}, \quad (154)$$

with new auxiliary quantities defined by

$$P_x = \frac{1-x_1}{1-x_2} P = X P, \quad M_x^2 = \frac{\chi(x_1; P^2; m_2^2, m_1^2) + x_2(m_3^2 - m_1^2)}{x_2(1-x_2)}. \quad (155)$$

Secondly, we combine the remaining propagators with Feynman parameters y_i , $i = 1, \dots, 3$: it follows

$$\begin{aligned} \pi^2 V^\kappa &= i \mu^{2\epsilon} \pi^{-\epsilon/2} \Gamma\left(4 + \frac{\epsilon}{2}\right) \int dS_2(\{x\}) [x_2(1-x_2)]^{-1-\epsilon/2} \int dS_3(\{y\}) y_3^{\epsilon/2} \\ &\times \int d^n q_2 \left[y_3 [123]_\kappa + (y_2 - y_3) [4]_\kappa + (1 - y_1) [5]_\kappa + (y_1 - y_2) [6]_\kappa \right]^{-4-\epsilon/2}, \end{aligned} \quad (156)$$

where $[123]_\kappa = q_2^2 + 2P_x \cdot q_2 + M_x^2$. After performing the q_2 -integration we obtain the following result:

$$V^\kappa = - \left(\frac{\mu^2}{\pi} \right)^\epsilon \Gamma(2 + \epsilon) \int dS_2(\{x\}) [x_2(1-x_2)]^{-1-\epsilon/2} \int dS_3(\{y\}) y_3^{\epsilon/2} U_\kappa^{-2-\epsilon}, \quad (157)$$

where the quadratic form U_κ is given by

$$U_\kappa = -[p_2 y_1 - P(y_2 - X y_3) + p_1]^2 + (P^2 - p_1^2 + m_6^2 - m_5^2) y_1 - (P^2 + m_6^2 - m_4^2) y_2 + (M_x^2 - m_4^2) y_3 + p_1^2 + m_5^2 \quad (158)$$

To proceed in our derivation we introduce $\bar{X} = 1 - X$ (with X given in Eq.(155)) and perform a change of variables, $y_2 = y'_2 + X y_3$, obtaining

$$\begin{aligned} V^\kappa &= - \left(\frac{\mu^2}{\pi} \right)^\epsilon \Gamma(2 + \epsilon) \int dS_2(\{x\}) [x_2(1-x_2)]^{-1-\epsilon/2} \int_0^1 dy_1 \int_{0, \bar{X} y_1}^{\bar{X} y_1, y_1} dy_2 \mathcal{Y}_{1\oplus 2; \kappa} \\ \mathcal{Y}_{i; \kappa} &= \int_0^{a_i} dy_3 y_3^{\epsilon/2} (A_\kappa y_3 + B_\kappa)^{-2-\epsilon}, \quad a_1 = \frac{y_2}{X}, \quad a_2 = \frac{y_1 - y_2}{X} \end{aligned} \quad (159)$$

where A_κ and B_κ are defined by

$$\begin{aligned} A_\kappa &= M_x^2 - \bar{X} m_4^2 - (P^2 + m_6^2) X \\ B_\kappa &= -(p_2 y_1 - P y_2 + p_1)^2 + (P^2 - p_1^2 + m_6^2 - m_5^2) y_1 - (P^2 + m_6^2 - m_4^2) y_2 + p_1^2 + m_5^2 \end{aligned} \quad (160)$$

The $\mathcal{Y}_{i; \kappa}$ functions of Eq.(159) can be expressed in terms of an hypergeometric function,

$$\mathcal{Y}_{i; \kappa} = \frac{\Gamma^2(1 + \epsilon/2)}{\Gamma(2 + \epsilon)} (A_\kappa B_\kappa)^{-1-\epsilon/2} - \frac{2}{2 + \epsilon} (a_i A_\kappa^2)^{-1-\epsilon/2} {}_2F_1(2 + \epsilon, 1 + \frac{\epsilon}{2}; 2 + \frac{\epsilon}{2}; -\frac{B_\kappa}{a_i A_\kappa}). \quad (161)$$

The first term in Eq.(161) does not depend on a_i ; therefore, we obtain,

$$\begin{aligned} V^\kappa &= - \left(\frac{\mu^2}{\pi} \right)^\epsilon \int dS_2(\{x\}) [x_2(1-x_2)]^{-1-\epsilon/2} \\ &\times \left[\Gamma^2\left(1 + \frac{\epsilon}{2}\right) \int dS_2(\{y\}) (A_\kappa B_\kappa)^{-1-\epsilon/2} - 2 \frac{\Gamma(2 + \epsilon)}{2 + \epsilon} \int_0^1 dy_1 \int_{0, \bar{X} y_1}^{\bar{X} y_1, y_1} dy_2 J_{1\oplus 2; \kappa} \right], \end{aligned} \quad (162)$$

where $J_{i; \kappa}$ is defined by

$$J_{i; \kappa} = (a_i A_\kappa^2)^{-1-\epsilon/2} {}_2F_1(2 + \epsilon, 1 + \frac{\epsilon}{2}; 2 + \frac{\epsilon}{2}; -\frac{B_\kappa}{a_i A_\kappa}). \quad (163)$$

Having derived the general result of Eq.(162) we proceed with separate evaluations of the four cases of Fig. 10.

5.6.1 Evaluation of V_a^K

For the configuration a) of Fig. 10 we have:

$$A_{a;\kappa} = \frac{V_{a;\kappa}(x_1, x_2)}{x_2(1-x_2)}, \quad B_{a;\kappa} = \beta(y_2, y_1; P^2, M^2, m^2), \quad (164)$$

$$V_{a;\kappa} = -P^2 x_1^2 + (P^2 - m^2 + M^2) x_1 x_2 + m^2 x_2^2 + (P^2 + m_1^2 - m_2^2) x_1 - (P^2 + M^2 - m_3^2 + m_1^2) x_2 + m_2^2.$$

After a transformation of variable, $y_2 \rightarrow y_1 y_2$, in the first integral of Eq.(162) the y_1 -integration can be carried out giving raise to the infrared pole. After that we put $\epsilon = 0$ in $I_{1;\kappa}$ and $I_{2;\kappa}$, thus obtaining:

$$V_a^K = \left(\frac{\mu^2}{\pi}\right)^\epsilon \Gamma^2\left(1 + \frac{\epsilon}{2}\right) \int dS_2(\{x\}) \left[\frac{1}{\epsilon} \int_0^1 dy_2 [V_{a;\kappa} \chi(y_2)]^{-1-\epsilon/2} + V_{a;\kappa}^{-1} \int_0^1 dy_1 \int_{0, \bar{X} y_1}^{\bar{X} y_1, y_1} dy_2 C_{1\oplus 2; a; \kappa}^{-1} \right], \quad (165)$$

where $C_{i, a; \kappa} = a_i A_{a; \kappa} + B_{a; \kappa}$ and χ is defined in Eq.(9). Henceforth we change variables in the last two integrals, $y_2 = y_1 y_2'$; the y_1 -integration can be performed, giving

$$V_a^K = \left(\frac{\mu^2}{\pi}\right)^\epsilon \Gamma^2\left(1 + \frac{\epsilon}{2}\right) \int dS_2(\{x\}) \left\{ \frac{1}{\epsilon} \int_0^1 dy_2 [V_{a;\kappa} \chi(y_2)]^{-1-\epsilon/2} + \sum_{i=1}^2 \int_0^{b_i} dy_2 \frac{1}{\alpha_i(y_2) V_{a;\kappa}} \ln \left[1 + \frac{x_2(1-x_2) b_i \alpha_i(y_2)}{y_2 V_{a;\kappa}} \right] \right\}, \quad (166)$$

where we have introduced

$$\alpha_1(y_2) = \bar{X}(y_2), \quad \alpha_2(y_2) = \chi(y_2), \quad b_1 = \bar{X}, \quad b_2 = X. \quad (167)$$

In the last two integrals of Eq.(166) we change, once again, variables:

$$\begin{aligned} x_1 &= x_1' + x_2, & x_2 &= 1 - x_2', & x_1 &\leftrightarrow x_2, & \text{for } i=1, \\ x_1 &= 1 - x_1', & x_2 &= 1 - x_2', & x_1 &\leftrightarrow x_2, & \text{for } i=2, \end{aligned} \quad (168)$$

thus obtaining

$$V_a^K = \frac{1}{\epsilon} \left(\frac{\mu^2}{\pi}\right)^\epsilon \Gamma^2\left(1 + \frac{\epsilon}{2}\right) \mathcal{X}_{a;\kappa} \mathcal{Y}_\kappa + J_{a,1;\kappa} + J_{a,2;\kappa}, \quad (169)$$

where the various ingredients are defined by

$$\begin{aligned} \mathcal{X}_{a;\kappa} &= \int dS_2(\{x\}) V_{a;\kappa}^{-1-\epsilon/2}(x_1, x_2), & \mathcal{Y}_\kappa &= \int_0^1 dy_2 \chi^{-1-\epsilon/2}(y_2) \\ J_{a,i;\kappa} &= \int dS_2(\{x\}) \int_0^{x_2/x_1} dy_2 \frac{1}{\alpha_i(y_2) V_{a,i;\kappa}} \ln \left[1 + \frac{x_2(1-x_1) \alpha_i(y_2)}{y_2 V_{a,i;\kappa}} \right]. \end{aligned} \quad (170)$$

The quadratic forms introduced in Eq.(170) are:

$$V_{a,i;\kappa}(x_1, x_2) = x^t H_{a,i} x + 2 K_{a,i}^t x + L_{a,i}, \quad i = 1, 2; \quad (171)$$

$$\begin{aligned} V_{a,1;\kappa} &= M^2 x_1^2 + (P^2 - M^2 + m^2) x_1 x_2 - P^2 x_2^2 + (m_2^2 - m_3^2 - M^2) x_1 + (m_1^2 - m_2^2 + M^2 - m^2) x_2 + m_3^2, \\ V_{a,2;\kappa} &= m^2 x_1^2 + (P^2 - m^2 + M^2) x_1 x_2 - P^2 x_2^2 + (m_1^2 - m_3^2 - m^2) x_1 + (m_2^2 - m_1^2 + m^2 - M^2) x_2 + m_3^2. \end{aligned}$$

To compute $\mathcal{X}_{a;\kappa}$ and \mathcal{Y}_κ , defined in Eq.(169), we use a BST relation. Given $V_{a;\kappa} = x^t H_a x + 2 K_a^t x + L_a$ we introduce $X_{a;\kappa}^0 = 1$, $X_{a;\kappa}^3 = 0$ and also

$$B_{a;\kappa} = L_a - K_a^t H_a^{-1} K_a, \quad X_{a;\kappa}^i = - \left(K_a^t H_a^{-1} \right)^i \quad i = 1, 2; \quad (172)$$

we obtain for $\mathcal{X}_{a;\kappa} = \mathcal{X}_{a;\kappa}^1 + \mathcal{X}_{a;\kappa}^2 \epsilon$

$$\mathcal{X}_{a;\kappa}^n = \frac{(-1)^{n+1}}{2^n n! B_{a;\kappa}} \left[2 \int dS_2 \ln^{n-1} V_{a;\kappa} \left(\ln V_{a;\kappa} + n \right) - \sum_{i=0}^2 (X_{a;\kappa}^i - X_{a;\kappa}^{i+1}) \int_0^1 dx \ln^n V_{a;\kappa}^i \right], \quad (173)$$

where the $V_{a;\kappa}^i$ quadratic forms are

$$V_{a;\kappa}^1 = V_{a;\kappa}(1, x), \quad V_{a;\kappa}^2 = V_{a;\kappa}(x, x), \quad V_{a;\kappa}^3 = V_{a;\kappa}(x, 0). \quad (174)$$

Similarly, for \mathcal{Y}_κ , we get

$$\mathcal{Y}_\kappa = \mathcal{Y}_\kappa^1 + \mathcal{Y}_\kappa^2 \epsilon, \quad \mathcal{Y}_\kappa^n = \frac{(-1)^{n+1}}{2^n n! B_\chi} \left\{ \int_0^1 dy \ln^{n-1} \chi(y) \left[\ln \chi(y) + 2n \right] - L_\chi^n \right\}, \quad (175)$$

where BST factor and co-factor are defined in Eq.(10) and L_χ^n in Eq.(84). To compute $J_{a,i;\kappa}$ we use Eq.(57) which in the present case reads:

$$\begin{aligned} \frac{1}{V_{a,i;\kappa}} \ln \left(1 - \frac{A_{a,i;\kappa}}{V_{a,i;\kappa}} \right) &= \frac{1}{B_{a;\kappa}} \left\{ \frac{1}{A_{a,i;\kappa}} \ln \left(1 - \frac{A_{a,i;\kappa}}{V_{a,i;\kappa}} \right) \left[1 - \frac{1}{2} \sum_{j=1}^2 (x_j - X_{a,i;\kappa}^j) \partial_{x_j} \right] A_{a,i;\kappa} \right. \\ &\quad \left. - \frac{1}{2} \sum_{j=1}^2 (x_j - X_{a,i;\kappa}^j) \partial_{x_j} \text{Li}_2 \left(\frac{A_{a,i;\kappa}}{V_{a,i;\kappa}} \right) \right\}. \end{aligned} \quad (176)$$

where $A_{a,i;\kappa} = -x_2(1-x_1)\alpha_i/y_2$ and BST factor and co-factors are

$$B_{a;\kappa} = L_{a,1} - K_{a,1}^t H_{a,1}^{-1} K_{a,1} = L_{a,2} - K_{a,2}^t H_{a,2}^{-1} K_{a,2} = L_a - K_a^t H_a^{-1} K_a, \quad X_{a,i;\kappa} = -K_{a,i}^t H_{a,i}^{-1}. \quad (177)$$

After integration by parts we obtain

$$\begin{aligned} J_{a,i;\kappa} &= \frac{1}{B_{a;\kappa}} \int_0^1 dy_2 \left\{ \int_0^1 dx_1 \int_{x_1}^{x_1} dx_2 \frac{1}{\alpha_i(y_2)} \left[\frac{1}{2} \left(\frac{1 - X_{a,i;\kappa}^1}{1 - x_1} + \frac{X_{a,i;\kappa}^2}{x_2} \right) \ln(1 + \eta_{a,i;\kappa}) + \text{Li}_2(-\eta_{a,i;\kappa}) \right] \right. \\ &\quad \left. - \frac{1}{2} \int_0^1 dx \left[\frac{X_{a,i;\kappa}^1 - X_{a,i;\kappa}^2}{\alpha_i(y_2)} \text{Li}_2(-\eta_{a,i;\kappa}^1) - \frac{y_2 X_{a,i;\kappa}^1 - X_{a,i;\kappa}^2}{\alpha_i(y_2)} \text{Li}_2(-\eta_{a,i;\kappa}^2) \right] \right\}, \end{aligned} \quad (178)$$

where the η -functions are defined by

$$\eta_{a,i;\kappa} = \frac{x_2(1-x_1)\alpha_i(y_2)}{y_2 V_{a,i;\kappa}(x_1, x_2)}, \quad \eta_{a,i;\kappa}^1 = \frac{x(1-x)\alpha_i(y_2)}{y_2 V_{a,i;\kappa}(x, x)}, \quad \eta_{a,i;\kappa}^2 = \frac{x(1-x)\alpha_i(y_2)}{V_{a,i;\kappa}(x, x y_2)}. \quad (179)$$

Collecting all pieces together, we get:

$$\boxed{V_a^\kappa} = - \left(\frac{\mu^2}{\pi} \right)^\epsilon \Gamma(1 + \epsilon) \left(\frac{1}{\epsilon} V_{-1}^{a;\kappa} + V_0^{a;\kappa} \right) \quad (180)$$

$$V_{-1}^{a;\kappa} = -\mathcal{X}_{a;\kappa}^1 \mathcal{Y}_\kappa^1, \quad V_0^{a;\kappa} = -\mathcal{X}_{a;\kappa}^1 \mathcal{Y}_\kappa^2 - \mathcal{X}_{a;\kappa}^2 \mathcal{Y}_\kappa^1 - J_{a,1;\kappa} - J_{a,2;\kappa}. \quad (181)$$

In the following section we will consider the b) configuration of Fig. 10.

5.6.2 Evaluation of V_b^κ

Configuration b) of Fig. 10 is a special case of a). Here the polynomial V takes the form (β is defined in Eq.(12))

$$V_{b;\kappa}(x_1, x_2) = \beta(1-x_1, 1-x_2; P^2; m^2, M^2) \quad (182)$$

which has a double zero at $x_1 = x_2 = 1$. The BST factor for the polynomial $V_{b;\kappa}$ is zero, revealing again the presence of a new infrared pole. For this reason we cannot put $\epsilon = 0$ from the beginning; instead we reexamine Eq.(159) which, in the present configuration, reads:

$$V_b^K = -\left(\frac{\mu^2}{\pi}\right)^\epsilon \Gamma(2 + \epsilon) \int dS_2(\{x\}) [x_2(1-x_2)]^{-1-\epsilon/2} \int_0^1 dy_1 \\ \times \int_{(0, \bar{x}, y_1)} dy_2 dy_3 y_3^{\epsilon/2} \left[\frac{\beta(1-x_1, 1-x_2)}{x_2(1-x_2)} y_3 + \bar{\beta}(y_2, y_1) \right]^{-2-\epsilon}, \quad (183)$$

In the first(second) integral of Eq.(183) we change variables according to:

$$x_1 \rightarrow x_1 + x_2, \quad x_2 \rightarrow 1 - x_2, \quad x_1 \rightarrow x_1 x_2 \quad \left(x_1 \rightarrow 1 - x_1, \quad x_2 \rightarrow 1 - x_2, \quad x_1 \rightarrow x_1 x_2 \right), \quad (184)$$

thus obtaining

$$V_b^K = -\left(\frac{\mu^2}{\pi}\right)^\epsilon \Gamma(2 + \epsilon) \int dC_3(\{x\}, y_1) \frac{[x_2(1-x_2)]^{-\epsilon/2}}{1-x_2} \sum_{i=1}^2 \int_{a_i}^{b_i} dy_2 \int_0^{d_i} dy_3 y_3^{\epsilon/2} \left[\frac{x_2 \alpha_i(x_1)}{1-x_2} y_3 + \bar{\beta}(y_2, y_1) \right]^{-2-\epsilon} \\ a_1 = 0, \quad b_1 = x_1 y_1, \quad d_1 = \frac{y_2}{x_1}, \quad a_2 = (1-x_1)y_1, \quad b_2 = y_1, \quad d_2 = \frac{y_1 - y_2}{x_1}. \quad (185)$$

where the functions α_i are defined in Eq.(167). We also transform the integration domain of y_2 and y_3 in the first(second) integral of Eq.(183) according to:

$$y_3 \rightarrow y_2 y_3 / x_1, \quad y_2 \rightarrow y_1 y_2, \quad \left(y_3 \rightarrow (y_1 - y_2) y_3 / x_1, \quad y_2 \rightarrow y_1 (1 - y_2) \right). \quad (186)$$

After this transformation we obtain

$$V_b^K = -\left(\frac{\mu^2}{\pi}\right)^\epsilon \Gamma(2 + \epsilon) \sum_{i=1}^2 \int dC_3(x_1, x_2, y_3) \int_0^{x_1} dy_2 [x_1(1-x_2)y_2]^{1+\epsilon/2} \left(\frac{y_3}{x_2}\right)^{\epsilon/2} \mathcal{Y}_{b,i;\kappa} \\ \mathcal{Y}_{b,i;\kappa} = \int_0^1 dy_1 y_1^{-\epsilon/2} [x_2 y_2 y_3 \alpha_i(x_1) + x_1(1-x_2) y_1 \alpha_i(y_2)]^{-2-\epsilon}. \quad (187)$$

$\mathcal{Y}_{b,i;\kappa}$ is then expressed in terms of an hypergeometric function:

$$\mathcal{Y}_{b,i;\kappa} = \frac{2}{2-\epsilon} [x_2 y_2 y_3 \alpha_i(x_1)]^{-2-\epsilon} {}_2F_1\left(2 + \epsilon, 1 - \frac{\epsilon}{2}; 2 - \frac{\epsilon}{2}; -\frac{x_1(1-x_2)\alpha_i(y_2)}{x_2 y_2 y_3 \alpha_i(x_1)}\right) \\ = B\left(1 - \frac{\epsilon}{2}, 1 + \frac{3}{2}\epsilon\right) [x_2 y_2 y_3 \alpha_i(x_1)]^{-1-3\epsilon/2} [x_1(1-x_2)\alpha_i(y_2)]^{-1+\epsilon/2} \\ - \frac{2}{2+3\epsilon} [x_1(1-x_2)\alpha_i(y_2)]^{-2-\epsilon} {}_2F_1\left(2 + \epsilon, 1 + \frac{3}{2}\epsilon; 2 + \frac{3}{2}\epsilon; -\frac{x_2 y_2 y_3 \alpha_i(x_1)}{x_1(1-x_2)\alpha_i(y_2)}\right). \quad (188)$$

Substituting this partial result in the expression for V_b^K and setting $\epsilon = 0$ where possible, we get:

$$V_b^K = -\left(\frac{\mu^2}{\pi}\right)^\epsilon \Gamma\left(1 - \frac{\epsilon}{2}\right) \Gamma\left(1 + \frac{3}{2}\epsilon\right) \left(V_{b,\epsilon}^K + V_{b,0}^K\right) \quad (189)$$

where we have defined

$$V_{b,\epsilon}^K = \sum_{i=1}^2 \int dC_3(x_1, x_2, y_3) \int_0^{x_1} dy_2 x_1^\epsilon x_2^{-1-2\epsilon} (1-x_2)^\epsilon y_2^{-\epsilon} y_3^{-1-\epsilon} \alpha_i^{-1-3/2\epsilon}(x_1) \alpha_i^{-1+\epsilon/2}(y_2) \\ V_{b,0}^K = -\sum_{i=1}^2 \int dC_3(x_1, x_2, y_3) \int_0^{x_1} dy_2 \frac{y_2}{\alpha_i(y_2)} [x_2 y_2 y_3 \alpha_i(x_1) + x_1(1-x_2)\alpha_i(y_2)]^{-1}. \quad (190)$$

After some straightforward integration the function of Eq.(190) become

$$\begin{aligned}
V_{b,\epsilon}^K &= \frac{1}{2\epsilon^2} \frac{\Gamma(1-2\epsilon)\Gamma(1+\epsilon)}{\Gamma(1-\epsilon)} \sum_{i=1}^2 \int_0^1 dx \int_0^x dy x^\epsilon y^{-\epsilon} \alpha_i^{-1-3/2\epsilon}(x) \alpha_i^{-1+\epsilon/2}(y) \\
V_{b,0}^K &= -\sum_{i=1}^2 \int dC_2(x_1, x_2) \int_0^{x_1} dy \frac{\ln(1+\eta_{b,i;\kappa})}{\alpha_i(x_1)\alpha_i(y)x_2}, \quad \eta_{b,i;\kappa} = \frac{x_2 y \alpha_i(x_1)}{x_1(1-x_2)\alpha_i(y)}
\end{aligned} \tag{191}$$

After a Laurent expansion in ϵ , $V_{b,\epsilon}^K$ has the following form:

$$V_{b,\epsilon}^K = \frac{1}{2} \sum_{n=-2}^0 \mathcal{R}_n^{b;\kappa} \epsilon^n, \tag{192}$$

$$\begin{aligned}
\mathcal{R}_{-2}^{b;\kappa} &= \left[\int_0^1 dx \chi^{-1}(x) \right]^2 = [J_0^0]^2 & \mathcal{R}_{-1}^{b;\kappa} &= -J_0^0 J_0^1 + \sum_{i=1}^2 \left[J_{10}^{00}(i) - J_{01}^{00}(i) \right] \\
\mathcal{R}_0^{b;\kappa} &= -\frac{3}{4} [J_0^1]^2 + \frac{5}{4} J_0^2 J_0^0 + 2\zeta(2) [J_0^0]^2 + \frac{1}{2} \sum_{i=1}^2 \left[-2 J_{11}^{00}(i) \right. \\
&\quad \left. + J_{20}^{00}(i) + J_{02}^{00}(i) - 3 J_{10}^{10}(i) + J_{10}^{01}(i) + 3 J_{01}^{10}(i) - J_{01}^{01}(i) \right].
\end{aligned} \tag{193}$$

In Eq.(193) we have introduced J_n^k and $J_{nm}^{kh}(i)$ defined by:

$$J_n^k = \int_0^1 dz \ln^n z \frac{\ln^k \chi(z)}{\chi(z)} \quad J_{nm}^{kh}(i) = \int_0^1 dx \int_0^x dy \ln^n x \ln^m y \frac{\ln^k \alpha_i(x)}{\alpha_i(x)} \frac{\ln^h \alpha_i(y)}{\alpha_i(y)} \tag{194}$$

J integrals of the first kind have already been considered in section 5.3.2 (see Eq.(132)). For J integrals of the second kind it is easy to verify that the following property holds:

$$\sum_{i=1}^2 J_{00}^{k_1 k_2}(i) = J_0^{k_1} J_0^{k_2} \tag{195}$$

The general analysis of J is reported in appendix D; here it is enough to say that for J we are always able to find a smooth integral representation. Finally, note that the residue of the double pole is exactly one half of the square of the residue for the single pole in the one-loop case. For $V_{b,0}^K$ we apply Eq.(57):

$$\frac{1}{\alpha_i(y)} \ln \left(1 - \frac{by}{\alpha_i(y)} \right) = \frac{1}{B_\chi} \left\{ \left(1 - \frac{y-Z_i}{2y} \right) \ln \left(1 - \frac{by}{\alpha_i(y)} \right) - \frac{y-Z_i}{2} \partial_y \text{Li}_2 \left(\frac{by}{\alpha_i(y)} \right) \right\}, \tag{196}$$

where $b = -x_2 \alpha_i(x_1)/x_1/(1-x_2)$, $Z_1 = \bar{X}_\chi$ and $Z_2 = X_\chi$. After integrating by parts, we obtain:

$$V_{b,0}^K = -\frac{1}{2B_\chi} \sum_{i=1}^2 \int dC_2(\{x\}) \int_0^{x_1} dy \frac{1}{x_2 \alpha_i(x_1)} \left[\left(1 + \frac{Z_i}{y} \right) \ln(1+\eta_{b,i;\kappa}) + \text{Li}_2(-\eta_{b,i;\kappa}) \right] \tag{197}$$

Collecting all pieces together, we get:

$$\boxed{V_b^K} = -\left(\frac{\mu^2}{\pi} \right)^\epsilon \Gamma(1+\epsilon) \left(\frac{1}{\epsilon^2} V_{-2}^{b;\kappa} + \frac{1}{\epsilon} V_{-1}^{b;\kappa} + V_0^{b;\kappa} \right) \tag{198}$$

$$V_{-2}^{b;\kappa} = \frac{1}{2} \mathcal{R}_{-2}^{b;\kappa} \quad V_{-1}^{b;\kappa} = \frac{1}{2} \mathcal{R}_{-1}^{b;\kappa} \quad V_0^{b;\kappa} = \frac{1}{2} \mathcal{R}_0^{b;\kappa} + \frac{3}{8} \zeta(2) \mathcal{R}_{-2}^{b;\kappa} + V_{b,0}^K \tag{199}$$

5.6.3 Evaluation of V_c^κ

For configuration c) of Fig. 10 we have

$$\begin{aligned} A_{c;\kappa} &= \frac{V_{c;\kappa}(x_1, x_2)}{x_2(1-x_2)}, & V_{c;\kappa}(x_1, x_2) &= \chi(x_1; -M^2; m_2^2, m_1^2) + x_2(m_3^2 - m_1^2) \\ B_{c;\kappa}(y_1, y_2) &= \beta(y_1 - y_2, 1 - y_2; P^2; m^2, M^2). \end{aligned} \quad (200)$$

For this configuration we transform variables according to $y_1 = y'_1 + y_2$ and $y_2 = 1 - y'_2$ in the first integral of Eq.(162) which will have the same form as the similar integral in case a) and we obtain:

$$V_c^\kappa = \left(\frac{\mu^2}{\pi}\right)^\epsilon \frac{1}{\epsilon} \Gamma^2\left(1 + \frac{\epsilon}{2}\right) \mathcal{X}_{c;\kappa} \mathcal{Y}_\kappa + J_{c,1;\kappa} + J_{c,2;\kappa}, \quad (201)$$

where the various components are defined by

$$\mathcal{X}_{c;\kappa} = \int dS_2(\{x\}) V_{c;\kappa}^{-1-\epsilon/2}(x_1, x_2), \quad \mathcal{Y}_\kappa = \int_0^1 dy_2 \chi^{-1-\epsilon/2}(y_2), \quad (202)$$

$$\sum_i J_{c,i;\kappa} = \int dS_2(\{x\}) \int_0^1 dy_1 \int_{0, \bar{X}_{y_1}}^{\bar{X}_{y_1, y_1}} dy_2 C_{1\oplus 2; c;\kappa}^{-1}, \quad C_{i,c;\kappa} = a_i A_{c;\kappa} + B_{c;\kappa}. \quad (203)$$

and $\chi(x)$ is defined in Eq.(9). \mathcal{Y}_κ has already been computed in Eq.(175), while for computing $\mathcal{X}_{c;\kappa}$ we can use the following BST relations:

$$V_{c;\kappa}^\mu = \frac{1}{m_3^2 - m_1^2} \frac{1}{\mu + 1} \partial_{x_2} V_{c;\kappa}^{\mu+1}, \quad V_{c;\kappa}^\mu = \frac{1}{b_{c;\kappa}} \left\{ 1 - \frac{1}{\mu + 1} \left[\frac{1}{2} (x_1 - X_{c;\kappa}) \partial_{x_1} + x_2 \partial_{x_2} \right] \right\} V_{c;\kappa}^{\mu+1}, \quad (204)$$

$$b_{c;\kappa} = -\frac{\lambda(M^2, m_1^2, m_2^2)}{4M^2}, \quad X_{c;\kappa} = \frac{M^2 - m_1^2 + m_2^2}{2M^2}, \quad \bar{X}_{c;\kappa} = 1 - X_{c;\kappa}. \quad (205)$$

After intergration by parts, we obtain the following two results:

$$\mathcal{X}_{c;\kappa} = \frac{1}{m_3^2 - m_1^2} \left(\mathcal{X}_{c;\kappa}^{11} - \frac{\epsilon}{4} \mathcal{X}_{c;\kappa}^{12} \right) \text{ if } m_1 \neq m_3, \quad \mathcal{X}_{c;\kappa} = \frac{1}{2b_{c;\kappa}} \left(\mathcal{X}_{c;\kappa}^{21} - \frac{\epsilon}{4} \mathcal{X}_{c;\kappa}^{22} \right) \text{ if } b_{c;\kappa} \neq 0. \quad (206)$$

$$\mathcal{X}_{c;\kappa}^{1n} = \int_0^1 dx \left[\ln^n V_{c;\kappa}(x, x) - \ln^n V_{c;\kappa}(x, 0) \right]; \quad (207)$$

$$\mathcal{X}_{c;\kappa}^{2n} = \int dS_2 \ln^{n-1} V_{c;\kappa} \left(3 \ln V_{c;\kappa} + 2n \right) - \int_0^1 dx \left[\bar{X}_{c;\kappa} \ln^n V_{c;\kappa}(1, x) + (x + X_{c;\kappa}) \ln^n V_{c;\kappa}(x, x) \right]. \quad (208)$$

Therefore, our result is also valid when $m_1 = m_3$ or $\lambda(M^2, m_1^2, m_2^2) = 0$, but not when the two conditions occur simultaneously. In the standard model this can actually happen only when $m_1 = m_3 = M$ and $m_2 = 0$ which corresponds to configuration d) to be analyzed in the next subsection.

In order to compute $J_{c,1;\kappa}$ and $J_{c,2;\kappa}$, we change variables according to:

$$\begin{aligned} x_1 &= x'_1 + x_2, & x_2 &= 1 - x'_2, & x_1 &\leftrightarrow x_2, & y_2 &= y_1 y'_2, & \text{for } i &= 1, \\ x_1 &= 1 - x'_1, & x_2 &= 1 - x'_2, & x_1 &\leftrightarrow x_2, & y_2 &= y_1 (1 - y'_2), & \text{for } i &= 2, \end{aligned} \quad (209)$$

thus obtaining

$$J_{c,i;\kappa} = \int dS_2(\{x\}) \int_0^1 dy_1 \int_0^{x_2/x_1} dy_2 \frac{1}{V_{c,i;\kappa}} \frac{x_2(1-x_1)y_1}{y_1 y_2 V_{c,i;\kappa} + x_2(1-x_1)B_{c,i;\kappa}}, \quad (210)$$

where we have introduced new quadratic forms $V_{c,i;\kappa}$:

$$\begin{aligned} V_{c,1;\kappa} &= \chi(1-x_1+x_2; -M^2; m_2^2, m_1^2) + (1-x_1)(m_3^2 - m_1^2), & B_{c,1;\kappa} &= B_{c;\kappa}(y_1, y_1 y_2) \\ V_{c,2;\kappa} &= \chi(1-x_2; -M^2; m_2^2, m_1^2) + (1-x_1)(m_3^2 - m_1^2), & B_{c,2;\kappa} &= B_{c;\kappa}(y_1, y_1(1-y_2)). \end{aligned} \quad (211)$$

For $V_{c,1;\kappa}$ and $V_{c,2;\kappa}$ two BST relations are available. Looking at the expression for $J_{c,i;\kappa}$, we immediately see that the required BST relations are of the form of Eq.(56). We have

$$\begin{aligned} \frac{1}{V_{c,i;\kappa}} \frac{A}{V_{c,i;\kappa} - A} &= \frac{1}{m_3^2 - m_1^2} \left[\frac{1}{V_{c,i;\kappa} - A} \mathcal{P}_{i,1} A + \mathcal{P}_{i,1} \ln \left(1 - \frac{A}{V_{c,i;\kappa}} \right) \right], \\ \frac{1}{V_{c,i;\kappa}} \frac{A}{V_{c,i;\kappa} - A} &= \frac{1}{b_{c;\kappa}} \left[\frac{1}{V_{c,i;\kappa} - A} (1 + \mathcal{P}_{i,2}) A + \mathcal{P}_{i,2} \ln \left(1 - \frac{A}{V_{c,i;\kappa}} \right) \right], \end{aligned} \quad (212)$$

where the explicit form of $\mathcal{P}_{i,j}$ is

$$\mathcal{P}_{1,1} = -\partial_{x_1} - \partial_{x_2}, \quad \mathcal{P}_{1,2} = (1-x_1)\partial_{x_1} + \frac{1}{2}(1-x_1-x_2+X_{c;\kappa})\partial_{x_2}, \quad (213)$$

$$\mathcal{P}_{2,1} = -\partial_{x_1}, \quad \mathcal{P}_{2,2} = (1-x_1)\partial_{x_1} + \frac{1}{2}(1-x_2-X_{c;\kappa})\partial_{x_2}. \quad (214)$$

In our case it is $A = -x_2(1-x_1)B_{c,i;\kappa}/(y_1 y_2)$, and we can define $a_{i,j}$ such that

$$\mathcal{P}_{i,1} A = a_{i,1} \frac{B_{c,i;\kappa}}{y_1 y_2}, \quad (1 + \mathcal{P}_{i,2}) A = \frac{a_{i,2}}{2} \frac{B_{c,i;\kappa}}{y_1 y_2}. \quad (215)$$

For a_{ij} we obtain:

$$\begin{aligned} a_{1,1} &= 1 - x_1 - x_2, & a_{1,2} &= (x_1 + x_2 - X_{c;\kappa} - 1)(1 - x_1), \\ a_{2,1} &= -x_2, & a_{2,2} &= -(1 - x_2 - X_{c;\kappa})(1 - x_1). \end{aligned} \quad (216)$$

After integration by parts the $J_{c,i;\kappa}$ can be expressed as

$$J_{c,i;\kappa} = \frac{1}{m_3^2 - m_1^2} \sum_{A=a}^d J_{i,1}^A \quad \text{if } m_1 \neq m_3, \quad J_{c,i;\kappa} = \frac{1}{2b_{c;\kappa}} \sum_{A=a}^d J_{i,2}^A \quad \text{if } b_{c;\kappa} \neq 0. \quad (217)$$

$$\begin{aligned} J_{i,j}^a &= - \int dS_2(\{x\}) a_{i,j} \int_0^1 dy_1 \int_0^{x_2/x_1} dy_2 \frac{y_1}{y_1 y_2 V_{c,i;\kappa} + x_2(1-x_1)B_{c,i;\kappa}}, \\ J_{i,j}^b &= \int dS_2(\{x\}) \int_0^1 dy_1 \int_0^{x_2/x_1} dy_2 b_{i,j} \frac{y_1}{B_{c,i;\kappa}} \ln \left(1 + \frac{x_2(1-x_1)B_{c,i;\kappa}}{y_1 y_2 V_{c,i;\kappa}} \right), \\ J_{i,j}^c &= \int dC_3(x \{y\}) c_{i,j} \frac{y_1}{B_{c,i;\kappa}} \ln \left(1 + \frac{x(1-x)B_{c,i;\kappa}}{y_1 y_2 V_{c,i;\kappa}(x, x)} \right), \\ J_{i,j}^d &= \int dC_3(x \{y\}) d_{i,j} \frac{y_1}{B_{c,i;\kappa}} \ln \left(1 + \frac{x(1-x)B_{c,i;\kappa}}{y_1 V_{c,i;\kappa}(x, x y_2)} \right), \end{aligned} \quad (218)$$

where $a_{i,j}$ is defined in Eq.(216), while the $b \cdots d$ coefficients are:

$$\begin{aligned} b_{1,1} &= 0, & c_{1,1} &= 0, & d_{1,1} &= -(1-y_2), \\ b_{2,1} &= 0, & c_{2,1} &= -1, & d_{2,1} &= y_2, \\ b_{1,2} &= -3, & c_{1,2} &= 1 - X_{c;\kappa}, & d_{1,2} &= 1 - x - 2y_2 + x y_2 + X_{c;\kappa}, \\ b_{2,2} &= -3, & c_{2,2} &= 1 - x + X_{c;\kappa}, & d_{2,2} &= 1 - 2y_2 + x y_2 - X_{c;\kappa}. \end{aligned} \quad (219)$$

All the quantities in Eq.(218) but $J_{i,j}^a$ are stable under numerical integration. For this integral we perform back the transformations of Eq.(209) and get:

$$J_{i,j}^a = \int dS_2(\{x\}) a'_{i,j} J_i^a \quad (220)$$

where the new coefficients $a'_{i,j}$ are

$$a'_{1,1} = x_1 - 2x_2, \quad a'_{1,2} = (2x_2 - x_1 + X_{c;\kappa}) x_2, \quad a'_{2,1} = x_1 - x_2, \quad a'_{2,2} = (\bar{X}_{c;\kappa} - x_1 + x_2) x_2. \quad (221)$$

The new integrals J_i^a are defined by

$$J_1^a = \int_0^1 dy_1 \int_0^{\bar{X} y_1} dy_2 \frac{1}{y_2 V_{c;\kappa} + x_2 (x_1 - x_2) B_{c;\kappa}}, \quad (222)$$

$$J_2^a = \int_0^1 dy_1 \int_{\bar{X} y_1}^{y_1} dy_2 \frac{1}{(y_1 - y_2) V_{c;\kappa} + x_2 (1 - x_1) B_{c;\kappa}}. \quad (223)$$

We transform according to $y_1 = y'_1 + y_2$, $y_2 = 1 - y'_2$, $y_1 \leftrightarrow y_2$, obtaining

$$J_1^a = \int_X^1 dy_1 \int_{(1-y_1)X/\bar{X}}^{y_1} dy_2 \frac{1}{(1-y_1) V_{c;\kappa} + x_2 (x_1 - x_2) \beta(y_2, y_1)}, \quad (224)$$

$$J_2^a = \left[\int_0^1 dy_1 \int_0^{y_1} dy_2 - \int_X^1 dy_1 \int_{(1-y_1)X/\bar{X}}^{y_1} dy_2 \right] \frac{1}{y_2 V_{c;\kappa} + x_2 (1 - x_1) \beta(y_2, y_1)}, \quad (225)$$

where the quadratic form β given in Eq.(12). For J_2^a we further transform $y_2 = y_1 y'_2$; as a consequence the y_1 integration becomes trivial giving:

$$J_2^a = \int_0^1 dy \frac{1}{x_2 (1 - x_1) \chi(y)} \ln \left\{ 1 + \frac{x_2 (1 - x_1)^2 \chi(y)}{y [1 - x_1 + (x_1 - x_2) y] V_{c;\kappa}} \right\}. \quad (226)$$

The χ function is defined in Eq.(9). For J_1^a we can use the fact that the B factor of the polynomial β is zero. In this way we can use Eq.(58):

$$\frac{1}{V - A} \left(\mathcal{P}_0 + \mathcal{P}_1^t \partial_x \right) A = -\mathcal{P}_1^t \partial_x \ln \left(1 - \frac{A}{V} \right). \quad (227)$$

To derive J_1^a we replace

$$V \rightarrow \beta(y_2, y_1), \quad A \rightarrow -\frac{(1-y_1)V_{c;\kappa}}{x_2(x_1-x_2)}, \quad \mathcal{P}_0 \rightarrow 2, \quad \mathcal{P}_1^t \partial_x \rightarrow -(y_1 \partial_{y_1} + y_2 \partial_{y_2}), \quad (228)$$

and obtain the equation

$$\left(\mathcal{P}_0 + \mathcal{P}_1^t \partial_x \right) A = -(2 - y_1) \frac{V_{c;\kappa}}{x_2 (x_1 - x_2)}. \quad (229)$$

Substituting in the expression for J_1^a , Eq.(224), after integration by parts, we get the final result for J_1^a ,

$$J_1^a = \frac{1}{V_{c;\kappa}} \int_X^1 dy_1 \int_{(1-y_1)X/\bar{X}}^{y_1} dy_2 \frac{4 - y_1}{(2 - y_1)^2} \ln \left\{ 1 + \frac{(1 - y_1) V_{c;\kappa}}{x_2 (x_1 - x_2) \beta(y_2, y_1)} \right\} \\ + \frac{1}{V_{c;\kappa}} \int_0^1 dy \frac{X}{1 + \bar{X} y} \ln \left\{ 1 + \frac{y \bar{X} V_{c;\kappa}}{x_2 (x_1 - x_2) \beta(X y, 1 - \bar{X} y)} \right\}. \quad (230)$$

Collecting all pieces together, we get:

$$\boxed{V_c^{\kappa}} = - \left(\frac{\mu^2}{\pi} \right)^\epsilon \Gamma(1 + \epsilon) \left(\frac{1}{\epsilon} V_{-1}^{c;\kappa} + V_0^{c;\kappa} \right) \quad (231)$$

$$\begin{aligned}
V_{-1}^{c;\kappa} &= -\frac{1}{m_3^2 - m_1^2} \mathcal{X}_{c;\kappa}^{11} \mathcal{Y}_\kappa^1 & V_0^{c;\kappa} &= -\frac{1}{m_3^2 - m_1^2} \left(\mathcal{X}_{c;\kappa}^{11} \mathcal{Y}_\kappa^2 + \mathcal{X}_{c;\kappa}^{12} \mathcal{Y}_\kappa^1 + \sum_{i=1}^2 \sum_{A=a}^d J_{i,1}^A \right) & \text{if } m_1 \neq m_3, \\
V_{-1}^{c;\kappa} &= -\frac{1}{2b_{c;\kappa}} \mathcal{X}_{c;\kappa}^{21} \mathcal{Y}_\kappa^1 & V_0^{c;\kappa} &= -\frac{1}{2b_{c;\kappa}} \left(\mathcal{X}_{c;\kappa}^{21} \mathcal{Y}_\kappa^2 + \mathcal{X}_{c;\kappa}^{22} \mathcal{Y}_\kappa^1 + \sum_{i=1}^2 \sum_{A=a}^d J_{i,1}^A \right) & \text{if } b_{c;\kappa} \neq 0. \quad (232)
\end{aligned}$$

5.6.4 Evaluation of V_d^K

Configuration d) of Fig. 10 is a special case of c). In fact the polynomial V_κ takes the form $V_{d;\kappa} = M^2 x_1^2$, which has a double zero for $x_1 = 0$. The BST factor for the polynomial $V_{d;\kappa}$ is also zero revealing the presence of a new infrared pole; we are not allowed to put $\epsilon = 0$ but reexamine instead Eq.(159) which now is:

$$\begin{aligned}
V_d^K &= -\left(\frac{\mu^2}{\pi}\right)^\epsilon \Gamma(2+\epsilon) \int dS_2(\{x\}) [x_2(1-x_2)]^{1+\epsilon/2} \int_0^1 dy_1 \int_{0, \bar{X}y_1}^{\bar{X}y_1, y_1} dy_2 \mathcal{Y}_{1\oplus 2; d; \kappa}, \\
\mathcal{Y}_{d,i;\kappa} &= \int_0^{a_i} dy_3 y_3^{\epsilon/2} \left[M^2 x_1^2 y_3 + x_2(1-x_2) B_{d;\kappa} \right]^{-2-\epsilon} \\
&= \frac{2}{2+\epsilon} [x_2(1-x_2)]^{-2-\epsilon} \left(\frac{a_i}{B_{d;\kappa}^2} \right)^{1+\epsilon/2} {}_2F_1 \left(-\frac{a_i M^2 x_1^2}{x_2(1-x_2) B_{d;\kappa}} \right). \quad (233)
\end{aligned}$$

where $a_1 = y_2/\bar{X}$, $a_2 = (y_1 - y_2)/X$ and $B_{d;\kappa}(y_1, y_2) = \beta(y_1 - y_2, 1 - y_2; P^2; m^2, M^2)$, with β defined in Eq.(12). We have also defined the shorthand notation ${}_2F_1(x) \equiv {}_2F_1(2+\epsilon, 1+\epsilon/2; 2+\epsilon/2; x)$. Now we split the integration region, $[\bar{X}y_1, y_1] = [0, y_1] \oplus [0, \bar{X}y_1]$, and use the properties of the hypergeometric functions to obtain

$$V_d^K = \left(\frac{\mu^2}{\pi}\right)^\epsilon \left(J_{d,0;\kappa} + J_{d,1;\kappa} + J_{d,2;\kappa} \right) \quad (234)$$

$$\begin{aligned}
J_{d,0;\kappa} &= -\frac{\Gamma(2+\epsilon)}{1+\epsilon/2} \int dS_2(\{x\}) \int dS_2(\{y\}) \left[\frac{y_1 - y_2}{x_2(1-x_1) B_{d;\kappa}^2} \right]^{1+\epsilon/2} {}_2F_1 \left(-\frac{M^2 x_1^2 (y_1 - y_2)}{x_2(1-x_1) B_{d;\kappa}} \right), \\
J_{d,1;\kappa} &= \frac{1}{M^2} \int dS_2(\{x\}) \int_0^1 dy_1 \int_0^{\bar{X}y_1} dy_2 \frac{x_2(x_1 - x_2)}{x_1^2} \frac{1}{M^2 x_1^2 y_2 + x_2(x_1 - x_2) B_{d;\kappa}}, \\
J_{d,2;\kappa} &= -\frac{1}{M^2} \int dS_2(\{x\}) \int_0^1 dy_1 \int_0^{\bar{X}y_1} dy_2 \frac{x_2(1-x_1)}{x_1^2} \frac{1}{M^2 x_1^2 (y_1 - y_2) + x_2(1-x_1) B_{d;\kappa}}. \quad (235)
\end{aligned}$$

We make the transformations $x_2 = x_1 x'_2$, $y_1 = y'_1 + y_2$, $y_2 = 1 - y'_2$, $y_1 \leftrightarrow y_2$, obtaining

$$\begin{aligned}
J_{d,0;\kappa} &= -\frac{\Gamma(2+\epsilon)}{1+\epsilon/2} \int dC_2(\{x\}) \int dS_2(\{y\}) x_1^{-\epsilon/2} \left[\frac{y_2}{x_2(1-x_1)\beta^2(y_2, y_1)} \right]^{1+\epsilon/2} {}_2F_1 \left(-\frac{M^2 x_1 y_2}{x_2(1-x_1)\beta(y_2, y_1)} \right), \\
J_{d,1;\kappa} &= \frac{1}{M^2} \int dC_2(\{x\}) \int_{X'}^1 dy_1 \int_{(1-y_1)X'/\bar{X}'}^{y_1} dy_2 \frac{x_2(1-x_2)}{x_1} \frac{1}{M^2(1-y_1) + x_2(1-x_2)\beta(y_2, y_1)}, \\
J_{d,2;\kappa} &= -\frac{1}{M^2} \int dC_2(\{x\}) \int_{X'}^1 dy_1 \int_{(1-y_1)X'/\bar{X}'}^{y_1} dy_2 \frac{x_2(1-x_1)}{x_1} \frac{1}{M^2 x_1 y_2 + x_2(1-x_1)\beta(y_2, y_1)}, \quad (236)
\end{aligned}$$

where β is defined in Eq.(12) and

$$X' = \frac{1-x_1}{1-x_1 x_2}, \quad \bar{X}' = 1 - X' = \frac{x_1(1-x_2)}{1-x_1 x_2}. \quad (237)$$

For $J_{d,1;\kappa}$ ($J_{d,2;\kappa}$) we apply the same technique already used in the previous subsection to treat J_1^a (J_2^a). We obtain

$$\begin{aligned}
J_{d,1;\kappa} &= \frac{1}{M^4} \int_0^1 dx_2 \int dS_2\{y\} \frac{4-y_1}{(2-y_1)^2} x_2 (1-x_2) \ln \left(1 + \frac{(1-x_2)y_2}{1-y_1} \right) \ln \left\{ 1 + \frac{(1-y_1)M^2}{x_2(1-x_2)\beta(y_2, y_1)} \right\} \\
&\quad + \frac{1}{M^4} \int dC_3(\{x\}, y) \frac{x_2(1-x_2)}{x_1} \frac{X'}{1+\bar{X}'y} \ln \left\{ 1 + \frac{x_1 y M^2}{x_2(1-x_1 x_2)\beta(X'y, 1-\bar{X}'y)} \right\}, \quad (238) \\
J_{d,2;\kappa} &= \frac{1}{M^2} \int dC_3(\{x\}, y) \frac{1}{x_1 \chi(y)} \ln \left\{ 1 - \frac{x_1 x_2 (1-x_1)(1-x_2) y \chi(y)}{[1-x_1+x_1(1-x_2)y][M^2 x_1 y + x_2(1-x_1)\chi(y)]} \right\}.
\end{aligned}$$

To extract the infrared poles from $J_{d,0;\kappa}$ of Eq.(236) we first transform according to $y_2 = y_1 y'_2$ and then perform a sector decomposition of the unit square in x_1 and y_1 : $[0, 1]^2 = [0, 1] \otimes [0, x_1] \oplus [0, 1] \otimes [0, y_1]$. Each sector is then mapped back into the unit square giving $J_{d,0;\kappa} = J_{\epsilon,1} + J_{\epsilon,2}$, with

$$\begin{aligned}
J_{\epsilon,1} &= -(M^2)^{-1-\epsilon/2} \Gamma^2(1+\epsilon/2) \int dC_3(x, \{y\}) x_1^{-1-2\epsilon} y_1^{-1-\epsilon} \chi(y_2)^{-1-\epsilon/2} \quad (239) \\
&\quad + \frac{\Gamma(2+\epsilon)}{1+\epsilon/2} \int dC_4(\{x\}, \{y\}) x_1^{-1-2\epsilon} y_1^{-\epsilon/2} \left[\frac{x_2(1-x_1)}{y_2 M^4} \right]^{1+\epsilon/2} {}_2F_1 \left(-\frac{x_2(1-x_1)y_1 \chi(y_2)}{M^2 y_2} \right), \\
J_{\epsilon,2} &= -\frac{\Gamma(2+\epsilon)}{1+\epsilon/2} \int dC_4(\{x\}, \{y\}) x_1^{-\epsilon/2} y_1^{-1-2\epsilon} \left[\frac{y_2}{x_2(1-x_1 y_1)\chi^2(y_2)} \right]^{1+\epsilon/2} {}_2F_1 \left(-\frac{M^2 x_1 y_2}{x_2(1-x_1 y_1)\chi(y_2)} \right).
\end{aligned}$$

For $J_{\epsilon,1}$ we have used the properties of the hypergeometric functions of related arguments (see app. C). In the first term of $J_{\epsilon,1}$, the integration over x_1 and y_1 is trivially performed giving the double infrared pole. The two terms containing the hypergeometric function are also divergent for $\epsilon \rightarrow 0$. The corresponding pole can be extracted as in Eq.(3). Setting $\epsilon = 0$ when possible, we get:

$$\begin{aligned}
J_{d,0;\kappa} &= -\frac{1}{2} \frac{1}{\epsilon^2} (M^2)^{-1-\epsilon/2} \Gamma^2 \left(1 + \frac{\epsilon}{2} \right) \mathcal{Y}_\kappa - \frac{\Gamma(2+\epsilon)}{1+\epsilon/2} \int dC_4(\{x\}, \{y\}) \tilde{J}_{d,0;\kappa}, \\
\tilde{J}_{d,0;\kappa} &= \frac{1}{2\epsilon} \left[y_1^{-\epsilon/2} \left(\frac{x_2}{y_2 M^4} \right)^{1+\epsilon/2} {}_2F_1 \left(-\frac{x_2 y_1 \chi(y_2)}{M^2 y_2} \right) - x_1^{-\epsilon/2} \left(\frac{y_2}{x_2 \chi^2(y_2)} \right)^{1+\epsilon/2} {}_2F_1 \left(-\frac{M^2 x_1 y_2}{x_2 \chi(y_2)} \right) \right] \\
&\quad - \frac{x_2}{M^2} \frac{1}{x_1} \frac{1-x_1}{x_2(1-x_1)y_1 \chi(y_2) + M^2 y_2} \Big|_+ + \frac{y_2}{\chi(y_2)} \frac{1}{y_1} \frac{1}{x_2(1-x_1 y_1)\chi(y_2) + M^2 x_1 y_2} \Big|_+. \quad (240)
\end{aligned}$$

\mathcal{Y}_κ has already been considered in section 5.6.1. The coefficients of its expansion $\mathcal{Y}_\kappa = \mathcal{Y}_\kappa^1 + \mathcal{Y}_\kappa^2 \epsilon + \mathcal{Y}_\kappa^3 \epsilon^2$ are given in Eq.(175). Now we expand the hypergeometric functions around $\epsilon = 0$ according to Eq.(326) and perform everywhere the x_1 and y_1 integrations. Using properties of the dilogarithm we obtain:

$$\begin{aligned}
\tilde{J}_{d,0;\kappa} &= \frac{\Gamma(1+\epsilon)}{M^2} \int_0^1 \frac{dx dy}{\chi(y)} \left\{ -\frac{1}{2\epsilon} \ln \eta_{d;\kappa} + \frac{1}{2} \left[\frac{1}{2} \ln \frac{x}{y} + \ln \chi(y) \right] \ln \eta_{d;\kappa} \right. \\
&\quad \left. - \text{Li}_2(\eta_{d;\kappa}) - \ln \eta_{d;\kappa} \ln(1-\eta_{d;\kappa}) + \frac{\zeta(2)}{2} \right\}. \quad \eta_{d;\kappa} = \frac{x \chi(y)}{y M^2} \quad (241)
\end{aligned}$$

The result of Eq.(241) can be cast in a form suited for numerical evaluation, by introducing the integrals J_n^k already treated in section 5.3.2 (see Eq.(132)). Combining all terms together we finally write $J_{d,0;\kappa}$ as

$$\boxed{V_d^\kappa} = - \left(\frac{\mu^2}{\pi} \right)^\epsilon \Gamma(1+\epsilon) \left(\frac{1}{\epsilon^2} V_{-2}^{d;\kappa} + \frac{1}{\epsilon} V_{-1}^{d;\kappa} + V_0^{d;\kappa} \right) \quad (242)$$

$$V_{-2}^{b;\kappa} = \frac{J_0^0}{2M^2}, \quad V_{-1}^{b;\kappa} = -\frac{1}{2M^2} \left[\left(\frac{3}{2} \ln M^2 + 1 \right) J_0^0 - \frac{1}{2} J_0^1 + J_1^0 \right],$$

$$V_0^{b;\kappa} = \frac{1}{2M^2} \left\{ \frac{1}{8} (\ln^2 M^2 - 4 \ln M^2 - 10 \zeta(2) - 8) J_0^0 + \frac{1}{4} (5 \ln M^2 + 6) J_0^1 - \frac{1}{2} (\ln M^2 + 2) J_1^0 \right. \\ \left. + \frac{3}{2} J_1^1 - \frac{7}{8} J_0^2 - \frac{1}{2} J_2^0 + 2 \int_0^1 dx dy \frac{1}{\chi(y)} \left[\text{Li}_2(\eta_{d;\kappa}) + \ln \eta_{d;\kappa} \ln(1 - \eta_{d;\kappa}) \right] \right\} - J_{d,1;\kappa} - J_{d,2;\kappa}. \quad (243)$$

5.7 The V^H diagram

Finally, we consider the V^H -family given in Fig. 11 which is representables as

$$\pi^4 V^H = \mu^{2\epsilon} \int d^n q_1 d^n q_2 \frac{1}{[1]_H [2]_H [3]_H [4]_H [5]_H [6]_H}, \quad (244)$$

with propagators

$$[1]_H = q_1^2 + m_1^2, \quad [2]_H = (q_1 - p_2)^2 + m_2^2, \quad [3]_H = (q_1 - q_2 + p_1)^2 + m_3^2, \quad (245)$$

$$[4]_H = (q_1 - q_2 - p_2)^2 + m_4^2, \quad [5]_H = q_2^2 + m_5^2, \quad [6]_H = (q_2 - p_1)^2 + m_6^2, \quad (246)$$

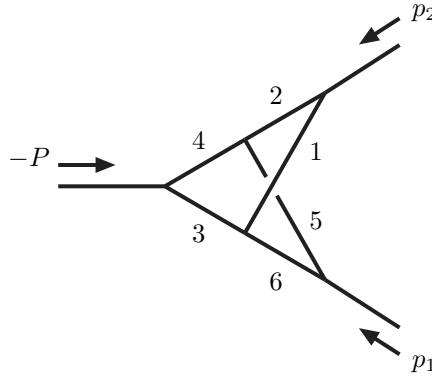


Figure 11: The irreducible two-loop vertex diagrams V^H . External momenta are flowing inwards.

This diagram has only one infrared configuration (shown in Fig. 12) which corresponds to $m_1 = m_5 = 0$, and $p_1^2 = -m_3^2 = -m_6^2 = -m^2$ $p_2^2 = -m_2^2 = -m_4^2 = -M^2$ At first we combine propagators $[1]_H - [4]_H$ with

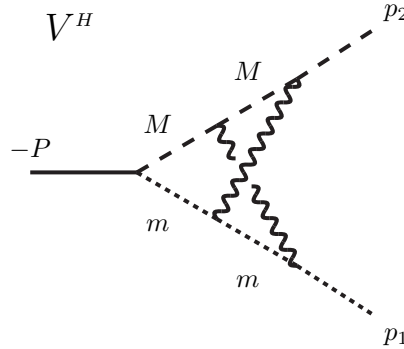


Figure 12: The V^H infrared configurations. The photon line represents a general massless particle while dashed and solid lines refer to different massive particles.

Feynman parameters x_1, x_2, x_3 ,

$$\pi^4 V^H = \mu^{2\epsilon} \Gamma(4) \int d^n q_1 d^n q_2 \int dS_3(\{x\}) \frac{1}{[5]_H [6]_H} \frac{1}{(q_1^2 + 2 R_x \cdot q_1 + Q_x^2)^4}, \quad (247)$$

where x -dependent quantities are

$$R_x = -x_2 q_2 - x_1 p_2 + x_3 P, \quad Q_x^2 = x_2 q_2^2 + 2 x_2 p_2 \cdot q_2 - 2 x_3 P \cdot q_2 \quad (248)$$

Integration over q_1 gives

$$\pi^2 V^H = i \frac{\mu^{2\epsilon}}{\pi^{\epsilon/2}} \Gamma\left(2 + \frac{\epsilon}{2}\right) \int dS_3(\{x\}) [x_2(1-x_2)]^{-2-\epsilon/2} \int \frac{d^n q_2}{(q_2^2 + 2 P_x \cdot q_2 + M_x^2)^{2+\epsilon/2} [5]_H [6]_H}, \quad (249)$$

with new auxiliary quantities defined by

$$P_x = \frac{1}{x_2(1-x_2)} [x_2(1-x_1)p_2 - x_3(1-x_2)P] \quad M_x^2 = -\frac{1}{x_2(1-x_2)} [x_1 p_2 - x_3 P]^2. \quad (250)$$

Secondly, we combine the remaining propagators with Feynman parameters y_1, y_2 : it follows

$$\pi^2 V^H = i \frac{\mu^{2\epsilon}}{\pi^{\epsilon/2}} \Gamma\left(4 + \frac{\epsilon}{2}\right) \int dS_3(\{x\}) [x_2(1-x_2)]^{-2-\epsilon/2} \int dS_2(\{y\}) y_2^{1+\epsilon/2} \int \frac{d^n q_2}{(q_2^2 + 2 R_y \cdot q_2 + Q_y^2)^{4+\epsilon/2}}, \quad (251)$$

where y -dependent quantities are $R_y = y_2 P_x - (y_1 - y_2) p_1$ and $Q_y^2 = y_2 M_x^2$. Integration over q_2 followed by a transformation $y_2 = y_1 y_2'$, gives

$$V^H = - \left(\frac{\mu^2}{\pi}\right)^\epsilon \Gamma(2+\epsilon) \int dS_3(\{x\}) \int dC_2(\{y\}) [x_2(1-x_2)]^{-2-\epsilon/2} y_1^{-\epsilon/2} y_2^{1+\epsilon/2} (A_H + B_H y_1)^{-2-\epsilon}, \quad (252)$$

where A_H and B_H are

$$A_H = M_x^2 y_2 = \frac{y_2}{x_2(1-x_2)} \bar{\beta}(x_3, x_1), \quad B_H = -[P_x y_2 - p_1(1-y_2)]^2 = \bar{\beta}\left(1 - \frac{x_2 - x_3}{x_2} y_2, 1 - \frac{x_1 - x_2}{1-x_2} y_2\right) \quad (253)$$

and the quadratic $\bar{\beta}$ is defined in Eq.(13). To proceed in the evaluation of the diagram we perform the following changes of variables

$$x_3 \rightarrow x_2 x_3, \quad y_2 \rightarrow \frac{1-x_2}{x_1-x_2} y_2, \quad x_2 \rightarrow x_1 x_2, \quad x_1 \rightarrow \frac{x_1}{1-(1-x_1)x_2}, \quad y_2 \rightarrow x_1 y_2, \quad (254)$$

and derive

$$V^H = - \left(\frac{\mu^2}{\pi}\right)^\epsilon \Gamma(2+\epsilon) \int dC_4(\{x\}, y_2) x_1^{-\epsilon/2} [1 - (1-x_1)x_2]^\epsilon [x_2(1-x_2)]^{-1-\epsilon/2} y_2^{1+\epsilon/2} \mathcal{Y}_H$$

$$\mathcal{Y}_H = \int_0^1 dy_1 y_1^{-\epsilon/2} (\mathcal{A}_H + \mathcal{B}_H y_1)^{-2-\epsilon} = \frac{2}{2-\epsilon} \mathcal{A}_H^{-2-\epsilon} {}_2F_1(2+\epsilon, 1-\frac{\epsilon}{2}; 2-\frac{\epsilon}{2}; -\frac{\mathcal{B}_H}{\mathcal{A}_H}) \quad (255)$$

where $\mathcal{A}_H, \mathcal{B}_H$ factors are

$$\mathcal{A}_H = \frac{x_1 y_2}{x_2(1-x_2)} \bar{\chi}(x_2 x_3), \quad \mathcal{B}_H = \bar{\beta}(1 - (1-x_3)y_2, 1 - x_1 y_2). \quad (256)$$

The quadratic form $\bar{\chi}$ is defined in Eq.(11). Using properties of the hypergeometric function and setting $\epsilon = 0$ whenever possible, we obtain:

$$V^H = - \left(\frac{\mu^2}{\pi}\right)^\epsilon \Gamma\left(1 - \frac{\epsilon}{2}\right) \Gamma\left(1 + \frac{3}{2}\epsilon\right) \int dC_4(\{x\}, y_2) \mathcal{B}_H^{-1+\epsilon/2} \mathcal{V}_H \quad (257)$$

$$\mathcal{V}^H = x_1^{-1-2\epsilon} \left[\frac{1 - (1-x_1)x_2}{y_2} \right]^\epsilon [x_2(1-x_2)]^\epsilon \bar{\chi}^{-1-3\epsilon/2}(x_2 x_3) + \frac{y_2}{x_1 y_2 \bar{\chi}(x_2 x_3) + x_2(1-x_2) \mathcal{B}_H}. \quad (258)$$

The first term in Eq.(258) is an integral of the type shown in Eq.(3) and the V^H diagram can be rewritten as

$$V^H = \left(\frac{\mu^2}{\pi} \right)^\epsilon \Gamma \left(1 - \frac{\epsilon}{2} \right) \Gamma \left(1 + \frac{3}{2} \epsilon \right) \left[\frac{1}{2\epsilon} \int_0^1 dx_3 J_x J_y - J \right] \quad (259)$$

$$J_x = \int_0^1 dx_2 x_2^\epsilon (1-x_2)^{2\epsilon} \bar{\chi}^{-1-3\epsilon/2}(x_2 x_3), \quad J_y = \int_0^1 dy_2 y_2^{-\epsilon} \bar{\chi}^{-1+\epsilon/2}(1 - (1-x_3)y_2), \quad (260)$$

$$J = \int dC_4(\{x\}, y_2) \frac{1}{x_1 \bar{\chi}(x_2 x_3)} \left[\frac{x_2(1-x_2)}{x_1 y_2 \bar{\chi}(x_2 x_3) + x_2(1-x_2) \mathcal{B}_H} - \frac{1}{\mathcal{B}_H^0} \right]. \quad (261)$$

Here we define $\mathcal{B}_H^0 = \mathcal{B}_H(x_1 = 0) = \bar{\chi}(1 - (1-x_3)y_2)$. The quadratic forms corresponding to J_x and J_y can be treated according to:

$$\begin{aligned} \bar{\chi}^\mu(x_2 x_3) &= \frac{1}{B_\chi} \left[1 - \frac{1}{2(\mu+1)} \left(x_2 - \frac{\bar{X}_\chi}{x_3} \right) \partial_{x_2} \right] \bar{\chi}^{\mu+1}(x_2 x_3) \\ \bar{\chi}^\mu(1 - (1-x_3)y_2) &= \frac{1}{B_\chi} \left[1 - \frac{1}{2(\mu+1)} \left(y_2 - \frac{X_\chi}{1-x_3} \right) \partial_{y_2} \right] \bar{\chi}^{\mu+1}(1 - (1-x_3)y_2). \end{aligned} \quad (262)$$

After integration by parts we write $J_{x,y}$ as

$$J_x = \frac{1}{2B_\chi} \int_0^1 dx_2 [I_x^0 + I_x^1 \epsilon] \quad J_y = \frac{1}{2B_\chi} \int_0^1 dy_2 [I_y^0 + I_y^1 \epsilon] \quad (263)$$

$$\begin{aligned} I_x^0 &= \ln \bar{\chi}(x_2 x_3) + \frac{\bar{X}_\chi}{x_3} \ln \frac{\bar{\chi}(x_3)}{\bar{\chi}(0)} - \ln \bar{\chi}(x_3) + 2 \\ I_x^1 &= -\frac{3}{4} \ln^2 \bar{\chi}(x_2 x_3) + (\ln x_2 + 2 \ln(1-x_2)) \ln \bar{\chi}(x_2 x_3) - \frac{\bar{X}_\chi}{x_2 x_3} \ln \frac{\bar{\chi}(x_2 x_3)}{\bar{\chi}(0)} \\ &\quad - \frac{2}{1-x_2} \left(1 - \frac{\bar{X}_\chi}{x_3} \right) \ln \frac{\bar{\chi}(x_2 x_3)}{\bar{\chi}(x_3)} - \frac{3}{4} \frac{\bar{X}_\chi}{x_3} \ln \frac{\bar{\chi}(x_3)}{\bar{\chi}(0)} \left[\ln \bar{\chi}(x_3) + \ln \bar{\chi}(0) \right] + \frac{3}{4} \ln^2 \bar{\chi}(x_3) - 6 \\ I_y^0 &= \ln \bar{\chi}(1 - (1-x_3)y) + \frac{X_\chi}{1-x_3} \ln \frac{\bar{\chi}(x_3)}{\bar{\chi}(1)} - \ln \bar{\chi}(x_3) + 2 \\ I_y^1 &= \frac{1}{4} \ln^2 \bar{\chi}(1 - (1-x_3)y) - \ln y \ln \bar{\chi}(1 - (1-x_3)y) + \frac{X_\chi}{y(1-x_3)} \ln \frac{\bar{\chi}(1 - (1-x_3)y)}{\bar{\chi}(1)} \\ &\quad + \frac{1}{4} \frac{X_\chi}{1-x_3} \ln \frac{\bar{\chi}(x_3)}{\bar{\chi}(1)} \left[\ln \bar{\chi}(x_3) + \ln \bar{\chi}(1) \right] - \frac{1}{4} \ln^2 \bar{\chi}(x_3) + 2 \end{aligned} \quad (264)$$

The computation of J , Eqs.(259)–(261), is actually more involved. First of all we transform variables according to $x'_1 = y_2 x_1$. For the term proportional to \mathcal{B}_H we write $1/x_1 = (1-x_1)^2/x_1 + (2-x_1)$. Now J is given by:

$$J = \int dC_3(\{x\}) \int_{x_1}^1 dy_2 \frac{1}{\bar{\chi}} \left\{ \frac{1}{x_1} \left[\frac{x_2(1-x_2)(1-x_1)^2}{x_1 \bar{\chi} + x_2(1-x_2) \bar{\beta}} - \frac{1}{\bar{\beta}_{x_1}} \right] + \frac{x_2(1-x_2)(2-x_1)}{x_1 \bar{\chi} + x_2(1-x_2) \bar{\beta}} \right\}, \quad (265)$$

We have introduced shorthand notations:

$$\bar{\chi} = \bar{\chi}(x_2 x_3), \quad \bar{\beta} = \bar{\beta}(1 - (1-x_3)y_2, 1-x_1), \quad \bar{\beta}_{x_1} = \bar{\chi}(1 - (1-x_3)y_2). \quad (266)$$

Both terms of Eq.(265) are split, i.e.

$$\begin{aligned}
J &= J_{11} + J_{12} + J_{21} + J_{22}, & J_{ij} &= \int dC_3(\{x\}) J'_{ij}, \\
J'_{11} &= \int_{x_1}^1 dy_2 \frac{1}{x_1 \bar{\chi}} \left[\frac{(1-x_1)^2}{\bar{\beta}} - \frac{1}{\bar{\beta}_{x_1}} \right], & J'_{12} &= - \int_{x_1}^1 dy_2 \frac{1}{\bar{\beta}} \frac{(1-x_1)^2}{x_1 \bar{\chi} + x_2 (1-x_2) \bar{\beta}}, \\
J'_{21} &= \int_{x_1}^1 dy_2 \frac{1-x_3}{\bar{\chi}} \frac{x_2 (1-x_2) (2-x_1)}{x_1 \bar{\chi} + x_2 (1-x_2) \bar{\beta}}, & J'_{22} &= \int_{x_1}^1 dy_2 \frac{x_3}{\bar{\chi}} \frac{x_2 (1-x_2) (2-x_1)}{x_1 \bar{\chi} + x_2 (1-x_2) \bar{\beta}},
\end{aligned} \tag{267}$$

In order to compute J_{11} , we use Eq.(262) to increase the power of $\bar{\chi}$ by one unit, while for $\bar{\beta}$ and $\bar{\beta}_{x_1}$ we use:

$$\frac{(1-x_1)^2}{\bar{\beta}} - \frac{1}{\bar{\beta}_{x_1}} = - \frac{1}{2B_\chi} \left[\left(y_2 - \frac{1-(1-x_1)\bar{X}_\chi}{1-x_3} \right) \partial_{y_2} \ln \bar{\beta} - \left(y_2 - \frac{1-\bar{X}_\chi}{1-x_3} \right) \partial_{y_2} \ln \bar{\beta}_{x_1} \right] \tag{268}$$

The presence of $(1-x_1)^2$ is crucial in preventing spurious singularities at $x_1 = 1$. This is the reason of our splitting $1/x_1 = (1-x_1)^2/x_1 + (2-x_1)$. After integration by parts we get:

$$J_{11} = \frac{1}{4B_\chi^2} \int dC_4(\{x\}, y_2) I_x^0 I_{11} \tag{269}$$

$$I_{11} = \frac{1-x_1}{x_1} \left[\ln \frac{\bar{\beta}_0}{\bar{\beta}_{00}} - \ln \frac{\bar{\beta}_2}{\bar{\beta}_{20}} \right] + \frac{x_3 - \bar{X}_\chi}{x_1 (1-x_3)} \ln \frac{\bar{\beta}_1 \bar{\beta}_{20}}{\bar{\beta}_2 \bar{\beta}_{10}} + \frac{\bar{X}_\chi}{1-x_3} \ln \frac{\bar{\beta}_1}{\bar{\beta}_2} \tag{270}$$

where I_x^0 is given in Eq.(264) and the new quadratic forms are given by

$$\begin{aligned}
\bar{\beta}_0 &= \bar{\beta}(x_3 + (1-x_1)(1-x_3)y, 1-x_1), & \bar{\beta}_{00} &= \bar{\chi}(x_3 + (1-x_1)(1-x_3)y), \\
\bar{\beta}_1 &= \bar{\beta}(x_3, 1-x_1), & \bar{\beta}_{10} &= \bar{\chi}(x_3), \\
\bar{\beta}_2 &= \bar{\beta}(1-(1-x_3)x_1, 1-x_1), & \bar{\beta}_{20} &= \bar{\chi}(1-(1-x_3)x_1),
\end{aligned} \tag{271}$$

It can be easily seen that the logarithms vanish when the denominator of the corresponding factor is zero. The result is then smooth enough to be integrated numerically.

For J_{12} , we use Eq.(56) which in the present case reads as follows:

$$\frac{1}{\bar{\beta}} \frac{(1-x_1)^2}{\bar{\xi}} = \frac{1}{B_\chi} \left[\frac{1}{\bar{\xi}} + \frac{1}{2x_1 \bar{\chi}} \left(y_2 - \frac{1-(1-x_1)\bar{X}_\chi}{1-x_3} \right) \partial_{y_2} \ln \left(1 + \frac{x_1 \bar{\chi}}{x_2 (1-x_2) \bar{\beta}} \right) \right], \tag{272}$$

$$\bar{\xi} = x_1 \bar{\chi}(x_2 x_3) + x_2 (1-x_2) \bar{\beta}(1-(1-x_3)y_2, 1-x_1). \tag{273}$$

Now we integrate by parts, obtaining:

$$J_{12} = \frac{1}{2B_\chi} \int dC_4(\{x\}, y_2) I_{12} - \frac{1}{B_\chi} J_{s1}, \quad J_{s1} = \int dC_3(\{x\}) \int_{x_1}^1 dy_2 \bar{\xi}^{-1}, \tag{274}$$

$$\begin{aligned}
I_{12} &= \frac{1-x_1}{x_1 \bar{\chi}} \left[\ln \left(1 + \frac{x_1 \bar{\chi}}{x_2 (1-x_2) \bar{\beta}_0} \right) - \ln \left(1 + \frac{x_1 \bar{\chi}}{x_2 (1-x_2) \bar{\beta}_2} \right) \right] \\
&+ \left(\bar{X}_\chi + \frac{x_3 - \bar{X}_\chi}{x_1} \right) \frac{1}{(1-x_3) \bar{\chi}} \left[\ln \left(1 + \frac{x_1 \bar{\chi}}{x_2 (1-x_2) \bar{\beta}_1} \right) - \ln \left(1 + \frac{x_1 \bar{\chi}}{x_2 (1-x_2) \bar{\beta}_2} \right) \right]
\end{aligned} \tag{275}$$

To compute J_{s1} we perform the change of variable $y_2 \rightarrow (1-y_2)/(1-x_3)$, i.e.

$$\int_0^1 dx_3 \int_{x_1}^1 dy_2 \rightarrow \left[\int_0^1 dy_2 \int_0^{y_2} dx_3 - \int_{1-x_1}^1 dy_2 \int_0^{1-(1-y_2)/x_1} dx_3 \right] \frac{1}{1-x_3} \tag{276}$$

and obtain:

$$J_{s1} = \int dC_3(\{x\}) \int_{x_3}^{1-(1-x_3)x_1} \frac{dy_2}{(1-x_3)\bar{\xi}_s}, \quad \bar{\xi}_s = x_1\bar{\chi} + x_2(1-x_2)\bar{\beta}_s, \quad \bar{\beta}_s = \bar{\beta}(y_2, 1-x_1). \quad (277)$$

For $\bar{\xi}_s$ we have the following BST relation:

$$\bar{\xi}_s^{-1} = \frac{1}{B_\chi \rho} \left\{ 1 - \frac{1}{2} \left[\left(x_3 - \frac{\bar{X}_\chi}{x_2} \right) \partial_{x_3} + \left(y_2 - (1-x_1)\bar{X}_\chi \right) \partial_{y_2} \right] \ln \bar{\xi}_s \right\}, \quad \rho = x_1 + x_2(1-x_2)(1-x_1)^2. \quad (278)$$

Integration by parts gives:

$$J_{s1} = \frac{1}{2B_\chi} \int dC_4(\{x\}, y_2) \frac{I_{s1}}{\rho} \quad (279)$$

$$\begin{aligned} I_{s1} = & \frac{1-x_1}{1-x_3} \left[\left(1 - \frac{\bar{X}_\chi}{x_2} \right) \ln \frac{\bar{\xi}_0}{\bar{\xi}_{01}} - \bar{X}_\chi \ln \frac{\bar{\xi}_1}{\bar{\xi}_2} \right] + \frac{1}{1-x_3} \left[\ln \frac{\bar{\xi}_{11}}{\bar{\xi}_{21}} + \frac{\bar{X}_\chi}{x_2} \ln \frac{\bar{\xi}_1}{\bar{\xi}_{11}} \right. \\ & \left. - \left(1-x_1 + x_1 \frac{\bar{X}_\chi}{x_2} \right) \ln \frac{\bar{\xi}_2}{\bar{\xi}_{21}} \right] + (1-x_1) \left[\ln \bar{\xi}_0 - \frac{\bar{X}_\chi}{x_2} \ln \frac{\bar{\xi}_3}{\bar{\xi}_{31}} - \ln \bar{\xi}_{31} + 2 \right], \end{aligned} \quad (280)$$

where the new quadratic forms, $\bar{\xi}_0$ etc, are given by

$$\begin{aligned} \bar{\xi}_0 &= x_1\bar{\chi} + x_2(1-x_2)\bar{\beta}_0, & \bar{\xi}_{01} &= x_1\bar{\chi}(x_2) + x_2(1-x_2)\bar{\beta}_0, \\ \bar{\xi}_1 &= x_1\bar{\chi} + x_2(1-x_2)\bar{\beta}_1, & \bar{\xi}_{11} &= x_1\bar{\chi}(x_2) + x_2(1-x_2)\bar{\beta}_1, \\ \bar{\xi}_2 &= x_1\bar{\chi} + x_2(1-x_2)\bar{\beta}_2, & \bar{\xi}_{21} &= x_1\bar{\chi}(x_2) + x_2(1-x_2)\bar{\beta}_2, \\ \bar{\xi}_3 &= x_1\bar{\chi}(0) + x_2(1-x_2)\bar{\beta}_3, & \bar{\xi}_{31} &= x_1\bar{\chi}(x_2) + x_2(1-x_2)\bar{\beta}_3, & \bar{\beta}_3 &= (1-x_1)^2\bar{\chi}(x_3). \end{aligned} \quad (281)$$

For J_{21} we perform the same change of variable made for J_{s1} (Eq.(276)), obtaining

$$J_{21} = \int_0^1 dx_1 dx_2 \left[\int_0^1 dy_2 \int_0^{y_2} dx_3 - \int_{1-x_1}^1 dy_2 \int_0^{1-(1-y_2)/x_1} dx_3 \right] \frac{x_2(1-x_2)(2-x_1)}{\bar{\chi}\bar{\xi}_s}. \quad (282)$$

Secondly, we use Eq.(56)

$$\frac{x_2(1-x_2)}{\bar{\chi}\bar{\xi}_s} = \frac{1}{B_\chi} \left[\frac{x_2(1-x_2)}{\bar{\xi}_s} + \frac{1}{2\bar{\beta}_s} \left(x_3 - \frac{\bar{X}_\chi}{x_2} \right) \partial_{x_3} \ln \left(1 + \frac{x_2(1-x_2)\bar{\beta}_s}{x_1\bar{\chi}} \right) \right], \quad (283)$$

Similarly for J_{22} we use:

$$\frac{x_2(1-x_2)}{\bar{\chi}\bar{\xi}} = \frac{1}{B_\chi} \left[\frac{x_2(1-x_2)}{\bar{\xi}} + \frac{1}{2\bar{\beta}_s} \left(x_2 - \frac{\bar{X}_\chi}{x_3} \right) \partial_{x_2} \ln \left(1 + \frac{x_2(1-x_2)\bar{\beta}}{x_1\bar{\chi}} \right) \right], \quad (284)$$

After integration by parts, we collect the results obtaining:

$$J_2 \equiv J_{21} + J_{22} = \frac{1}{2B_\chi} \int dC_4(\{x\}, y_2) (2-x_1) I_2 + \frac{1}{2B_\chi} J_{s2}, \quad (285)$$

$$\begin{aligned} I_2 = & -\frac{1-x_1}{\bar{\beta}_0} \ln \left(1 + \frac{x_2(1-x_2)\bar{\beta}_0}{x_1\bar{\chi}} \right) + \left(x_3 - \frac{\bar{X}_\chi}{x_2} \right) \frac{1}{\bar{\beta}_1} \ln \left(1 + \frac{x_2(1-x_2)\bar{\beta}_1}{x_1\bar{\chi}} \right) \\ & - \left(x_3 - \frac{\bar{X}_\chi}{x_2} \right) \frac{x_1}{\bar{\beta}_2} \ln \left(1 + \frac{x_2(1-x_2)\bar{\beta}_2}{x_1\bar{\chi}} \right) + \frac{\bar{X}_\chi}{x_2} \frac{1-x_1}{\bar{\beta}_3} \ln \left(1 + \frac{x_2(1-x_2)\bar{\beta}_3}{x_1\bar{\chi}(0)} \right), \end{aligned} \quad (286)$$

$$J_{s2} = \int dC_3(\{x\}) \int_{x_1}^1 dy_2 (2-x_1) \frac{x_2 X_\chi + (1-x_2) \bar{X}_\chi + x_2(1-2x_2)(1-x_3)}{x_1 \bar{\chi} + x_2(1-x_2) \bar{\beta}}. \quad (287)$$

To compute J_{s2} we use the same techniques already used for J_{s1} and obtain

$$\begin{aligned} J_{s2} &= \frac{1}{2B_\chi} \int dC_4(\{x\}, y_2) (2-x_1) \left[\frac{x_2 X_\chi + (1-x_2) \bar{X}_\chi}{\rho} I_{s1} + \frac{1-2x_2}{\rho} I_{s2} \right], \\ I_{s2} &= 2x_2(1-x_1)(1-x_3) \ln \bar{\xi}_0 + \left[1 - (1-x_1)x_2 \right] \bar{X}_\chi \ln \bar{\xi}_1 \\ &\quad - \left[x_2(1-x_1)X_\chi + x_1 \bar{X}_\chi \right] \ln \bar{\xi}_2 - (1-x_1) \bar{X}_\chi \ln \bar{\xi}_3 + 2x_2(1-x_1)(1-x_3) \end{aligned} \quad (288)$$

Summarising, we write the result for V^H as

$$\boxed{V^H} = - \left(\frac{\mu^2}{\pi} \right)^\epsilon \Gamma(1+\epsilon) \left(\frac{1}{\epsilon} V_{-1}^H + V_0^H \right) \quad (289)$$

$$\begin{aligned} V_{-1}^H &= -\frac{1}{8B_\chi^2} \int dC_4(\{x\}, y_2) I_x^0 I_y^0, \\ V_0^H &= \int dC_4(\{x\}, y_2) \left\{ \frac{1}{2B_\chi} \left[I_{12} + (2-x_1)I_2 \right] + \frac{1}{4B_\chi^2} \left[-\frac{1}{2} (I_x^0 I_y^1 + I_x^1 I_y^0) \right. \right. \\ &\quad \left. \left. + I_x^0 I_{11} + \frac{(2-x_1)[x_2 X_\chi + (1-x_2) \bar{X}_\chi] - 2}{\rho} I_{s1} + (2-x_1) \frac{1-2x_2}{\rho} I_{s2} \right] \right\}, \end{aligned} \quad (290)$$

5.8 Collinear limits of V^H

In the previous section we have derived a suitable integral representation for the V^H diagram in a generic infrared configuration and for arbitrary value of the masses. The resulting representation is stable and can be computed numerically even if it contains several polynomial denominators depending on the integration variables. This is made possible because each denominator is multiplied by a logarithm or a polylogarithm which vanishes exactly at the zeros of the denominator. However it can happen that, for some values of the masses, this compensation is delayed and there we encounter numerical instabilities, revealing a region where the integrand has strong peaks. This is always the case when one of the two masses in the diagram (or both) is vanishing, i.e. in the collinear region.

For example, if we consider the expression of I_x^0 of Eq.(264) the second term is proportional to:

$$\frac{1}{x_3} \ln \frac{\bar{\chi}(x_3)}{\bar{\chi}(0)} = \frac{1}{x_3} \ln \left(1 + \frac{-P^2 x_3 + P^2 - M^2 + m^2}{M^2} x_3 \right) \quad (291)$$

In this term the stability around $x_3 = 0$ is at stake when M^2 is small compared to $|P^2|$.

In all these cases one has to compute explicitly the leading behaviour of the diagram, leaving a stable remainder. We have considered the following collinear limits of V^H : a) $m^2 = M^2 \ll |P^2|$ and b) $m^2 \ll M^2 \ll |P^2|$. In both cases, we have found that it is better to change Feynman parametrization and proceed in the following way (see also [5] section 10.2). Starting from Eq.(244), we first combine propagators $[1]_H - [2]_H$ with parameter z_1 , propagators $[3]_H - [4]_H$ with z_2 and $[5]_H - [6]_H$ with z_3 :

$$\pi^4 V_0^H = \mu^{2\epsilon} \int dC_3(\{z\}) \int d^n q_1 d^n q_2 \frac{1}{[12]_H^2 [34]_H^2 [56]_H^2}, \quad (292)$$

$$[12]_H = [1]_H (1-z_1) + [2]_H z_1, \quad [34]_H = [4]_H (1-z_2) + [3]_H z_2, \quad [56]_H = [5]_H (1-z_3) + [6]_H z_3. \quad (293)$$

Next we combine $[12]_H - [34]_H$ with parameter x and integrate in q_1 , obtaining:

$$\pi^2 V_0^H = \mu^{2\epsilon} i \pi^{-\epsilon/2} \Gamma\left(2 + \frac{\epsilon}{2}\right) \int_0^1 dx \int dC_3(\{z\}) [x(1-x)]^{-1-\epsilon/2} \int d^n q_2 \frac{1}{[1234]_H^{2+\epsilon/2} [56]_H^2}, \quad (294)$$

$$[1234]_H = [q_2 + (1 - z_1)p_2 - z_2 P]^2 + \frac{\chi(z_1; p_2^2; m_1^2, m_2^2)}{x} + \frac{\chi(z_2; P^2; m_4^2, m_3^2)}{1 - x}, \quad (295)$$

with χ defined in Eq.(9). Finally we introduce the parameter y for the remaining two denominators and integrate in q_2 :

$$V_0^H = - \left(\frac{\mu^2}{\pi} \right)^\epsilon \Gamma(2 + \epsilon) \int_0^1 dx \int_0^1 dy \int dC_3(\{z\}) [xy(1-x)]^{1+\epsilon/2} (1-y) U_H^{-2-\epsilon} \quad (296)$$

$$U_H = xy(1-x)(1-y) [-P^2(z_2-z_3)(1-z_1-z_2) + p_1^2(z_2-z_3)(1-z_1-z_3) + p_2^2(1-z_1-z_3)(1-z_1-z_2)] \\ + y(1-x)\chi(z_1; p_2^2; m_1^2, m_2^2) + xy\chi(z_2; P^2; m_4^2, m_3^2) + x(1-x)(1-y)\chi(z_3; p_1^2; m_5^2, m_6^2) \quad (297)$$

Inserting the values corresponding to the infrared configuration of Fig. 12 we get (after the change of variable $z_3 \rightarrow 1 - z_3$):

$$V_0^H = - \left(\frac{\mu^2}{P^2 \pi} \right)^\epsilon \frac{\Gamma(2 + \epsilon)}{P^4} \int dC_5(x, y, \{z\}) [xy(1-x)]^{1+\epsilon/2} (1-y) (a_0 + a_m \epsilon_m + a_M \epsilon_M)^{-2-\epsilon} \quad (298)$$

$$a_0 = xy \left\{ (1-x)(1-y) [z_1 z_2 z_3 + (1-z_1)(1-z_2)(1-z_3)] + (x+y-xy) z_2 (1-z_2) \right\} \quad (299)$$

$$a_m = x \left\{ y(1-x)(1-y) [z_1 z_2 + z_2(1-z_3) + (1-z_1)(1-z_3)] + (1-x)(1-y)^2(1-z_3)^2 + y(x+y-xy) z_2 \right\}$$

$$a_M = y \left\{ x(1-x)(1-y) [z_1 z_3 + z_1(1-z_2) + (1-z_2)(1-z_3)] + (1-x)(1-x+xy) z_1^2 + x(x+y-xy)(1-z_2) \right\}$$

We have also introduced the (small) ratios $\epsilon_m = m^2/P^2$ and $\epsilon_M = M^2/P^2$. The polynomials a_0 , a_1 and a_2 are positive definite in the integration region, but vanish at the hedge. These zeros are responsible for the infrared pole and the collinear divergencies.

At first we perform a Mellin-Barnes splitting, once for case a) and twice for case b):

$$\text{a) } V_0^H = - \left(\frac{\mu^2}{P^2 \pi} \right)^\epsilon \frac{\Gamma(2 + \epsilon)}{P^4} \frac{1}{2\pi i} \int_{-i\infty}^{+i\infty} ds \text{ B}(s, 2 + \epsilon - s) \\ \times \int dC_5(x, y, \{z\}) [xy(1-x)]^{1+\epsilon/2} (1-y) a_0^{-s} (a_m + a_M)^{s-2-\epsilon} \epsilon_m^{s-2-\epsilon}$$

$$\text{b) } V_0^H = - \left(\frac{\mu^2}{P^2 \pi} \right)^\epsilon \frac{\Gamma(2 + \epsilon)}{P^4} \left(\frac{1}{2\pi i} \right)^2 \int_{-i\infty}^{+i\infty} ds dt \text{ B}(s, 2 + \epsilon - s) \text{ B}(t, s - t) \\ \times \int dC_5(x, y, \{z\}) [xy(1-x)]^{1+\epsilon/2} (1-y) a_0^{-t} (a_m \epsilon_m)^{s-2-\epsilon} (a_M \epsilon_M)^{t-s} \quad (300)$$

where $0 < \text{Re } s < 2 + \epsilon$ and $0 < \text{Re } t < \text{Re } s$. For the s and t integrations we close the integration contour in the positive real half-plane and compute the residues at the poles of s and t (which are $t \sim s \sim n + \alpha\epsilon$, $n \geq 2$). Since we are interested in the leading behaviour in $\epsilon_m \rightarrow 0$ and $\epsilon_M \rightarrow 0$, we restrict our attention to the poles at $n = 2$ (higher values of n would lead to terms proportional to ϵ_m^{n-2} or ϵ_M^{n-2}).

A problem connected to case b) is the appearance of poles at $t = 2 + \epsilon$ together with poles at $t = s$ and $s = 2 + \epsilon$. The residue of these poles in t generates terms containing all powers of ϵ_m/ϵ_M ; without an assumption on the value of the ratio ϵ_m/ϵ_M , we would be forced to consider all poles at $s = n + \alpha\epsilon$ ($n \geq 2$) and to resum the series. For this reason we limit our analysis to $m^2 \ll M^2$ and neglect in this way all contributions proportional to m^2/M^2 .

The poles in s and t come from the integration over Feynman parameters and are, obviously, related to the zeros of a_0 , a_1 and a_2 . These three polynomials can vanish only at the end point of the integration region; in order to bring all the zeros to the origin, we first split the integration domain of each variable (for x and y this is actually not necessary) according to the following rule:

$$\int_0^1 dz f(z) = \left[\int_0^{1/2} dz + \int_{1/2}^1 dz \right] f(z) = \frac{1}{2} \int_0^1 dz \left[f\left(\frac{z}{2}\right) + f\left(\frac{2-z}{2}\right) \right]. \quad (301)$$

In this way we disentangle $z = 0$ from $z = 1$; then we remap each sector into $[0, 1]$, moving all end-point singularities in $z = 0$. Applying this decomposition to the z_i integrals we obtain eight new integrals. Consider one of the integrals generated in case a) where the poles are at $s = 2 + \alpha \epsilon$,

$$I(s) = \int dC_5(x, y, \{z\}) (xy)^{1-s+\epsilon/2} (1-x)^{1+\epsilon/2} (1-y) A_{a_1}^{-s} (B_{a_1} \epsilon_m)^{s-2-\epsilon} \quad (302)$$

$$\begin{aligned} A_{a_1} &= (1-x)(1-y) [z_1 z_2 z_3 + (2-z_1)(2-z_2)(2-z_3)] + 2(x+y-xy) z_2 (2-z_2) \\ B_{a_1} &= (1-x) \left[2xy(1-y)(4-2z_3+z_1 z_3) + y(1-x+xy) z_1^2 + x(1-y)^2 (2-z_3)^2 \right] + 4xy(x+y-xy) \end{aligned} \quad (303)$$

To extract the proper behaviour around $x = y = 0$, we apply a sector decomposition (see section 3.2):

$$\begin{aligned} I(s) &= \int dC_5(x, y, \{z\}) (xy)^{1-s} (1-xy) \left[y^{\epsilon/2} (1-x)^{1+\epsilon/2} A_{a_{1,1}}^{-s} B_{a_{1,1}}^{s-2-\epsilon} \right. \\ &\quad \left. + x^{\epsilon/2} (1-xy)^{\epsilon/2} (1-y) A_{a_{1,2}}^{-s} B_{a_{1,2}}^{s-2-\epsilon} \right] \epsilon_m^{s-2-\epsilon} \end{aligned} \quad (304)$$

$$\begin{aligned} A_{a_{1,1}} &= (1-x)(1-xy) [z_1 z_2 z_3 + (2-z_1)(2-z_2)(2-z_3)] + 2x(1+y-xy) z_2 (2-z_2) \\ B_{a_{1,1}} &= 2xy(1-x)(1-xy)(4-2z_3+z_1 z_3) + y(1-x)(1-x+x^2 y) z_1^2 \\ &\quad + (1-x)(1-xy)^2 (2-z_3)^2 + 4x^2 y (1+y-xy) \\ A_{a_{1,2}} &= (1-xy)(1-y) [z_1 z_2 z_3 + (2-z_1)(2-z_2)(2-z_3)] + 2y(1+x-xy) z_2 (2-z_2) \\ B_{a_{1,2}} &= 2xy(1-xy)(1-y)(4-2z_3+z_1 z_3) + (1-xy)(1-xy+xy^2) z_1^2 \\ &\quad + x(1-xy)(1-y)^2 (2-z_3)^2 + 4xy^2 (1+x-xy) \end{aligned} \quad (305)$$

The poles are at $s = 2 + \epsilon/2$ and $s = 2$ (both $B_{a_{1,1}}$ and $B_{a_{1,2}}$ are not vanishing at $x = y = 0$). and we use Eq.(3) to extract the poles. All integrals that appear in the evaluation of the diagram have been analyzed according to this strategy. The coefficients of the collinear logarithms are computed with a numerical integration with a result that agrees with all analytical expansions which have been presented in the literature. Our numerical findings can be summarized by means of the following formulas:

$$V^H = - \left(\frac{\mu^2}{P^2 \pi} \right)^\epsilon \Gamma(1+\epsilon) \left[V_{-1}^H \epsilon^{-1} + V_0^H \right], \quad (306)$$

For case a) we obtain

$$V_i^H = -\frac{1}{P^4} \sum_{n=0}^4 a_n^{(i)} \ln^n \frac{m^2}{P^2} + \mathcal{O} \left(\frac{m^2}{P^2} \right) + \mathcal{O} \left(\frac{m^2 - M^2}{m^2 + M^2} \right), \quad i = -1, 0 \quad (307)$$

$$\begin{aligned} a_0^{(-1)} &= -2.40409(3), & a_1^{(-1)} &= -3.289868(2), & a_2^{(-1)} &= 0, & a_3^{(-1)} &= -\frac{2}{3}, & a_4^{(-1)} &= 0, \\ a_0^{(0)} &= -10.007(2), & a_1^{(0)} &= 1.2020(2), & a_2^{(0)} &= 4.934802(8), & a_3^{(0)} &= 0, & a_4^{(0)} &= \frac{1}{6}. \end{aligned} \quad (308)$$

For case b)

$$V_i^H = -\frac{1}{P^4} \sum_{n,k=0}^4 b_{n,k}^{(i)} \ln^n \frac{m^2}{P^2} \ln^k \frac{M^2}{P^2} + \mathcal{O} \left(\frac{m^2}{P^2} \right) + \mathcal{O} \left(\frac{m^2}{M^2} \right), \quad i = -1, 0 \quad (309)$$

$$\begin{aligned} b_{0,0}^{(-1)} &= -2.40411(3), & b_{1,0}^{(-1)} &= b_{1,0}^{(-1)} = -1.644834(1), \\ b_{2,0}^{(-1)} &= b_{1,1}^{(-1)} = b_{0,2}^{(-1)} = 0, & b_{3,0}^{(-1)} &= b_{0,3}^{(-1)} = -\frac{1}{12}, & b_{2,1}^{(-1)} &= b_{1,2}^{(-1)} = -\frac{1}{4}, \\ b_{4,0}^{(-1)} &= b_{3,1}^{(-1)} = b_{2,2}^{(-1)} = b_{1,3}^{(-1)} = b_{0,4}^{(-1)} = 0, \end{aligned} \quad (310)$$

$$\begin{aligned} b_{0,0}^{(0)} &= 0.8118(3), & b_{1,0}^{(0)} &= 3.00514(3), & b_{1,0}^{(0)} &= -4.20720(5), \\ b_{2,0}^{(0)} &= 1.23370(1), & b_{1,1}^{(0)} &= 0.82246(3), & b_{0,2}^{(0)} &= 2.87863(1), & b_{3,0}^{(0)} &= b_{2,1}^{(0)} = b_{1,2}^{(0)} b_{0,3}^{(0)} = 0, \\ b_{4,0}^{(0)} &= \frac{1}{24}, & b_{3,1}^{(0)} &= \frac{1}{12}, & b_{2,2}^{(0)} &= 0, & b_{1,3}^{(0)} &= -\frac{1}{12}, & b_{0,4}^{(0)} &= \frac{1}{8}, \end{aligned} \quad (311)$$

5.9 A detailed study of the V^H configurations

We use V^H as a prototype for discussing the classification of configurations that, for each family of diagrams, are infrared divergent (at least the QED-like). The tools are the corresponding Landau equations and a necessary condition for some configuration to be infrared divergent is that the Landau equations are satisfied. At first we enumerate internal masses and internal vertices of V^H , as done in Fig. 13. Then we

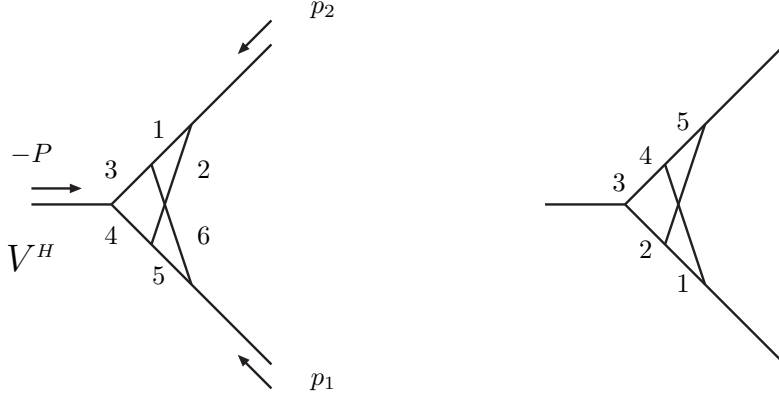


Figure 13: Enumeration of internal masses and of internal vertices for V^H .

look for a non-trivial solution of the Landau equations where P^2 or $p_1^2(p_2^2)$ are unconstrained and one or two internal masses are zero, according to the rules of the standard model: there is no tri-linear vertex with two photon lines. In this operation particular care must be devoted in recognizing topologically equivalent diagrams. An example is illustrated in Fig. 14 where it would be enough to compute our standard definition

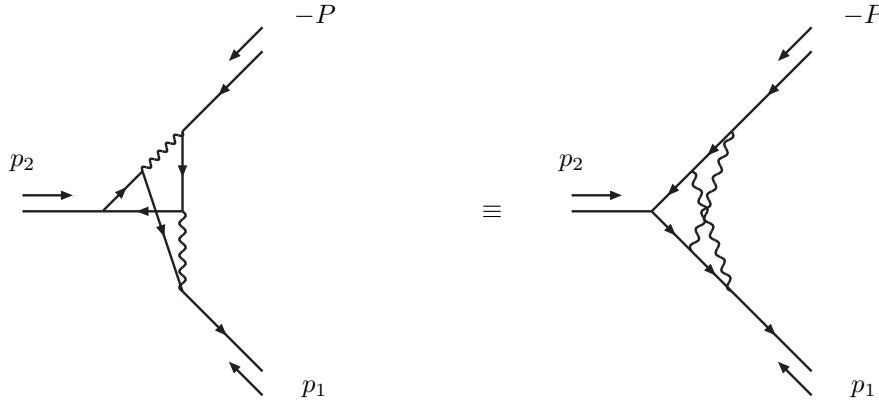


Figure 14: Equivalence of two configurations of the V^H -type containing two internal photonic lines.

for V^H and to perform a permutation of its arguments. The equivalence can be shown by simply enumerating the internal vertices and corresponds to $(12345) \leftrightarrow (34521)$. A second example is given in Fig. 15 where the equivalence is $(12345) \leftrightarrow (14325)$. For all diagrams but V^H we can solve the set of Landau equations, looking for the leading or the sub-leading singularities, in the general case and we have an explicit condition on internal masses and external momenta which express the singular configurations. For V^H there is no known general expression and the set of eight equations that we can write must be examined configuration by configuration. For instance, given propagators $[i]_H$, $i = 1 \dots 6$, the *standard* configuration with $p_1^2 = -M^2$, $p_2^2 = -m^2$, $m_1 = m_3 = m$, and $m_4 = m_5 = M$, $m_2 = m_6 = 0$, has a solution with P^2 unconstrained, $\alpha_2, \alpha_6 \neq 0$ and $\alpha_1 = \alpha_3 = \alpha_4 = \alpha_5 = 0$. Clearly, this has to be put in correspondence with a non-leading singularity; we stress that to have a non-trivial solution is the necessary condition for a singularity, but the

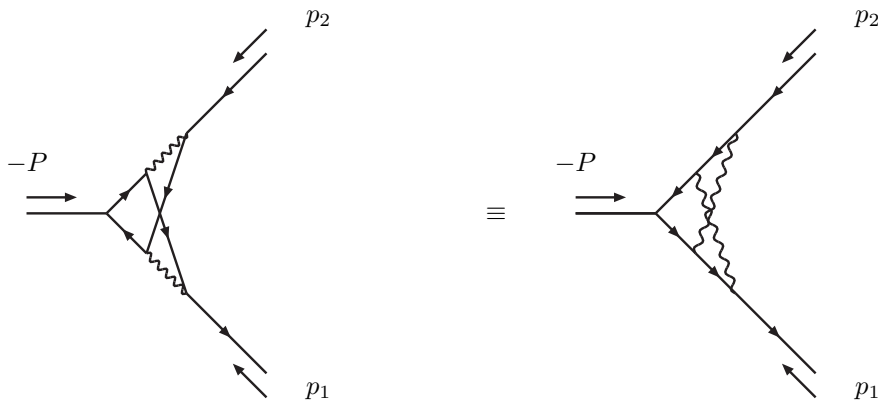


Figure 15: Equivalence of two configurations of the V^H -type containing two internal photonic lines.

final presence of the singularity follows from infrared power-counting. Indeed, this configuration of V^H has a single pole at $\epsilon = 0$, as well-known.

The configuration where $m_1 = m_5 = 0$ needs not to be considered, given the equivalence of Fig. 15. This exhausts the configurations where we have two internal photons, no tri-linear couplings with two photonic legs and both photons attached to a current with one external, on-shell, line. If the last condition is relaxed we can consider a configuration $m_1 = m_4 = 0$, $m_3 = m_6 = m$, $m_2 = m_5 = M$ where we only require that both lines attached to a photon have the same mass. From the system of Landau equations we observe a possible solution with only $\alpha_1 \neq 0$ which requires $p_2^2 = -M^2$ (on-shell condition) and some peculiar relation between P^2 and p_1^2 , namely $p_1^2 = -2(-Mm + 1/2 M^2 - 1/2 P^2)$. Finally, we consider the case of only one internal photon. The typical configuration has $p_1^2 = -M^2$, $p_2^2 = -m^2$, and $m_1 = m_3 = m$, $m_4 = m_5 = M_1$, $m_2 = 0$, $m_6 = M_2$. This is a non-trivial solution but infrared power counting shows that it does not correspond to a singularity. One starts from some parametrization of the diagram, performs sector decomposition and obtains expressions of the form given in Eq.(27) with $A \geq 0$.

6 Behaviour of two - loop vertices in the collinear limit

All results derived in this paper have a common property: diagrams are given in terms of integral representations where integrands are smooth functions thus allowing for a stable numerical integration. These integral representations have been obtained in several ways: we have used BST functional relations which force the appearance of B_χ factors in the denominator; their zeros correspond to anomalous (normal) thresholds of the diagram. Far from threshold we register very good stability in the numerical integration, but even near threshold we have been able to find quite stable results.

For those cases where we have not been able to find the proper BST algorithm we, nevertheless, succeeded in writing an integral representation of the following form:

$$\int dC_k(\{x\}) \frac{1}{A} \ln \left(1 + \frac{A}{B} \right) \quad \text{or} \quad \int dC_k(\{x\}) \frac{1}{A} \text{Li}_n \left(\frac{A}{B} \right) \quad (312)$$

where A, B are multivariate polynomials in the Feynman parameters. These representations generalize the class of Nielsen polylogarithms where we only deal with monomials in one variable. In a word, two - loop diagrams are always reducible to combinations of integrals of the type given in Eq.(312) where the usual monomials that appear in the integral representation of Nielsen - Goncharov generalized polylogarithms are replaced by multivariate polynomials of arbitrary degree. We have made no attempt towards an analytical classification of these new transcendental functions; rather, we compute them numerically, possibly after the elimination of apparent singularities by means of sector decomposition techniques.

Problems with numerical integration arise whenever A and B become small in the same region of Feynman parameters and this usually occurs when some mass is much smaller than the largest scale of the diagram,

i.e. in the collinear regions. In order to have a better understanding of the collinear limit, we consider the case of Eq.(243); here one of the terms in our representation is

$$\int_0^1 dx dy \frac{1}{\chi(y)} \text{Li}_2 \left(\frac{x \chi(y)}{y M^2} \right) \quad A \equiv x \chi(y) = x \left[-P^2 y^2 + (P^2 - m^2 + M^2) y + m^2 \right], \quad B \equiv M^2 y. \quad (313)$$

Here numerical instabilities may arise from two specific regions: M^2 is much smaller than A which means that B is always small, m^2 is much smaller than $|P^2|$ so that one zero of A is near $y = 0$, where also B vanishes. Both regions are indeed of collinear nature. To conclude this section we list some useful expansions of one-dimensional integrals which often occur in our results. The following formulae are used to extract collinear logarithms in order to obtain numerical stability in the collinear regions.

The expansions have been implemented in the procedure of numerical integration which decides if we need to compute the diagram in the collinear region or not and uses the collinear expansion or the initial integral representation.

All collinear divergencies occur at the border of the integration domain which, for one-dimensional integrals means $x = 0$ or $x = 1$. The latter case can always be eliminated with a change of variable, $x \rightarrow 1 - x$. Therefore, all integrals in collinear regions which occur in our results can be cast in one of the following forms, where $Q(x) = ax^2 + bx + c - i\delta$, with $\delta \rightarrow 0_+$ and $R(x) = Q(x)/(dx)$:

$$I_0^{k,n} = \int_0^1 dx \frac{\ln^k x}{x} \ln^n \frac{Q(x)}{d} \Big|_+, \quad I_1^1 = \int_0^1 \frac{dx}{x} \ln \left(1 + \frac{1}{R(x)} \right), \quad I_1^n = \int_0^1 \frac{dx}{x} \text{Li}_n \left(-\frac{1}{R(x)} \right), \quad (314)$$

$$I_2^1 = \int_0^1 \frac{dx}{Q(x)} \ln(1+R(x)), \quad I_2^n = \int_0^1 \frac{dx}{Q(x)} \text{Li}_n(-R(x)), \quad I_3 = \int_0^1 \frac{dx}{Q(x)} \ln R(x) \ln(1-R(x)).$$

In our example we find a I_2^2 and the two unstable cases correspond respectively to $d \rightarrow 0$ and $c \rightarrow 0$.

When $d \rightarrow 0$, the behaviour of $I_0^{k,n}$ is trivial and I_1^1 is regular. Furthermore, to extract the divergency for I_2^1 and I_2^2 it is enough to use well-known relations among (poly)logarithms of argument z and $1/z$ and then apply the BST method (Eq.(57) and Eq.(54)). After integration by parts, the logarithmic behaviour in d arises naturally without any expansion. The results, collected in appendix E, are therefore valid everywhere. In order to extract the divergent behaviour for $c \rightarrow 0$, we proceed in the following way:

$$\int_0^1 dx f(x, Q(x)) = \int_0^1 dx [f(x, Q(x)) - f(x, bx)] + \int_0^1 dx f(x, bx + c) + \int_0^1 dx [f(x, bx) - f(x, bx + c)], \quad (315)$$

where f is one of the (poly)logarithms of Eq.(315). Only the second integral in Eq.(315) is divergent when $c \rightarrow 0$, we can set $c = 0$ in the first (subtracted) term and the third one is $\mathcal{O}(c)$. The results for the expansion are again listed in appendix E.

7 Numerical Results

In this section we present numerical results for infrared configurations corresponding to two-loop three-point scalar functions. All results are computed numerically using the analytical expressions given in this paper. A particular attention has been devoted to collinear regions where the mass of the outgoing particles is small compared to the incoming momentum.

In our general program, aimed to a numerical evaluation of multi-loop, multi-leg Feynman diagrams we have developed a set of FORTRAN/77 codes which go from standard A_0, \dots, D_0 functions to diagrams presented in this paper. This new ensemble of programs which includes the treatment of complex poles [32] will succeed to the corresponding Library of TOPAZO [33].

The whole collection of codes is heavily based on the NAG-library [30]; while completing the analysis it became natural to consider a migration of the whole set of programs to a stand-alone, FORTRAN/95 version. The outcome of our decision is a brand-new version of our numerical code, *LoopBack* [34], which is fully based on quasi - Montecarlo methods (with a possible extension to a parallelized version) and is presently

under construction. Our FORTRAN/95 version has been adapted from the automatic multi-dimensional integration subroutine DKBVRC, written by Alan Genz; DKBVRC uses randomized Korobov rules [28]

In the migration to FORTRAN/95 we have experienced huge gains in CPU-time, a better numerical precision and we foresee a future release of the code, although the numbers produced for this paper still rely on the (by now) old version. For present numerical results all the vertices are evaluated using the routine D01GDF or D01EAF [30]. The first routine is based on the Korobov-Conroy [29] number theoretic method with a Monte-Carlo error estimate, while the second one uses an adaptive subdivision strategy.

For those configurations where we could compare with analytical results we have adapted our setup to match the known examples. Alternatively we have considered few physically relevant cases, selected among those not presented in the literature, and extracted from processes like $Z^* \rightarrow \bar{f}f$, $H^* \rightarrow W^+W^-$, $t \rightarrow W^+b$, etc. In this paper we use the following input parameter set:

$$\begin{aligned} M_W &= 80.380 \text{ GeV}, & M_Z &= 91.1875 \text{ GeV}, & M_H &= 150 \text{ GeV} \\ m_t &= 174.3 \text{ GeV}, & m_b &= 4 \text{ GeV}, & m_e &= 0.510999 \text{ MeV} \end{aligned} \quad (316)$$

Comparisons have been performed with [15] and the results are shown in Tab. 1, Tab. 3, Tab. 5, Tab. 8, Tab. 10, Tab. 12 and Tab. 13; with [12] and the results are shown in Tab. 14; with [13] and the results are shown in Tab. 15. In the comparison with the work of Bonciani - Mastrolia - Remiddi [15], the evaluated finite part is defined through the following ϵ expansion ²:

$$V_{a;l} = V_{a;l}^{-2} \frac{1}{\epsilon^2} + V_{a;l}^{-1} \frac{1}{\epsilon} + V_{a;l}^0, \quad \text{etc.} \quad (317)$$

For the comparison with the work of Davydychev - Kalmykov [12] we use V_a^K of Fig. 10 with $m_1 = m_2 = m_3 (= 180 \text{ GeV})$, $m_i = 0, i \geq 4$ and $p_i^2 = 0$ (which is related to $H^* \rightarrow gg$). We compute

$$V_a^K = \left(\frac{\mu^2}{\pi} \right)^\epsilon \Gamma^2 \left(1 + \frac{\epsilon}{2} \right) (V_{-2;\kappa} \frac{1}{\epsilon^2} + V_{-1;\kappa} \frac{1}{\epsilon} + V_{0;\kappa}). \quad (318)$$

Note that the presence of a double pole in Eq.(318) reflects a collinear singularity besides the infrared one. For the comparison with the work of Davydychev-Smirnov [13] we consider the diagram V_c^K of Fig. 10 with $m_1 = m_4 = m$ and $m_2 = m_6 = M$. The analytical calculation is valid in the region $m^2 \ll M^2, |P|^2$, and we define

$$V_c^K = \left(\frac{\mu^2}{\pi} \right)^\epsilon \Gamma(2 + \epsilon) (V_{-2;\kappa} \frac{1}{\epsilon^2} + V_{-1;\kappa} \frac{1}{\epsilon} + V_{0;\kappa}). \quad (319)$$

For all comparisons performed in this paper we have found an excellent agreement with analytical calculations,³ therefore signaling a satisfactory status of the overall goodness of our numerical algorithms. Needless to say, we have been able to produce results having no counter-examples in the literature.

In Tab. 16 we give a sample of results for the numerical integration of tensor integrals. The relevant message is that all analytical expressions which have been implemented in our code for tensor integrals has been derived using the same techniques already used for scalar configurations.

The topology chosen for tensor integrals is $V_{c;\kappa}$, which enters in the computation of the fermionic corrections to $\sin^2 \theta_{\text{eff}}$ and these results have been already used in [7]; this emphasizes the overall relevance of our results.

The tensor structure considered in this brief example is:

$$\begin{aligned} V_{c;\kappa} &= \frac{\mu^{2\epsilon}}{\pi^4} \int \frac{d^n q_1 d^n q_2}{\prod_{l=1}^6 [l]_\kappa}, & V_{c;\kappa|i}^\mu &= \frac{\mu^{2\epsilon}}{\pi^4} \int d^n q_1 d^n q_2 \frac{q_i^\mu}{\prod_{l=1}^6 [l]_\kappa} = \sum_{j=1}^2 V_{c;\kappa|ij} p_j^\mu, \\ V_{c;\kappa|i_1 i_2}^{\mu\nu} &= \frac{\mu^{2\epsilon}}{\pi^4} \int d^n q_1 d^n q_2 \frac{q_{i_1}^\mu q_{i_2}^\nu}{\prod_{l=1}^6 [l]_\kappa} = \sum_{j_1, j_2=1}^2 V_{c;\kappa|i_1 j_1 i_2 j_2} p_{j_1}^\mu p_{j_2}^\nu + V_{c;\kappa|i_1 0 i_2 0} \delta^{\mu\nu}, \end{aligned} \quad (320)$$

where $[l]_\kappa$ has been defined in Eq.(148). The ϵ expansion for the coefficients is $V_{c;\kappa} = V_{c;\kappa}^{-1} / \epsilon + V_{c;\kappa}^0$.

²Note that these authors define $n = 4 - 2\epsilon$. Therefore the ϵ of the following formula corresponds to 2ϵ of [15]

³In several cases we had to code the analytical results since the authors did not present explicit numerical results

8 Conclusions

In this paper we have analyzed a special component of our project aimed to a numerical evaluation of physical observables at the two-loop level: since QED/QCD are an integral part of any realistic theory and they are characterized by the exchange/emission of massless gauge-bosons leading to infrared divergent parts we had to prove that infrared and also collinear configurations can be treated within the same class of algorithms which we have used for massive configurations or, at least, within some simple extension of them.

The main result, therefore, has been to assemble relatively simple expressions for scalar two-loop vertices in a systematic and coherent manner so that they can be used for practical calculations. Our results introduce integral representations which are well suited for numerical integration and represent a generalization of the familiar Nielsen - Goncharov multivariate polylogarithms.

Confining most of the paper to scalar configurations should not be confused with a limitation of the method. Tensor integrals that arise in any non-trivial theory, due to the spin structure, simply add extra polynomials of Feynman parameters in the integral representations of the diagrams. One can easily see, for instance from Eq.(73), that these additional polynomials can only change the numerator structure inside Eq.(76) which is at the basis of our results: we simply get an hypergeometric function with a different list of arguments and the whole derivation can be carried through along the same lines used for a scalar integrand.

Another important issue that has been addressed in this paper concerns the systematization of any procedure for implementing infrared divergent graphs in a realistic calculation, at least when using a modern language and when considering QED (and also QCD) as embedded into a larger theory. Indeed, QED alone with a massive regulator has been treated long ago in a seminal paper by Cvitanovic and Kinoshita [24].

In the final stage of our project we will generate diagrams with the help of *GraphShot* [31]: each diagram where an internal photon (or gluon) line appears will be subjected to a special investigation, namely the corresponding Landau equations will be examined. As soon as they are fulfilled by the kinematical configuration that we are scanning and as soon as the filter of infrared power-counting is passed we know that the configuration is infrared singular and the appropriate subroutine will be initialized returning numerical answers for the residues and the finite part. Understanding these motivations will hopefully explain our preference for extending the numerical treatment to infrared divergent configuration despite the recent, spectacular, progress in analytical evaluation.

For instance, one of our configurations, V^κ , has been already computed by Davydychev and Smirnov [13] in the limit $m^2 \ll M^2, |P^2|$; we have found excellent agreement and have able to extend the numerical results to all values of m , therefore allowing for QCD corrections to the top quark decay without approximations for internal masses. For another setup of the same V^κ configuration we have another result by Davydychev and Kalmykov [12] which is relevant for Higgs decay into two photons or two gluons; again we found excellent agreement and are able to produce numerical results for the same diagram embedded into the standard model, e.g. also with W -lines and not only gluons outside the inner massive quark loop. Furthermore, we have been able to perform a numerical test of several analytical results by Bonciani, Mastrolia and Remiddi [15] corresponding to the whole set of two-loop topologies.

To summarize, we have been able to present all formulas that form the basis for numerical evaluation of infrared residues and infrared finite parts of arbitrary infrared configurations of two-loop vertices. The language may sound unfamiliar but our results have far reaching consequences; for instance, some of the results presented here have already been used for computing two - loop electroweak pseudo - observables [7].

Acknowledgments

We gratefully acknowledge discussions and comparisons with Andrei Davydychev, Misha Kalmykov and Volodya Smirnov. We would like to express our gratitude to Roberto Bonciani, Pierpaolo Mastrolia and Ettore Remiddi for discussions and comparisons. The contribution of Andrea Ferroglia to an early stage of this paper is also gratefully acknowledged. We recognize the role played by Stefano Actis in several steps of our global project. S.U. is indebted to W. Hollik for hospitality at MPI where part of the manuscript was written and would like to thank Ulrich Meier for cross-checking some of the results.

A Taylor and Laurent expansion of Euler's functions

Here we collect results needed in expanding Euler's functions; γ is the Euler constant and $\zeta(x)$ is the Riemann zeta function.

$$\begin{aligned}\Gamma(1+z) &= 1 + \sum_{n=1}^{\infty} G_n z^n, & \Gamma(z) &= \frac{\Gamma(1+z)}{z} = \frac{1}{z} + \sum_{n=0}^{\infty} G_{n+1} z^n, \\ G_1 &= -\gamma, & G_2 &= \frac{1}{2} [\gamma^2 + \zeta(2)], & G_3 &= -\frac{1}{6} [\gamma^3 + 3\zeta(2)\gamma + 2\zeta(3)], \\ G_4 &= \frac{1}{24} \gamma^4 + \frac{1}{4} \zeta(2) \gamma^2 + \frac{1}{8} \zeta^2(2) + \frac{1}{3} \zeta(3) \gamma + \frac{1}{4} \zeta(4).\end{aligned}\quad (321)$$

B Nielsen polylogarithms

Throughout the paper we have used (n, p are positive integers)

$$S_{n,p}(z) = \frac{(-1)^{n+p-1}}{(n-1)! p!} \int_0^1 dx \frac{dx}{x} \ln^{n-1} x \ln^p(1-zx), \quad S_{n-1,1}(z) = \text{Li}_n(z) \quad (322)$$

C Properties of the hypergeometric function

The Gauss hypergeometric function [27] is defined by:

$${}_2F_1(a, b; c; x) = \frac{\Gamma(c)}{\Gamma(b)\Gamma(c-b)} \int_0^1 dz z^{b-1} (1-z)^{c-b-1} (1-xz)^{-a}, \quad \text{Re } b > \text{Re } c > 0. \quad (323)$$

The special case $c = b + 1$ frequently occurs in this paper. Sometimes the Gauss hypergeometric series is used (circle of convergence $|x| = 1$):

$${}_2F_1(a, b; b+1; x) = \sum_{n=0}^{\infty} \frac{\Gamma(a+n)}{\Gamma(a)} \frac{b}{b+n} \frac{x^n}{\Gamma(n+1)}. \quad (324)$$

An important property of ${}_2F_1$ used in our paper is ($1-c, b-a, c-b-a$ are not integers):

$${}_2F_1(a, b; b+1; x) = \frac{b}{b-a} (-x)^{-a} {}_2F_1(a, a-b; a-b+1; \frac{1}{x}) + \frac{\Gamma(b+1)\Gamma(a-b)}{\Gamma(a)} (-x)^{-b}, \quad (325)$$

where $|\arg(-x)| < \pi$. In other cases we need an expansion around a vanishing ϵ ; few examples are listed below (see also [35]):

$$\begin{aligned}{}_2F_1(1+\alpha\epsilon, 1+\beta\epsilon; 2+\beta\epsilon; x) &= (1+\beta\epsilon) \left\{ -\frac{\ln(1-x)}{x} + \epsilon \left[\frac{\alpha}{2} \frac{\ln^2(1-x)}{x} - \beta \frac{\text{Li}_2(x)}{x} \right] \right\}, \\ {}_2F_1(2+\alpha\epsilon, 1+\beta\epsilon; 2+\beta\epsilon; x) &= \frac{1+\beta\epsilon}{1+\alpha\epsilon} \left\{ \frac{1}{1-x} + \epsilon \left[(\beta-\alpha) \frac{\ln(1-x)}{x} - \alpha \frac{\ln(1-x)}{1-x} \right] \right\}, \\ {}_2F_1(2+\alpha\epsilon, 2+\beta\epsilon; 3+\beta\epsilon; x) &= \frac{2+\beta\epsilon}{1+\alpha\epsilon} \left\{ \frac{1}{x} \left[\frac{1}{x} \ln(1-x) + \frac{1}{1-x} \right] \right. \\ &\quad \left. + \epsilon \left[\beta \frac{\text{Li}_2(x) + \ln(1-x)}{x^2} - \frac{\alpha}{2} \frac{\ln^2(1-x)}{x^2} - \alpha \frac{\ln(1-x)}{x(1-x)} \right] \right\}, \\ {}_2F_1(2+\alpha\epsilon, \beta\epsilon; 1+\beta\epsilon; x) &= \frac{1}{1+\alpha\epsilon} \left\{ 1 + \epsilon \left[(\alpha-\beta) - \beta \ln(1-x) + \frac{\beta}{1-x} \right] + \epsilon^2 \beta \left[(\alpha-\beta) \text{Li}_2(x) \right. \right. \\ &\quad \left. \left. + \frac{\alpha}{2} \ln^2(1-x) - (\alpha-\beta) \ln(1-x) - \alpha \frac{\ln(1-x)}{1-x} \right] \right\}.\end{aligned}\quad (326)$$

In several cases the hypergeometric function (with integer arguments) leads to elementary transcendental functions:

$${}_2F_1(1, 2; 3; z) = -\frac{2}{z} \left[\frac{1}{z} \ln(1-z) + 1 \right], \quad {}_2F_1(1, 1; 2; z) = -\frac{1}{z} \ln(1-z), \quad (327)$$

$${}_2F_1(2, 2; 3; z) = \frac{2}{z} \left[\frac{1}{z} \ln(1-z) + 1 \right] + \frac{2}{1-z}, \quad {}_2F_1(2, 1; 2; z) = \frac{1}{1-z}. \quad (328)$$

D Computation of the integral $J_{nm}^{kh}(i)$

The function $J_{nm}^{kh}(i)$ is defined by:

$$J_{nm}^{kh}(i) = \int_0^1 dx \int_0^x dy \ln^n x \ln^m y \frac{\ln^k \alpha_i(x)}{\alpha_i(x)} \frac{\ln^h \alpha_i(y)}{\alpha_i(y)}, \quad \alpha_1(z) = \bar{\chi}(z), \quad \alpha_2(z) = \chi(z), \quad (329)$$

where χ and $\bar{\chi}$ are defined in Eq.(9) and Eq.(11), respectively. The integral in Eq.(329) can be computed by using BST functional relations. We first use the following relation:

$$\alpha_i^{-1}(y) \ln^k \alpha_i(y) = \frac{1}{B_\chi} \left[\ln^k \alpha_i(y) - \frac{y - Z_i}{2(k+1)} \partial_y (\ln^{k+1} \alpha_i(y) - \ln^{k+1} \alpha_i(0)) \right], \quad (330)$$

where $Z_1 = \bar{X}_\chi$ and $Z_2 = X_\chi$ (see, once again, Eq.(9)). With respect to the usual BST relation (see Eq.(51)) with have added a term, $\partial_y \ln^{k+1} \alpha_i(0)$, which is actually zero. After the integration by parts, we treat the x -integral through another BST relation:

$$\begin{aligned} \alpha_i^{-1}(x) \ln^k \alpha_i(x) &= \frac{1}{B_\chi} \left[\ln^k \alpha_i(x) - \frac{x - Z_i}{2(k+1)} \partial_x \ln^{k+1} \alpha_i(x) \right]. \\ (x - Z_i) \alpha_i^{-1}(x) \ln^k \alpha_i(x) &= -\frac{1}{2P^2} \frac{\partial_x}{k+1} \ln^{k+1} \alpha_i(x). \end{aligned} \quad (331)$$

The second integration by parts gives:

$$J_{nm}^{k-1, h-1}(i) = \frac{1}{4B_\chi h} \left[\frac{B_{nm}^{k-1, h-1}(i)}{B_\chi k} + \frac{H_{nm}^{k-1, h-1}(i)}{P^2(k+h)} \right], \quad (332)$$

where, new, auxiliary quantities have been introduced:

$$\begin{aligned} B_{nm}^{k-1, h-1}(i) &= \int_0^1 dx \int_0^x dy L_m^{h-1}(y) \ln^{n-1} x \left\{ \ln x l_i^{k-1}(x) [l_i(x) + 2k] + n(x - Z_i) \frac{l_i^k(x)}{x} \right\} \\ &\quad - \sum_{p=0}^m \frac{m!}{p!} (-1)^{m-p} l_i^h(0) \int_0^1 dx \left\{ x \ln^{n+p} x l_i^{k-1}(x) [l_i(x) + 2k] \right. \\ &\quad \left. + (\ln x + n + p)(x - Z_i) \ln^{n+p-1} x l_i^k(x) \right\} - \int_0^1 dy L_m^{h-1}(y) \\ &\quad \times \left[\delta_{n,0} (1 - Z_i) l_i^k(1) - (y - Z_i) \ln^n y l_i^k(y) \right] + \delta_{n,0} (-1)^m m! (1 - Z_i) l_i^k(1) l_i^h(0) \\ H_{nm}^{k-1, h-1}(i) &= (n+m) \int_0^1 dx \ln^{n+m-1} x \left[\frac{l_i^{k+h}(x)}{x} \Big|_+ - \left(1 + \frac{h}{k}\right) l_i^h(0) \frac{l_i^k(x)}{x} \Big|_+ \right] \\ &\quad + \delta_{n,0} \delta_{m,0} \left[l_i^{k+h}(1) - \left(1 + \frac{h}{k}\right) l_i^k(1) l_i^h(0) + \frac{h}{k} l_i^{k+h}(0) \right]. \end{aligned} \quad (333)$$

Furthermore, we have defined:

$$l_i(x) = \ln \alpha_i(x), \quad L_n^{k-1}(y) = \ln^n y l_i^{k-1}(y) [l_i(y) + 2k] + n(y - Z_i) \ln^{n-1} y \frac{l_i^k(y)}{y} \Big|_+ \quad (334)$$

E Useful expansions

Here we discuss various expansions of $I_0^{k,n}$ (defined in Section 6) for $c \rightarrow 0$ in terms of polylogarithms (Eq.(322)). Let $Q(x) = ax^2 + bx + c$ and $e = a + b + c$; we have

$$I_0^{k,n}(a, b, c, d) \equiv \int_0^1 dx \frac{\ln^k x}{x} \ln^n \frac{Q(x)}{d} \Big|_+ = \sum_{h=1}^n (-1)^{k+h} n! \left[\sum_{l=0}^{n-h} \frac{(-1)^l (k+l)!}{l! (n-h-l)!} \ln^{n-h-l} \left(\frac{b}{d} \right) S_{k+l+1,h} \left(-\frac{a}{b} \right) + \frac{k!}{(n-h)!} \ln^{n-h} \left(\frac{c}{d} \right) S_{k+1,h} \left(-\frac{b}{c} \right) \right] + \mathcal{O}(c). \quad (335)$$

Then we consider a class of integrals which generalizes Eq.(130):

$$J_n^k(a, b, c, d) \equiv \int_0^1 dx \frac{\ln^n x}{Q(x)} \ln^k \frac{Q(x)}{d}, \quad (336)$$

They can be computed by using the BST relation Eq.(51) which in the present case reads as follows:

$$\frac{1}{Q(x)} \ln^k \frac{Q(x)}{d} = \frac{1}{B} \left[\ln^k \frac{Q(x)}{d} - \frac{x-X}{2(k+1)} \partial_x \ln^{k+1} \frac{Q(x)}{d} \right], \quad X = -\frac{b}{2a}, \quad B = -\frac{b^2 - 4ac}{4a}. \quad (337)$$

After integration by parts, we get:

$$\begin{aligned} J_n^0 &= \frac{1}{2B} \left\{ \int_0^1 dx (n \ln^{n-1} x + \ln^n x) \ln \frac{Q(x)}{c} - nX I_0^{n-1,1} + 2(-1)^n \Gamma(n+1) \right\}, \\ J_n^{k-1} &= \frac{1}{2Bk} \left\{ \int_0^1 dx \left[2k \ln^n x \ln^{k-1} \frac{Q(x)}{d} + (n \ln^{n-1} x + \ln^n x) \ln^k \frac{Q(x)}{d} \right] - nX I_0^{n-1,k} \right\}, \\ J_0^{k-1} &= \frac{1}{2Bk} \left\{ \int_0^1 dx \ln^{k-1} \frac{Q(x)}{d} \left[\ln \frac{Q(x)}{d} + 2k \right] - (1-X) \ln^k \frac{e}{d} - X \ln^k \frac{c}{d} \right\}, \end{aligned} \quad (338)$$

where for the first two results $n \geq 1$. Now we give the expansion of I_1^n for $c \rightarrow 0$:

$$\begin{aligned} I_1^1 &\equiv \int_0^1 \frac{dx}{x} \ln \left(1 + \frac{dx}{Q(x)} \right) = -\text{Li}_2 \left(-\frac{a}{b+d} \right) + \text{Li}_2 \left(-\frac{a}{b} \right) + \ln \left(\frac{b}{c} \right) \ln \left(1 + \frac{d}{b} \right) + \frac{1}{2} \ln^2 \left(1 + \frac{d}{b} \right) + \mathcal{O}(c), \\ I_1^n &\equiv \int_0^1 \frac{dx}{x} \text{Li}_n \left(-\frac{dx}{Q(x)} \right) = \int_0^1 \frac{dx}{x} \text{Li}_n \left(-\frac{d}{ax+b} \right) \Big|_+ + \ln \left(\frac{b}{c} \right) \text{Li}_n \left(-\frac{d}{b} \right) - S_{n-1,2} \left(-\frac{d}{b} \right) + \mathcal{O}(c), \end{aligned} \quad (339)$$

with $n \geq 2$. Next we give the results for I_2^1 and I_2^2 for $d \rightarrow 0$. The final expression has been derived following the strategy sketched in Section 6 and is valid also for d far from zero.

$$\begin{aligned} I_2^1 &\equiv \int_0^1 \frac{dx}{Q(x)} \ln \left(1 + \frac{Q(x)}{dx} \right) = -\frac{1}{2B} \left\{ \int_0^1 dx \left[\ln \left(1 + \frac{dx}{Q(x)} \right) + \text{Li}_2 \left(-\frac{dx}{Q(x)} \right) \right] \right. \\ &\quad \left. - (1-X) \text{Li}_2 \left(-\frac{d}{e} \right) + X I_1^1 \right\} - J_0^1 + J_1^0, \\ I_2^2 &\equiv \int_0^1 \frac{dx}{Q(x)} \text{Li}_2 \left(-\frac{Q(x)}{dx} \right) = -\frac{1}{2B} \left\{ \int_0^1 dx \left[\text{Li}_2 \left(-\frac{dx}{Q(x)} \right) - \text{Li}_3 \left(-\frac{dx}{Q(x)} \right) \right] \right. \\ &\quad \left. + (1-X) \text{Li}_3 \left(-\frac{d}{e} \right) + X I_1^2 \right\} - \zeta(2) J_0^0 - \frac{1}{2} J_0^2 - \frac{1}{2} J_2^0 + J_1^1. \end{aligned} \quad (340)$$

Finally, expanding I_2^n for $c \rightarrow 0$ we obtain:

$$\begin{aligned} I_2^1 &= \frac{1}{b} \left\{ -\text{Li}_2 \left(-\frac{a}{b+d} \right) + \text{Li}_2 \left(-\frac{a+b}{d} \right) + \ln \frac{d}{c} \ln \left(1 + \frac{b}{d} \right) + \frac{1}{2} \ln^2 \left(1 + \frac{b}{d} \right) - 2\text{Li}_2 \left(-\frac{b}{d} \right) + \mathcal{O}(c) \right\}, \\ I_2^n &= \frac{1}{b} \left\{ \int_0^1 \frac{dx}{x} \text{Li}_n \left(-\frac{ax+b}{d} \right) \Big|_+ - \text{Li}_{n+1} \left(-\frac{a+b}{d} \right) \right. \\ &\quad \left. + \ln \frac{d}{c} \text{Li}_n \left(-\frac{b}{d} \right) - S_{n-1,2} \left(-\frac{b}{d} \right) + (n+1) \text{Li}_{n+1} \left(-\frac{b}{d} \right) + \mathcal{O}(c) \right\}. \end{aligned} \quad (341)$$

F Tables of numerical results

In this section we collect a sample of our numerical results, based on the setup of Eq.(316).

	s	$\text{Re } V_{a;l}^0$	$\text{Im } V_{a;l}^0$
Our	$[500 \text{ GeV}]^2$	$-2.4142(1) \times 10^{-2}$	$4.12(1) \times 10^{-3}$
BMR		-2.414166×10^{-2}	4.121472×10^{-3}
Our	M_Z^2	$-0.61103(4)$	$9.447(6) \times 10^{-2}$
BMR		-0.6110145	9.446769×10^{-2}
Our	$100 m_e^2$	$-6.04493(6) \times 10^7$	$3.0986(2) \times 10^7$
BMR		-6.044903×10^7	3.098533×10^7
Our	$4.0001 m_e^2$	-6.878781×10^{10}	3.906172×10^{11}
BMR		-6.878781×10^{10}	3.906172×10^{11}
Our	m_e^2	8.533838×10^8	0
BMR		not available	0
Our	$-100 m_e^2$	5.463023×10^7	0
BMR		5.463023×10^7	0

Table 1: **Diagram $\mathbf{V}_{a;l}$** . Comparison with the results of [15] (BMR). The setup for Fig. 5 is: $m_1 = m_2 = m = M = m_e$. The unit of mass μ is 1 GeV. Only the infrared finite part is shown. The results are in GeV^{-2} . Unless indicated our relative error is below 10^{-7} .

Process	s	M, m	m_1, m_2	$\text{Re } V_{a;l}^0$	$\text{Im } V_{a;l}^0$
$Z^* \rightarrow e^+e^-$	$[500 \text{ GeV}]^2$	m_e, m_e	m_b, m_b	$-4.7574(4) \times 10^{-2}$	$2.55694(6) \times 10^{-2}$
	$[500 \text{ GeV}]^2$	m_e, m_e	m_t, m_t	$-1.147833(1) \times 10^{-2}$	$4.303633(8) \times 10^{-3}$
$Z \rightarrow e^+e^-$	M_Z^2	m_e, m_e	m_b, m_b	$-7.91577(3) \times 10^{-2}$	$4.74278(5) \times 10^{-2}$
	M_Z^2	m_e, m_e	m_t, m_t	-0.2243587	$9.752214(1) \times 10^{-2}$
$Z^* \rightarrow e^+e^-$	$100 m_e^2$	m_e, m_e	m_b, m_b	-5.665645×10^6	9.745030×10^5
	$100 m_e^2$	m_e, m_e	m_t, m_t	1.987627×10^5	4.155691×10^5
$W \rightarrow e^+\nu_e$	M_W^2	m_e, m_ν	m_t, m_t	-0.7168993	0.1227244
$W^* \rightarrow t\bar{b}$	$[200 \text{ GeV}]^2$	m_t, m_b	m_b, m_b	$-7.158(2) \times 10^{-3}$	$3.3638(2) \times 10^{-2}$
$t \rightarrow W^+b$	m_t^2	m_b, M_W	M_W, M_W	$-2.709610(3) \times 10^{-2}$	$3.182718(2) \times 10^{-2}$

Table 2: **Diagram $\mathbf{V}_{a;l}$** The setup refers to the diagram of Fig. 5 The neutrino mass has been arbitrarily set to $m_\nu = 0.1 \text{ eV}$ The unit of mass μ is 1 GeV Only the infrared finite part is shown. The results are in GeV^{-2} Unless indicated our relative error is below 10^{-7} .

	s	$\text{Re } V_{b,l}^0$	$\text{Im } V_{b,l}^0$
Our	$[500 \text{ GeV}]^2$	-7.102762×10^{-2}	1.914262×10^{-2}
BMR		-7.102885×10^{-2}	1.914295×10^{-2}
Our	M_Z^2	-1.590738	0.4462335
BMR		-1.590738	0.4462335
Our	$100 m_e^2$	-7.073558×10^7	$4.1480(2) \times 10^7$
BMR		-7.073558×10^7	4.148499×10^7
Our	$4.0001 m_e^2$	$-7.264768(2) \times 10^{10}$	4.364353×10^{11}
BMR		-7.264767×10^{10}	4.364353×10^{11}
Our	m_e^2	1.000079×10^9	0
BMR		not available	0
Our	$-100 m_e^2$	6.714222×10^7	0
BMR		6.714222×10^7	0

Table 3: **Diagram $V_{b,l}$** . Comparison with the results of [15] (BMR). The setup for the diagram of Fig. 5 is: $m_1 = m = M = m_e$, $m_2 = 0$. The unit of mass μ is 1 GeV. Only the infrared finite part is shown. The results are in GeV^{-2} . Unless indicated our relative error is below 10^{-7} .

Process	s	M, m	m_1, m_2	$\text{Re } V_{b,l}^0$	$\text{Im } V_{b,l}^0$
$Z^* \rightarrow e^+e^-$	$[500 \text{ GeV}]^2$	m_e, m_e	m_e, M_Z	-8.675940×10^{-3}	4.466520×10^{-3}
	$[500 \text{ GeV}]^2$	m_e, m_e	m_ν, M_W	-8.462338×10^{-3}	4.491430×10^{-3}
$Z \rightarrow e^+e^-$	M_Z^2	m_e, m_e	m_e, M_Z	-0.1618863	7.892145×10^{-2}
	M_Z^2	m_e, m_e	m_ν, M_W	-0.1551424	7.718541×10^{-2}
$Z^* \rightarrow e^+e^-$	$100 m_e^2$	m_e, m_e	m_e, M_Z	-5.936619×10^5	-9.349849×10^4
	$100 m_e^2$	m_e, m_e	m_ν, M_W	-7.285072×10^5	-1.167232×10^5
$W^* \rightarrow t\bar{b}$	$[200 \text{ GeV}]^2$	m_t, m_b	m_b, M_W	-2.383592×10^{-2}	5.899083×10^{-2}
	$[200 \text{ GeV}]^2$	m_t, m_b	m_t, M_H	-3.364485×10^{-2}	7.477385×10^{-2}
$H^* \rightarrow W^+W^-$	$[200 \text{ GeV}]^2$	M_W, M_W	M_W, M_H	-7.102816×10^{-3}	3.303713×10^{-2}

Table 4: **Diagram $V_{b,l}$** . The setup refers to the diagram of Fig. 5. The neutrino mass has been arbitrarily set to $m_\nu = 0.1 \text{ eV}$. The unit of mass μ is 1 GeV. Only the infrared finite part is shown. The results are in GeV^{-2} . Unless indicated our relative error is below 10^{-7} .

	s	$\text{Re } V_{a;M}^0$	$\text{Im } V_{a;M}^0$
Our	$[500 \text{ GeV}]^2$	$2.0928(5) \times 10^3$	$-1.95(3) \times 10^2$
BMR		2.092863×10^3	-1.941897×10^2
Our	M_Z^2	$5.659(1) \times 10^4$	$-5.84(3) \times 10^3$
BMR		5.658944×10^4	-5.837323×10^3
Our	$100 m_e^2$	$6.28283(2) \times 10^{12}$	$-1.70618(2) \times 10^{12}$
BMR		6.282796×10^{12}	-1.706180×10^{12}
Our	$4.0001 m_e^2$	-1.447472×10^{20}	$1.6161(6) \times 10^{21}$
BMR		-1.447472×10^{20}	1.616432×10^{21}
Our	m_e^2	$-3.11237240 \times 10^{14}$	0
BMR		not available	0
Our	$-100 m_e^2$	-6.544718×10^{12}	0
BMR		-6.544718×10^{12}	0

Table 5: **Diagram** $V_{a;M}$. Comparison with the results of [15] (BMR). The setup refers to the diagram of Fig. 7: $m_1 = m_2 = m = M = m_e$. The unit of mass μ is 1 GeV. Only the infrared finite part is shown. The results are in GeV^{-4} . Unless indicated our relative error is below 10^{-7} .

Process	s	M, m	m_1, m_2	$\text{Re } V_{a;M}^0$	$\text{Im } V_{a;M}^0$
$Z^* \rightarrow e^+e^-$	$[500 \text{ GeV}]^2$	m_e, m_e	m_b, m_b	91.02032	$1.5233(1) \times 10^{-6}$
	$[500 \text{ GeV}]^2$	m_e, m_e	m_t, m_t	-24.61950	$-9.6641(1) \times 10^{-10}$
$Z \rightarrow e^+e^-$	M_Z^2	m_e, m_e	m_b, m_b	2.736577×10^3	$4.4153(1) \times 10^{-5}$
	M_Z^2	m_e, m_e	m_t, m_t	-7.401994×10^2	-2.114765×10^{-6}
$Z^* \rightarrow e^+e^-$	$100 m_e^2$	m_e, m_e	m_b, m_b	8.061021×10^{11}	3.308893×10^{10}
	$100 m_e^2$	m_e, m_e	m_t, m_t	-2.392478×10^{11}	-4.086825×10^{10}
$W^* \rightarrow t\bar{b}$	$[200 \text{ GeV}]^2$	m_t, m_b	m_b, m_b	$-6.5246(4) \times 10^{-5}$	$3.5182(7) \times 10^{-5}$
	$[200 \text{ GeV}]^2$	m_t, m_b	m_t, m_t	-6.132929×10^{-5}	-6.549233×10^{-6}
$H^* \rightarrow W^+W^-$	$[200 \text{ GeV}]^2$	M_W, M_W	M_W, M_W	$-1.493808(2) \times 10^{-7}$	$-3.513014(2) \times 10^{-7}$
$t \rightarrow W^+b$	m_t^2	M_W, m_b	m_b, m_b	$-3.5328(2) \times 10^{-5}$	$1.5688(4) \times 10^{-5}$
	m_t^2	M_W, m_b	M_W, M_W	-2.341537×10^{-5}	$-2.486382(2) \times 10^{-7}$

Table 6: **Diagram** $V_{a;M}$. The setup refers to the diagram of Fig. 7. The unit of mass μ is 1 GeV. Only the infrared finite part is shown. The results are in GeV^{-4} . Unless indicated our relative error is below 10^{-7} .

Process	s	M, m	m_1, m_2	$\text{Re } V_{b;M}^0$	$\text{Im } V_{b;M}^0$
$Z^* \rightarrow e^+e^-$	$[500 \text{ GeV}]^2$	m_e, m_e	m_e, M_Z	-25.86641	2.008353×10^{-8}
	$[500 \text{ GeV}]^2$	m_e, m_e	m_ν, M_W	-29.73137	2.488703×10^{-8}
$Z \rightarrow e^+e^-$	M_Z^2	m_e, m_e	m_e, M_Z	-7.776883×10^2	2.316778×10^{-6}
	M_Z^2	m_e, m_e	m_ν, M_W	-8.938906×10^2	2.416842×10^{-6}
$Z^* \rightarrow e^+e^-$	$100 m_e^2$	m_e, m_e	m_e, M_Z	-2.171299×10^{11}	8.580100×10^9
	$100 m_e^2$	m_e, m_e	m_ν, M_W	-2.520681×10^{11}	6.108271×10^9
$W^* \rightarrow t\bar{b}$	$[200 \text{ GeV}]^2$	m_t, m_b	m_b, M_W	-2.248708×10^{-7}	1.048569×10^{-6}
	$[200 \text{ GeV}]^2$	m_t, m_b	m_t, M_H	-4.763299×10^{-7}	1.548612×10^{-6}
$H^* \rightarrow W^+W^-$	$[200 \text{ GeV}]^2$	M_W, M_W	M_W, M_H	1.109640×10^{-7}	4.589289×10^{-7}
$t \rightarrow W^+b$	m_t^2	M_W, m_b	m_e, m_ν	3.567051×10^{-7}	-2.586087×10^{-7}
	m_t^2	M_W, m_b	M_W, M_Z	-1.412470×10^{-7}	3.224342×10^{-7}

Table 7: **Diagram** $V_{b;M}$. The setup refers to the diagram of Fig. 7. The neutrino mass has been arbitrarily set to $m_\nu = 0.1 \text{ eV}$. The unit of mass μ is 1 GeV. Only the infrared finite part is shown. The results are in GeV^{-4} . Unless indicated our relative error is below 10^{-7} .

	s	$\text{Re } V_{c;M}^0$	$\text{Im } V_{c;M}^0$
Our	$[500 \text{ GeV}]^2$	-1.819980×10^5	4.273610×10^4
BMR		-1.820011×10^5	4.273685×10^4
Our	M_Z^2	-4.194142×10^6	1.086325×10^6
BMR		-4.194142×10^6	1.086325×10^6
Our	$100 m_e^2$	-9.234450×10^{13}	8.726096×10^{13}
BMR		-9.234450×10^{13}	8.726096×10^{13}
Our	$4.0001 m_e^2$	1.449091×10^{20}	-1.754699×10^{21}
BMR		1.449091×10^{20}	-1.754699×10^{21}
Our	m_e^2	1.377881×10^{15}	0
BMR		not available	0
Our	$-100 m_e^2$	1.038162×10^{14}	0
BMR		1.038162×10^{14}	0

Table 8: **Diagram** $V_{c;M}$. Comparison with the results of [15] (BMR). The setup referring to the diagram of Fig. 7 is: $m = M = m_e$. The unit of mass μ is 1 GeV. Only the infrared finite part is shown. The results are in GeV^{-4} . Our relative error is everywhere below 10^{-7} .

Process	s	M, m	m_1, m_2, m_3	$\text{Re } V_{a;K}^0$	$\text{Im } V_{a;K}^0$
$Z \rightarrow e^+e^-$	$[500 \text{ GeV}]^2$	m_e, m_e	m_e, m_e, M_Z	$-8.6239(5) \times 10^{-9}$	$4.86523(5) \times 10^{-8}$
	$[500 \text{ GeV}]^2$	m_e, m_e	M_W, M_W, m_ν	$-1.706(4) \times 10^{-8}$	$7.109(3) \times 10^{-8}$
$Z \rightarrow e^+e^-$	M_Z^2	m_e, m_e	m_e, m_e, M_Z	$5.11313(2) \times 10^{-6}$	$5.05866(2) \times 10^{-6}$
	M_Z^2	m_e, m_e	M_W, M_W, m_ν	$4.552503(7) \times 10^{-6}$	$-1.269944(6) \times 10^{-6}$
$Z^* \rightarrow e^+e^-$	$100 m_e^2$	m_e, m_e	m_e, m_e, M_Z	-6.700055×10^3	1.226283×10^3
	$100 m_e^2$	m_e, m_e	M_W, M_W, m_ν	-86.21982	-11.84965
$W^* \rightarrow t\bar{b}$	$[200 \text{ GeV}]^2$	m_t, m_b	m_b, m_t, M_Z	$1.0060(2) \times 10^{-6}$	$-6.2131(5) \times 10^{-7}$
	$[200 \text{ GeV}]^2$	m_t, m_b	M_W, M_H, m_t	$1.894547(1) \times 10^{-7}$	-3.017159×10^{-7}
$H^* \rightarrow W^+W^-$	$[200 \text{ GeV}]^2$	M_W, M_W	m_t, m_t, m_b	$4.216966(3) \times 10^{-8}$	-1.225831×10^{-7}
$t \rightarrow W^+b$	m_t^2	M_W, m_b	M_W, m_b, m_t	$3.4389(8) \times 10^{-7}$	$6.082(2) \times 10^{-8}$
	m_t^2	M_W, m_b	m_b, M_W, M_Z	$6.3629(3) \times 10^{-7}$	$3.0576(8) \times 10^{-7}$

Table 9: **Diagram $V_{a;K}$** . The setup refers to the diagram of Fig. 10. The neutrino mass has been arbitrarily set to $m_\nu = 0.1 \text{ eV}$. The unit of mass μ is 1 GeV. Only the infrared finite part is shown. The results are in GeV^{-4} . Unless indicated our relative error is below 10^{-7} .

	s	$\text{Re } V_{b;K}^0$	$\text{Im } V_{b;K}^0$
Our	$[500 \text{ GeV}]^2$	$-2.6228(2) \times 10^{-4}$	$8.7973(7) \times 10^{-5}$
BMR		-2.622920×10^{-4}	8.797302×10^{-5}
Our	M_Z^2	$-1.64386(8) \times 10^{-3}$	$5.8676(7) \times 10^{-4}$
BMR		$-1.6438612 \times 10^{-3}$	5.867706×10^{-4}
Our	$100 m_e^2$	$-3.8356(4) \times 10^{12}$	$7.7519(4) \times 10^{12}$
BMR		-3.835560×10^{12}	7.751602×10^{12}
Our	$4.0001 m_e^2$	$1.844(3) \times 10^{20}$	unstable
BMR		1.842500×10^{20}	5.160917×10^{19}
Our	m_e^2	-1.177792×10^{15}	0
BMR		not available	0
Our	$-100 m_e^2$	-5.682692×10^{12}	0
BMR		-5.682692×10^{12}	0

Table 10: **Diagram $V_{b;K}$** . Comparison with the results of [15] (BMR). The setup referring to the diagram of Fig. 10 is: $m = M = m_e$. The unit of mass μ is 1 GeV. Only the infrared finite part is shown. The results are in GeV^{-4} . Unless indicated our relative error is below 10^{-7} .

Process	s	M, m	m_1, m_2, m_3	$\text{Re } V_{c;\kappa}^0$	$\text{Im } V_{c;\kappa}^0$
$Z \rightarrow e^+e^-$	$[500 \text{ GeV}]^2$	m_e, m_e	m_e, M_Z, m_e	$-2.1336(8) \times 10^{-6}$	$6.87(2) \times 10^{-7}$
$Z \rightarrow e^+e^-$	M_Z^2	m_e, m_e	m_e, M_Z, m_e	$-5.0064(3) \times 10^{-5}$	$1.862(2) \times 10^{-6}$
	m_e^2	M_Z, m_e	m_t, m_t, m_t	-2.656960×10^{-7}	$2.424(5) \times 10^{-20}$
	m_e^2	M_Z, m_e	m_b, m_b, m_b	$6.8986(3) \times 10^{-6}$	$-6.3053(4) \times 10^{-6}$
$Z^* \rightarrow e^+e^-$	$100 m_e^2$	m_e, m_e	m_e, M_Z, m_e	$-7.19834(2) \times 10^3$	$3.73760(1) \times 10^3$
$W^* \rightarrow t\bar{b}$	$[200 \text{ GeV}]^2$	m_t, m_b	m_t, M_Z, m_t	$1.43046(3) \times 10^{-7}$	$-2.256417(8) \times 10^{-7}$
	$[200 \text{ GeV}]^2$	m_t, m_b	M_W, m_b, M_W	$5.962(5) \times 10^{-7}$	$6.528(3) \times 10^{-7}$
$H^* \rightarrow W^+W^-$	$[200 \text{ GeV}]^2$	M_W, M_W	m_t, m_b, m_t	$3.62055(7) \times 10^{-8}$	$-1.075947(8) \times 10^{-7}$
$t \rightarrow W^+b$	m_t^2	M_W, m_b	m_t, m_b, m_t	$1.22769(4) \times 10^{-7}$	$-1.084614(6) \times 10^{-7}$
	m_t^2	M_W, m_b	M_W, M_H, M_W	$1.6920(4) \times 10^{-7}$	$-1.49596(9) \times 10^{-7}$

Table 11: **Diagram $V_{c;\kappa}$** . The setup refers to the diagram of Fig. 10. The unit of mass μ is 1 GeV. Only the infrared finite part is shown. The results are in GeV^{-4} . Unless indicated our relative error is below 10^{-7} .

	s	$\text{Re } V_{d;\kappa}^0$	$\text{Im } V_{d;\kappa}^0$
Our	$[500 \text{ GeV}]^2$	$1.58634(5) \times 10^5$	$-3.868(8) \times 10^4$
BMR		1.586339×10^5	-3.878825×10^4
Our	M_Z^2	$3.61488(4) \times 10^6$	$-9.75(2) \times 10^5$
BMR		3.614876×10^6	-9.774586×10^5
Our	$100 m_e^2$	$6.7595(2) \times 10^{13}$	$-7.0650(4) \times 10^{13}$
BMR		6.759415×10^{13}	-7.065317×10^{13}
Our	$4.0001 m_e^2$	$-1.680564(3) \times 10^{17}$	$1.1570(6) \times 10^{17}$
BMR		-1.680565×10^{17}	1.156966×10^{17}
Our	m_e^2	-7.970954×10^{14}	0
BMR		not available	0
Our	$-100 m_e^2$	-7.782868×10^{13}	0
BMR		-7.782868×10^{13}	0

Table 12: **Diagram $V_{d;\kappa}$** . Comparison with the results of [15] (BMR). The setup referring to the diagram of Fig. 10 is: $m = M = m_e$. The unit of mass μ is 1 GeV. Only the infrared finite part is shown. The results are in GeV^{-4} . Unless indicated our relative error is below 10^{-7} .

	s	$\text{Re } V_H^0$	$\text{Im } V_H^0$
Our	500^2 GeV^2	-1.342815×10^{-6}	1.052948×10^{-6}
BMR		-1.342815×10^{-6}	1.052948×10^{-6}
Our	M_Z^2	-4.562983×10^{-4}	5.478876×10^{-4}
BMR		-4.552983×10^{-4}	5.478876×10^{-4}
Our	$100 m_e^2$	$2.801(1) \times 10^{11}$	$-2.0846(8) \times 10^{12}$
BMR		2.801721×10^{11}	-2.084294×10^{12}
Our	$4.01 m_e^2$	$-1.87(1) \times 10^{16}$	$2.185(32) \times 10^{16}$
BMR		-1.866708×10^{16}	2.152803×10^{16}
Our	m_e^2	1.424912×10^{14}	0
BMR		not available	0
Our	$-100 m_e^2$	$1.21504(6) \times 10^{12}$	0
BMR		1.214934×10^{12}	0

Table 13: **Diagram V_H** . Comparison with the results of [15] (BMR). The setup referring to the diagram of Fig. 12 is: $m = M = m_e$. The unit of mass μ is 1 GeV. Only the infrared finite part is shown. The results are in GeV^{-4} . We have found numerical instabilities for values of s too close to the normal threshold, Unless indicated our relative error is below 10^{-7} .

	\sqrt{s} [GeV]	$\text{Re } V_{0;K}$ [GeV^{-4}]	$\text{Im } V_{0;K}$ [GeV^{-4}]
Our	400	$5.1343(1) \times 10^{-8}$	$1.94009(8) \times 10^{-8}$
DK		5.13445×10^{-8}	1.94008×10^{-8}
Our	300	5.68801×10^{-8}	-1.61218×10^{-8}
DK		5.68801×10^{-8}	-1.61218×10^{-8}
Our	200	9.36340×10^{-8}	-2.84232×10^{-8}
DK		9.36340×10^{-8}	-2.84232×10^{-8}
Our	100	2.94726×10^{-7}	-9.74218×10^{-8}
DK		2.94726×10^{-7}	-9.74218×10^{-8}
	$\sqrt{-t}$ [GeV]	$\text{Re } V_{0;K}$ [GeV^{-4}]	$\text{Im } V_{0;K}$ [GeV^{-4}]
Our	100	-2.85709×10^{-7}	0
DK		-2.85709×10^{-7}	0
Our	200	-7.61695×10^{-8}	0
DK		-7.61695×10^{-8}	0
Our	300	-3.29938×10^{-8}	0
DK		-3.29938×10^{-8}	0
Our	400	-1.74228×10^{-8}	0
DK		-1.74228×10^{-8}	0

Table 14: Comparison with the results of [12] (DK) in the setup of Eq.(318). Only the infrared finite part is shown. Unless indicated our relative error is below 10^{-5} .

	s [GeV ²]	Re $V_{0;\kappa}$ [GeV ⁻⁴]	Im $V_{0;\kappa}$ [GeV ⁻⁴]
Our	10.2	16.346(5)	-18.059(4)
DS		16.3459	-18.0590
Our	9.2	19.928(6)	-22.175(4)
DS		19.9189	-22.1755
Our	8.2	24.898(8)	-27.980(4)
DS		24.9015	-27.9753
Our	7.2	32.185(8)	-36.547(8)
DS		32.1805	-36.5550
Our	6.2	43.51(1)	-50.114(8)
DS		43.4927	-50.1010
Our	5.2	62.62(2)	-73.51(2)
DS		62.6575	-73.5359
Our	4.2	99.58(3)	-120.09(2)
DS		99.6039	-120.086
Our	3.2	188.04(5)	-237.07(5)
DS		188.017	-237.028

Table 15: Comparison with the results of [13] (DK) in the setup of Eq.(319). Only the infrared finite part is shown.

Tensor coeff.	Real part	Imaginary part
$V_{c;\kappa}^0$	$6.8986(3) \times 10^{-6}$	$-6.3053(4) \times 10^{-6}$
$V_{c;\kappa 11}^0$	$-4.210(2) \times 10^{-6}$	$3.423(3) \times 10^{-6}$
$V_{c;\kappa 12}^0$	$-2.9453(4) \times 10^{-6}$	$2.4067(6) \times 10^{-6}$
$V_{c;\kappa 11 11}^0$	$3.043(2) \times 10^{-6}$	$-2.372(3) \times 10^{-6}$
$V_{c;\kappa 11 12}^0$	$2.1699(3) \times 10^{-6}$	$-1.7005(4) \times 10^{-6}$
$V_{c;\kappa 12 12}^0$	$1.7392(2) \times 10^{-6}$	$-1.5014(2) \times 10^{-6}$

Table 16: **Tensor Diagrams.** Results for the tensor coefficients of rank 0, 1 and 2 for the diagram $V_{c;\kappa}$, see Eq.(320), with setup $m_1 = m_2 = m_3 = m_b$, $M = M_Z$, $m = m_e$ and $s = M_Z^2$ (see Fig. 10). The unit of mass μ is 1 GeV. Only the infrared finite part is shown. The results are in GeV⁻⁴.

References

- [1] G. Passarino, Nucl. Phys. B **619** (2001) 257 [arXiv:hep-ph/0108252].
- [2] G. Passarino and S. Uccirati, Nucl. Phys. B **629** (2002) 97 [arXiv:hep-ph/0112004].
- [3] A. Ferroglia, M. Passera, G. Passarino and S. Uccirati, Nucl. Phys. B **650** (2003) 162 [arXiv:hep-ph/0209219].
- [4] A. Ferroglia, G. Passarino, M. Passera and S. Uccirati, *Prepared for 31st International Conference on High Energy Physics (ICHEP 2002), Amsterdam, The Netherlands*;
A. Ferroglia, G. Passarino, S. Uccirati and M. Passera, Nucl. Instrum. Meth. A **502** (2003) 391.
- [5] A. Ferroglia, M. Passera, G. Passarino and S. Uccirati, Nucl. Phys. B **680** (2004) 199 [arXiv:hep-ph/0311186].
- [6] S. Actis, A. Ferroglia, G. Passarino, M. Passera and S. Uccirati, Nucl. Phys. B **703**, 3 (2004) [arXiv:hep-ph/0402132].
- [7] W. Hollik, U. Meier and S. Uccirati, Nucl. Phys. B **731** (2005) 213 [arXiv:hep-ph/0507158];
W. Hollik, U. Meier and S. Uccirati, Phys. Lett. B **632** (2006) 680 [arXiv:hep-ph/0509302].
- [8] R. Gastmans, J. Verwaest and R. Meuldermans, Nucl. Phys. B **105** (1976) 454;
W. J. Marciano and A. Sirlin, Nucl. Phys. B **88** (1975) 86;
W. J. Marciano, Phys. Rev. D **12** (1975) 3861.
- [9] L.D. Landau, Nucl. Phys. **13** (1959) 181.
- [10] T. Binoth and G. Heinrich, Nucl. Phys. B **585** (2000) 741 [arXiv:hep-ph/0004013];
C. Anastasiou, K. Melnikov and F. Petriello, arXiv:hep-ph/0501130. C. Anastasiou, K. Melnikov and F. Petriello, Phys. Rev. D **69** (2004) 076010 [arXiv:hep-ph/0311311]. C. Anastasiou and A. Daleo, arXiv:hep-ph/0511176;
A. Denner, M. Melles and S. Pozzorini, Nucl. Phys. B **662** (2003) 299 [arXiv:hep-ph/0301241];
K. Hepp, Commun. Math. Phys. **2** (1966) 301.
- [11] T. Binoth and G. Heinrich, Nucl. Phys. B **693** (2004) 134 [arXiv:hep-ph/0402265]; G. Heinrich, arXiv:hep-ph/0601232; G. Heinrich, arXiv:hep-ph/0601062.
- [12] A. I. Davydychev and M. Y. Kalmykov, arXiv:hep-th/0303162.
- [13] A. I. Davydychev and V. A. Smirnov, Nucl. Instrum. Meth. A **502** (2003) 621 [arXiv:hep-ph/0210171].
- [14] R. Bonciani, P. Mastrolia and E. Remiddi, arXiv:hep-ph/0311145;
R. Bonciani, P. Mastrolia and E. Remiddi, arXiv:hep-ph/0307295;
- [15] R. Bonciani, P. Mastrolia and E. Remiddi, Nucl. Phys. B **661** (2003) 289 [arXiv:hep-ph/0301170];
U. Aglietti and R. Bonciani, Nucl. Phys. B **668** (2003) 3 [arXiv:hep-ph/0304028].
- [16] T. G. Birtwright, E. W. N. Glover and P. Marquard, JHEP **0409** (2004) 042 [arXiv:hep-ph/0407343];
R. Bonciani, P. Mastrolia and E. Remiddi, Nucl. Phys. B **661** (2003) 289 [Erratum-ibid. B **702** (2004) 359] [arXiv:hep-ph/0301170];
S. Groote and M. M. Knodel, arXiv:hep-ph/0508173;
J. Fleischer, V. A. Smirnov, A. Frink, J. G. Korner, D. Kreimer, K. Schilcher and J. B. Tausk, Eur. Phys. J. C **2** (1998) 747 [arXiv:hep-ph/9704353].
- [17] J. Bernstein, Modules over a ring of differential operators, Functional Analysis and its Applications 5(1971);
M. Sato, Nagoya Mat. J. **120** (1990) 1;
S. C. Coutinho, A Primer of Algebraic D -Modules, LMS Student Text 33 (1995);

- [18] D. Y. Bardin and G. Passarino, The standard model in the making: Precision study of the electroweak interactions, OUP 1999.
- [19] J. van der Bij and M. J. Veltman, Nucl. Phys. B **231** (1984) 205.
- [20] P. Cvitanovic and T. Kinoshita, Phys. Rev. D **10** (1974) 3978.
- [21] G. Passarino, Nucl. Phys. Proc. Suppl. **135** (2004) 265.
- [22] M. Roth and A. Denner, Nucl. Phys. B **479** (1996) 495 [arXiv:hep-ph/9605420].
- [23] R.J. Eden, P.V. Landshoff, D.I. Olive, and J.C. Polkinghorne, *The Analytic S-Matrix*, Cambridge Univ. Press, 1966.
- [24] P. Cvitanovic and T. Kinoshita, Phys. Rev. D **10** (1974) 3991.
- [25] F. V. Tkachov, Nucl. Instrum. Meth. A **389** (1997) 309 [hep-ph/9609429];
L. N. Bertstein, Functional Analysis and its Applications, **6**(1972)66.
- [26] K. S. Kolbig, SIAM J. Math. Anal. **17** (1986) 1232;
N. Nielsen, Nova Acta Leopoldina (Halle) **90** (1909) 123;
L. Lewin, Polylogarithms and associated functions, North Holland, Amsterdam, 1981;
A. B. Goncharov, Math. Res. Lett. **5** (1998) 497.
- [27] R. Erdelyi et al., *Higher Transcendental Functions vol. 2*, Bateman Manuscript Project (*McGraw-Hill 1953*);
L. J. Slater, *Generalized Hypergeometric Functions* Cambridge Univ. Press, 1966.
- [28] R. Cranley and T. N. L. Patterson, Randomization of Number Theoretic Methods for Multiple Integration, SIAM J Numer Anal **13**, pp. 904-14;
P. Keast, Optimal parameters for Multidimensional Integration, SIAM J Numer Anal **10**, pp.831-838;
H. Niederreiter, On a Number-Theoretical Integration Method, Aequationes Mathematicae, **8**(1972) 304;
- [29] N. M. Korobov, Dokl. Acad. Nauk USSR **115** (1957) 1062;
H. Conroy, J. Chem. Phys **47** (1967) 5307;
R. Cranley and T. N. L. Patterson, SIAM J. Numer. Anal. **137** (1976) 904.
- [30] NAG Fortran Library, Mark 19, The Numerical Algorithms Group Ltd, Oxford UK. 1999.
- [31] S. Actis, A. Ferroglia, G. Passarino and M. Passera, *GraphShot*, a FORM package for automatic generation of one- and two-loop Feynman diagrams, work in progress.
- [32] E. N. Argyres *et al.*, Phys. Lett. B **358** (1995) 339 [arXiv:hep-ph/9507216];
W. Beenakker *et al.*, Nucl. Phys. B **500** (1997) 255 [arXiv:hep-ph/9612260].
- [33] G. Montagna, F. Piccinini, O. Nicrosini, G. Passarino and R. Pittau, Comput. Phys. Commun. **76** (1993) 328;
G. Montagna, O. Nicrosini, F. Piccinini and G. Passarino, Comput. Phys. Commun. **117**, 278 (1999). [arXiv:hep-ph/9804211];
G. Montagna, F. Piccinini, O. Nicrosini, G. Passarino and R. Pittau, Nucl. Phys. B **401** (1993) 3.
- [34] G. Passarino and S. Uccirati, *LoopBack*, a FORTRAN/95 code for numerical evaluation of one- and two-loop Feynman diagrams, work in progress.
- [35] M. Y. Kalmykov, arXiv:hep-th/0602028.